Analysis of the performance of ensemble methods in reservoir simulation history matching

by

Junzhe Jiang, M.S.

A Dissertation

In

Petroleum Engineering

Submitted to the Graduate Faculty
of Texas Tech University in
Partial Fulfillment of
the Requirements for
the Degree of

DOCTOR OF PHILOSOPHY

Approved

Sheldon Gorell, Ph.D.
Chair of the Committee

James Sheng, Ph.D.
Qingwang Yuan, Ph.D.

Mark Sheridan, Ph.D.
Dean of the Graduate School

August, 2021

ACKNOWLEDGMENTS

I want to express my sincere thanks and appreciation to my thesis committee, which consisted of Dr. Sheldon Gorell, Dr. James J Sheng and Dr. Qingwang Yuan.

I would especially like to thank Dr. Sheldon Gorell for contributing so generously of his time, advice, understanding and encouragement during this study, for providing this opportunity for this study, and for assisting me during the study and reviewing this work several times. I am extremely grateful and indebted to him for his expert, sincere and valuable guidance and encouragement extended to me.

I would like to thank Mr. Zihou Cao for giving valuable advice and encouragement, also for his understanding and friendship.

I take this opportunity to express my sincere thanks to all the faculty members of the Department of Bob L Herd Department of Petroleum Engineering for their help and encouragement. I would also like to thank my parents for their love and support.

TABLE OF CONTENTS

ACKNOWLEDGMENTS ii
ABSTRACT v
LIST OF TABLES vii
LIST OF FIGURES viii
I. INTRODUCTION 1
1.1 Background 1
1.2 Overview 2
1.3 Problem Statement 8
1.3.1 The problems in the history matching for the conventional reservoirs 9
1.3.2 The problems in the history matching for the unconventional reservoirs 12
1.4 Research Objectives 15
II. ANALYSIS OF PARAMETERIZATION AND LOCALIZATION WITH SINGULAR VALUE DECOMPOSITION (SVD) ANALYTICAL SOLUTION 17
2.1 The relationship between ill-posedness and spurious correlation 17
2.2 The relationship between SVD parameterization and Localization 19
2.3 Generality from covariance localization to cross covariance localization and analysis of different correlation function 23
2.3.1 Generality in the first role 23
2.3.2 Generality in the second role 25
2.4 SVD supported localization 27
2.5 Experiments and results 30
2.5.1 Experimental design 30
2.5.2 The Criteria for Comparing Models 32
2.5.3 Example 1 33
2.5.4 Example 2 40
2.6 Conclusion 47
III. THE IMPORTANCE OF PRIOR INFORMATION ON THE FRACTURE GEOMETRY INVERSION WITH ENSEMBLE METHODS 49
3.1 Methods 49
3.2 Numerical Experiments 52
3.2.1 Example 1 53

3.2.2 Example 2 62
3.2.3 Example 3 67
Conclusion 73
IV. THE PERFORMANCE ANALYSIS OF EDFM WITH DIFFERENT TOTAL GRID NUMBER 75
4.1 The Verification of the Simulator 75
4.2 EDFM models with complex fracture geometry 76
4.3 EDFM models with single fracture 79
4.4 Improve the simulation accuracy of pressure drop around fracture 81
4.5 Improve the simulation quality with the tip effect 83
4.6 Improve the grid diagonal effect 89
4.7 Single fracture model with low fracture permeability 91
V. CONCLUSIONS 94
BIBLIOGRAPHY 95

ABSTRACT

The establishment of a reliable geological model is the basis of efficient reservoir evaluation, management, and development, as well as a guarantee for the performance prediction of reservoirs and wells. In the history matching process of reservoir simulation, Bayesian theory has been successfully used in automatic history matching algorithms. By replacing partitions with Bayesian estimation, and using prior statistical information of unknown parameters, the history matching problem becomes easier to determine in a statistical sense. The ensemble Kalman filter extended by Bayesian theory has also achieved gratifying results in the application of automatic history matching research. However, when the parameters and measurement errors are not normally distributed, the relationship between the model and the parameters is not linear, or the available data scale is very limited, the strict implementation of Bayesian estimation will become extremely complex and cumbersome. With an unstrict implementation of Bayesian estimation, the quality of the fitting results is also unstable.

For the conventional reservoirs, the history matching of the permeability field is a hot topic in the research of automatic history matching algorithms. The most important feature of the permeability field history matching problem is the large scale of parameters to be fitted. The huge difference in scale between the data used for history matching and the parameters that need to be fitted can cause serious overfitting problems. This dissertation introduces a novel localized Kalman filter based on singular value decomposition (SVD). it also demonstrates the improvement of over-fitting problems when applicating this algorithm in the automatic history matching process of reservoir simulation. At the same time, this dissertation also analyzes and summarizes the two functions of the covariance localization method at the theoretical level with an analytical solution of the objective function based on SVD. It also compares the performance of the localization methods using different correlation functions in the automatic history matching of the reservoir.

With the rapid development of the global economy and the continuous increase in energy consumption and demand, the shortage of conventional oil and gas resources has become a bottleneck restricting economic development. The exploration and development of fractured oil and gas reservoirs have become a research hotspot and have received more and more attention. Compared with conventional oil and gas reservoirs, the distribution of hydraulic fractures and nature fractures in fractured reservoirs, such as shale reservoirs, is extremely complicated. Fractures have a significant impact on fluid flow in the reservoir and need to be correctly described in the simulator. To guide the efficient development of fractured oil and gas reservoirs, first of all, it is necessary to be able to accurately describe the geometric characteristics and distribution of the fracture network in fractured oil and gas reservoirs. This dissertation investigates the use of ensemble methods to invert the position and shape of the fracture network because it is a promising direction. However, the relationship between the position of the fractures is highly non-linear. This dissertation demonstrates the proper prior information as an extremely critical factor for a successful history matching. The methods to generate the initial fields with proper prior information are also discussed.

At the same time, the scales of different types of fractures vary greatly in the fractured rservoir. Even if the fractures are the same type, there can be scale differences. The use of dense grids to completely and explicitly present all the fractures will lead to a huge waste of computing resources. The automatic history matching using the ensemble method is computationally intensive. The numerical model may need to be run thousands of times in an automatic history matching process, which requires a higher efficiency for the numerical simulator integrated into the automatic history matching program. However, fractured reservoirs, such as the shale gas reservoir requires a high simulation accuracy to capture the sharp pressure change around the fracture which is caused by the enormous permeability contrast between the fracture and matrix. the trade-off between the ensemble history matching program integrated simulator's efficiency and accuracy will be discussed through several numerical cases.

LIST OF TABLES

1. Example 1, Correlation length for each well 37
2. Example 1, misfit and spread of different history matching methods 40
3. Example 2, Correlation length for each well 43
4. Example 2, misfit and spread of different history matching methods 47
5. MSE of Example 1 62
6. MSE of Example 2 66
7. MSE of Example 3 73
8. Reservoir properties 78
9. Reservoir properties 80

LIST OF FIGURES

1. Localization Matrix 21
2. Comparison of different correlation functions 25
3. Comparison of Gaspari and Cohn correlation function and Gaussian function from Gaspari & Cohn (1999) 27
4. Elliptical area used to fit flow area 28
5. Example 1, Reference permeability (left) and log-permeability (right) field. 35
6. Example 1, water cut history matching result from EnKF without localization. 36
7. Example 1, the flow area maps for producer 1 and streamline map 36
8. Example 1, Comparison of log-permeability field history matching results from different history matching methods. 38
9. Example 1, Comparison of production rate history matching results from different history matching methods for Producer 4 38
10. Example 1, Comparison of water cut history matching results from different history matching methods for Producer 39
11. Example 2, Reference permeability field 42
12. Example 2, Comparison of log-permeability field history matching results from different history matching methods. 43
13. Example 2, water cut history matching result from EnKF without localization 44
14. Fracture in Cartesian coordinates 51
15. Hough field with local maximums 52
16. Saturation map of Example 1 reference model after 4 years simulation 54
17. Mean map of initial Hough value fields in Type 1 initial fields. 55
18. Fracture map used to generate initial Hough fields in Type 2 initial field. 56
19. Mean map of initial Hough value fields in Type 1 initial fields. 56
20. Mean map of initial Hough value fields after Gaussian filter in Type 1 initial fields. 56
21. Cartesian map with random points. 57

22. A representative of the Original Hough value fields and Hough value fields after Gaussian filter in Type 3 initial fields. 58
23. Mean map of initial Hough value fields after Gaussian filter in Type 3 initial fields. 58
24. Mean of Hough value fields history matching results. (From the top to the bottom: Type 1, Type 2, Type 3) 60
25. Fracture geometry history matching results. (From the left to the right: Type 1, Type 2, Type 3) 61
26. The production history matching results 62
27. Pressure map of Example 3 reference model 63
28. Mean of Hough value fields history matching results. (From the top to the bottom: Type 1, Type 2, Type 3) 64
29. Fracture geometry history matching results. (From the left to the right: Type 1, Type 2, Type 3) 65
30. The production history matching results 66
31. Saturation map of Example 4 reference model after 4 years simulation. 67
32. Fracture map used to generate initial Hough fields in Type 2 initial field. 69
33. Mean map of initial Hough value fields after Gaussian filter in Type 2 initial fields. 69
34. A representative of the point maps. 70
35. Mean map of initial Hough value fields after Gaussian filter in Type 3 initial fields. 70
36. Mean of Hough value fields history matching results. (From the top to the bottom: Type 1, Type 2, Type 3) 72
37. Fracture geometry history matching results. (From the left to the right: Type 1, Type 2, Type 3) 72
38. The production history matching results. 73
39. Comparison of gas flow rate (a) and cumulative production (b), (Bin Wang, 2020) 76
40. The grid mesh of the simulation models 77
41. The pressure maps after 30 years simulation 78
42. The production rate plot and cumulative production plot 79
43. The grid mesh of the simulation models 80

44. The pressure maps after 30 years simulation 80
45. The production rate plot and cumulative production plot 81
46. The grid mesh of the LGR models and Zoom-in plots for the matrix cell containing the fracture tip 82
47. The pressure maps after 30 years simulation 83
48. The production rate plot and cumulative production plot of the Model 1 83
49. The production rate plot and cumulative production plot of the Model 2 83
50. The illustration of the semi-analytical transmissibility (Shao, 2020) 84
51. The grid mesh of the simulation models and the pressure map at the end of the simulation of the model with LGR 86
52. The production rate plot and cumulative production plot of the model with LGR 86
53. The grid mesh of the simulation models and the pressure map at the end of the simulation of the model without LGR 87
54. The production rate plot and cumulative production plot of the model without LGR 87
55. Production rate plot analysis 88
56. The pressure-drop around the facture 88
57. The illustration of the fracture and its neighboring cells 89
58. The pressure maps after 30 years simulation 90
59. The production rate plot and cumulative production plot 90
60. The pressure map after 30 years simulation 91
61. The production rate plot and cumulative production plot of the model without improvement methods 91
62. The production rate plot and cumulative production plot of the model with improvement methods 92

CHAPTER I

INTRODUCTION

1.1 Background

The establishment of a reliable geological model is the basis for the reservoir's evaluation, management, and development. It is a basic requirement for the dynamic prediction of the flow in the reservoir. Reservoir geological modeling requires data's high quantity and high quality at the same time. It also requires the modeler's experience and knowledge. The uncertainty in the modeling process is common and complicated, which causes the geological model to be different from the real reservoir. Therefore, the geology model needs to be modified based on existing data, especially dynamic ones, to make the numerical model closer to the real reservoir. Compared with static data, dynamic data contains important geological information based on production response, which can evaluate geological models more comprehensively and accurately. The dynamic data is compared with the simulation results from the geological model (history matching) to evaluate the vast difference in parameters between the geological model and the real reservoir. The dynamic history matching method is currently widely used to modify and optimize the geological model. Automatic history matching is the process of automatically adjusting the parameters of the geological model with an optimization algorithm so that the reservoir model can reproduce the historical dynamics of the real reservoir. The basic principle is constructing an objective function that measures the error between the reservoir model and the observed data. The it finds the optimal reservoir parameters by minimizing the objective function through an optimization algorithm. Automatic history matching that modified with a large number of unknown parameters in the model with limited observed data (comparing to the grid number in the model), is a typical inverse problem with multiple solutions. Thus, the ultimate goal of the automatic history matching is to reduce the uncertainty of the model parameters and to make the geological model closer to the real reservoir. So that a more reliable geological model can be obtained.

1.2 Overview

History matching can be divided into manual history matching and automatic history matching depending on its development process and realization. Manually history matching is "trial and error". That is, the user manually analyzes and modifies one or more reservoir parameters based on the error between the calculated value from the simulation and the actual observation (Saleri & Toronyi, 1988; Mattax & Dalton, 1990). Actual oil and gas reservoirs are often highly heterogeneous and need a huge number of parameters to describe their properties precisely, leading to the existence of a large grid number in reservoir models. Manual history matching is usually time-consuming and laborious. Manual history matching the long-term developed and large-scale reservoir models is not realistic. Therefore, computers and optimization algorithms were introduced to modify reservoir parameters, gradually developing automatic history matching technology. Although the path of using computers to conduct history began as early as 1950s, the history matching algorithm with "automatic" significance only began to appear in the mid-1960s (Jacquard & Jain, 1965). The automatic history matching algorithm mainly includes two parts: objective function and optimization. When computational capabilities improve or the mathematical algorithms advance, the study of history matching sees an uptake. Not only the researcher's interest in history matching continues to increase, but also the researcher's ability continues to improve. The history matchings application has also developed from the early small simulation, simple model to the later three-dimensional three-phase complex model (Oliver & Chen, 2011).

In 1965, Jacquard and Jain (1965) tried to use regression analysis instead of "trial and error" for the first time, who introduce the experience from the electrical model into the reservoir model. By dividing the reservoir into multiple heterogeneous blocks, the properties on the blocks are continuously changed until the least-squares error between pressure observed value and calculated value was minimized. This pioneered the research of automatic history matching. However, due to the lack of experience in using this method and the limitations of computer performance at the time, the author did not

consider the feasibility of this technology. Jahns (1966) used the objective function and the parameter change rate to solve the linear problem derived from the least-squares method, and obtained the updated values of the model parameters, and suggested using the regression analysis method to correct the model parameter. Coats et al (1970) introduced the parameter value stochastic method and used linear programming to solve the problem, which avoided the situation that the updated value of the parameter appeared to have a negative value. Slater and Durrer (1971) used the mixed method to update the model parameters, which not only solved the parameter update according to the linear programming method of Coats but also modified the parameters in a certain direction which makes the objective function reaches minimum. Thomas et al. (1972) took the lead in solving the least-squares linear equation problem with implicit parameter changes, using the updated values of the parameters for numerical simulation until the least-squares error reached the minimum. The period from 1965 to 1972 was the embryonic stage of the study of automatic history matching. During this period, automatic history matching used perturbation theory to divide the reservoir model (including conductivity, storage coefficient, grid, etc.) at will (Jacquard and Jain, 1965; Jahns, 1966; Coats et al, 1970; Slater and Durrer, 1971; Dougherty, 1972; Veatch and Thomas, 1971), use the least-squares method to solve the problem multiple times and regard the problem as adjusting the nonlinear form or nonlinear programming problem. The stability problem of the solution has not been dealt with well and can only be applied Single-phase simple model. Chen et al (1973) used the optimal control theory to improve the previous gradient-based history matching method, treating the history matching problem as an optimal control problem, and treating the reservoir properties as a continuous function of location instead of discrete area values This greatly reduced the time required for history matching. Wasserman et al (1975) used the method proposed by Chen et al to study the quasi-multiphase problem and showed the wide practicability of optimal control theory for multiphase fluid models. Chavent et al (1975) extended the research of optimal control history matching method, further verified the advantages of using optimal control theory for automatic history matching

and found that optimal control theory can avoid unreal parameter values. For the first time, Gavala et al (1976) used Bayesian theory for automatic reservoir history matching, replacing partitions with Bayesian estimation, and using prior statistical information of unknown parameters, making the history fitting problem statistically easier to determine. However, if the parameters and measurement errors are not normally distributed, and the relationship between the model and the parameters is not linear, the strict implementation of Bayesian estimation becomes extremely tedious and cumbersome, so it is rarely used. Moreover, Gavala's article does not get rid of the traces of the gradient method. Bosch and Seinfeld (1977) studied the studied the automatic history matching of incompressible oil-water two-phase flow, and extended the single-phase automatic history matching to the two-phase automatic history matching stage.. Watson et al (1980) used GPST (Generalized Hypothesis Technology) to perform an automatic pressure history trajectory on a two-dimensional micro-compressible linear model based on the optimal control theory for a two-phase reservoir. Two-dimensional systems are also applicable. Agarwal et al (1987) used regression technology combined with a dynamic parameter selection method to fit the phase behavior of the fluid and the parameters of the equation of state. MacMillan (1987) used standard automatic history matching technology to fit the relative permeability curve in the microscopic water drive experiment. Yang and Watson (1988) improved the automatic history method of optimal control theory with a variable scale method. Tan and Kalogerakis (1991,1992) extended the study of nonlinear regression methods and extended automatic history fitting to three-dimensional three-phase models.

1973-1992 was the formative stage of the automatic history matching research. Earlier methods, such as the nonlinear regression method, gradient method, and Gauss-Newton method, were further improved and perfected; the sensitivity coefficient calculation method required in the calculation process was also emphasized and developed, and a "standard process" for the automatic history matching has gradually formed. In addition, optimal control theory was also introduced and gradually developed and perfected. At the same time, the applicable models for automatic history matching

have evolved from the initial one-dimensional single-phase reservoir model to the three-dimensional three-phase reservoir model. In 1993, Ouenes et al (1993) applied the simulated annealing algorithm to the automatic history matching process, which improved the reliability of the global optimal solution. Sen and Datta-Gupta (1995) introduced the genetic algorithm into the automatic history matching process and compared the differences between three different algorithms based on the hybrid optimization process and generated a random distribution field of permeability. Gao Huimin (1994) used the Powell method to reverse the formation parameters and compared the effects of three different methods. Wang Shuguang (1998) applied the non-linear programming method—Nelder-Mead simplex method to automatic reservoir history matching and achieved good results. Schiozer et al (1999) applied parallel computing in the direct optimization algorithm to improve the calculation speed. Gomez et al (1999) introduced the tunnel algorithm to extend the gradient-based local optimization to global optimization. Schulze Riegert et al (2002) used an evolutionary algorithm with good stability and less sensitivity to nonlinearity and discontinuity to perform automatic history matching. The practical application shows that this method has a good effect in early modeling.

1993-2002 was the development stage of automatic history matching research. With the deepening of research on automatic history matching, in addition to (non-)linear regression, optimal control, and Bayesian estimation-based automatic history matching methods were discussed, improved, and perfected, more and more methods were introduced into reservoir history matching. The basic methods of automatic history matching have evolved from direct and gradient methods to stochastic methods and intelligent algorithms. A number of heuristic automatic history matching methods have gradually formed.

Naevdal et al. (2002) introduced the ensemble Kalman filter method (ENKF) into the field of petroleum engineering, and Liu and Oliver (2005) studied the ensemble Kalman filter method in terms of sedimentary facies boundary fitting. Zhang et al. (2003) conducted a case study and discussion on the automatic history matching of

Bayesian estimation. Gao and Reynolds (2004) used the synchronous disturbance random approximation method to fit the multiphase flow model and generated the search direction for each parameter in the synchronous disturbance iteration step. Sahni and Horne (2004) introduced a wavelet for automatic history matching, which is different from the previous automatic history matching algorithm. This method not only ensures the consistency of the model after fitting but also contains the uncertainty of production data. Cullick et al. (2006) compared the effects of two automatic history matching processes (directly on the model and replacing the model with a neural network) to update reservoir and well parameters and found that replacing the model can improve the efficiency and stability of automatic history matching. Haugen et al. (2006) and Zafari and Reynolds (2005) extended the application of the ensemble Kalman filter in the research of automatic history matching and achieved gratifying results. Kazemi and Stephen (2010) and Yan Xia et al. (2011) used streamline simulation to replace the traditional reservoir simulator, which greatly improved the simulation speed. Hajizadeh (2010) introduced the ant colony optimization algorithm to study the history matching problem and proved that the ant colony optimization algorithm has a better effect than other methods in the history matching of high-dimensional complex reservoirs. While various new algorithms are continuously being introduced into automatic history matching, various hybrid algorithms are also constantly appearing. For example, probability and ensemble Kalman filters are mixed (Zeng et al., 2011), and global and local optimization algorithms are mixed (Yin et al., 2011). In addition, optimization algorithms based on various mathematic theories before improvements are also emerging (Nasralla et al., 2011; Zhang et al., 2012; Xavier et al., 2013; Kaydani et al., 2014; Costa et al., 2014).

From 2003 to the present was the rapid development stage of automatic history matching research. Stochastic methods and intelligent algorithms have been increasingly used in dynamic geological modeling. A number of more promising automatic history matching algorithms have been developed, such as ensemble Kalman filtering methods and various hybrid algorithms. With the improvement of people's

understanding of the accuracy and uncertainty of oil and gas reservoir modeling, a single "fitting" model can no longer meet the needs, and the automatic history matching technology is moving in the direction of generating multiple "fitting" models at the same time. At the same time, in order to improve the speed of automatic history matching of large-scale complex geological models, a variety of auxiliary automatic history matching methods have been developed and improved.

Besides the continued progress on the \algorithm, there also has been noticeable efforts to apply the history matching methods, especially the automatic ones to more and more new-raised practical problems in reservoir engineering. After 2010, with the rapid development of unconventional reservoirs, the history matching of the fracture reservoirs gained more and more attention. Fractures, both natural and hydraulically induced, often show a critical influence on the sub-surface flow. As introduced before, fractures' different locations and geometry can lead to dramatically different flow behavior and different Stimulated Reservoir Volume (SRV) in the reservoir. Fracture propagation modeling is a very promising research direction to determine the geometry of fractures. A noticeable work has been done by Bryant and Hwang (2015) where they proposed a finite volume-based arbitrary fracture propagation model. A single-phase flow model was coupled with Biot's displacement and in-situ stress tensor equations in a poroelastic reservoir domain. This model can simulate the propagation of single non-planar fractures. However, it still faces difficulties in describing the propagation process of a fracture with bifurcation or fractures that contacted each other. As a general problem in fracture propagation modeling, the initial and boundary conditions are necessary for forwarding modeling. Also, the material properties, such as the weak planes in the rock, play a decisive role in the direction of fractures' propagation. In many real problems, these conditions are hard to measure accurately.

Due to the problems in the forward modeling, there have been many attempts to directly obtain the geometry and position of fractures from production data using inversion. Chen & Liao (2016, 2017, 2017 September) obtained semi-analytical solutions of the sub-surface flow equations of horizontal wells with multiple hydraulic

fractures. Fracture properties and simple fracture-geometry information, such as fracture length, can be determined from pressure decline curves. After comparing the production data with several typical fracture geometries' decline curves, the most similar fractures' geometry is picked. This method shows limitation for fractures with more random distributions, whose geometry is not included in the typical type curves. For example, the nature fractures in carbonate are hard to obtain type curves and determine fracture geometries.

Numerical automatic history matching methods, especially the Ensemble methods, have gained attention for solving the inverse problem with production data to determine fracture position and geometry due to limitations of analytical methods. Ping & Zhang (2013) first applied the Ensemble Kalman filter (EnKF) for fracture geometry inversion. The parameterization method is necessary to transform the fracture geometry problem into a continuous field inversion problem with ensemble methods. The level set method was introduced as a parametrization method in their paper. Lu & Zhang (2015) then introduced another parameterization method, Hough transformation. Different ensemble methods' performance has also been researched before. Iterative ensemble methods were observed to exhibit better performance in Lu & Zhang's paper. Then, Yao & Chang combined the Levenberg-Marquardt method with iterative ensemble methods to get faster convergence. Recently, Chang & Zhang (2018) researched the potential to directly invert the SRV's geometry and properties with ensemble methods. However, it was difficult to obtain the correct shape and properties of the SRV area from their numerical experiments.

1.3 Problem Statement

From the introduction above, ensemble methods based on probability theory and Monte-Carlo simulation are promising approaches to solve history matching problems. Due to the different parameters we want to match, the ensemble history matching program may face the following problems: Due to the limitation of computing resources, the ensemble size of the history matching program with the ensemble method cannot be very huge. There may be a huge contrast between the ensemble's scale and

the parameter field's scale. This will influence the performance of the ensemble methods. The Ensemble methods were initially built for the linear problems. When facing the highly non-linear problem in the reservoir history matching, the different initial fields will make a dramatic influence on the results. Nowadays, the simulation of fractured reservoirs is a hot topic. To accurately simulate fractured reservoir always needs modifications to the simulator, which increases the calculation burden. In the automatic history matching process, computation resources are very precious. Thus, we will test and discuss the trade-off between efficiency and accuracy. The detail of each problem is discussed below.

1.3.1 The problems in the history matching for the conventional reservoirs

The ensemble methods and the hybrid algorithms based on them avoid the explicit calculation of gradients. Ensemble Kalman filter (EnKF) is a representative method. To study the factors that will influence the performance of EnKF in the conventional reservoirs, a classic automatic history matching problem was selected for this dissertation. The history matching problem of the permeability field is a large-scale problem spatially. The observations are commonly production data gathered from wells, which is sparse in spatial location. In addition, the production data is always 2D data with value and time axes. Thus, history matching is an extremely difficult task that uses spatially sparse and 2D data to estimate a spatially dense, 3D, and anisotropic permeability field. The conclusion from the permeability field history matching can be applied to other spatial parameters in the reservoir model, like the porosity. Because of the scale difference between the data and parameter field, history matching has been described as highly ill-posedness which will challenge the stability and accuracy of the ensemble methods (Zafari & Reynolds, 2005). The covariance matrix used in the update equation is estimated from the ensemble of reservoir model realizations. If the ensemble size is relatively small compared to the number of model parameters, this can cause problems like spurious correlation and filter divergence. Localization is a common method to solve the spurious correlation problem. Thus, proper localization methods for the reservoir history matching should be developed

In addition, there is also another problem that was researched in this chapter. Because the sensitivity or gradient matrix G is unknown in reservoir simulation, the traditional covariance localization cannot be applied to ensemble methods in reservoir history matching directly. To deal with this issue, a transform from the covariance localization to cross-covariance localization was introduced to reservoir history matching. The transformation of localization was first proposed by Houtekamer (2001) from the weather forecasting industry:

$$\mathrm{K} = [(\rho \circ P)H^T][\mathrm{H}(\rho \circ \mathrm{P})\mathrm{H}^{\mathrm{T}} + \mathrm{R}]^{-1} \quad (1)$$

$$\mathrm{K} = [\rho \circ (\mathrm{PH}^{\mathrm{T}})][\rho \circ (\mathrm{HPH}) + \mathrm{R}]^{-1} \quad (2)$$

The above equations show the Kalman gain matrix (K) that is used in weather forecasting from Houtekamer's paper (2001). H is the gradient between the parameter field and the observation. The parameter field can be the permeability/porosity field matrix in the reservoir simulation history matching, while the observation is usually the well's production. H is written as G in this dissertation. R is the observation error covariance matrix that is also written as $\mathrm{C_D}$ in this dissertation. P is the forecast error covariance matrix of the ensemble that equals to $\mathrm{C_M}$. ρ represents localization matrices in Eq. 1 and Eq. 2. Instead of applying the localization matrices directly on the forecast error covariance matrix (Eq. 1), Eq. 2 applies the localization matrices on the matrix's multiplication PH^{T} and HPH. The localization shown in Eq.2 is called cross-covariance localization. In Houtekamer's paper (2001), the localization matrices are represented by ρ in Eq. 1 and Eq. 2. However, they are not the same. In particular, they have different dimensions. Even the two localization matrices in Eq. 2 are different from each other. Thus, it is more reasonable to denote Eq. 2 as:

$$\mathrm{K} = [\rho_1 \circ (\mathrm{PH}^{\mathrm{T}})][\rho_2 \circ (\mathrm{HPH}) + \mathrm{R}]^{-1} \quad (3)$$

Due to Houtekamer's work, the same dependence on distance (such as Gaspari and Cohn's correlation function) can be used for both localization matrices. The localization matrices ρ in Eq.1 consider the distance between all pairs of analysis grid

points, while the first localization matrix ρ_1 in Eq. 3 considers the distance between analysis points and observation points and the second localization matrix ρ_2 considers the distance between all pairs of observation points. (Houtekamer, personal communication).

In Eq. 1, 2, and 3, Houtekamer discusses data assimilation with the main purpose to interpolate the true state to the observed quantities. Thus, the Kalman gain consists of a forward interpolation H. In weather forecasting, H may be a simple interpolation from a model grid to observation locations for direct observations, for example, winds or temperature from radiosondes. H can also perform additional complex transformations of model variables to, for example, satellite radiances. However, if H performs additional complex transformations, the non-linearity's influence on the transformation from Eq. 1 to Eq. 2 was not discussed in Houterkamer (2001). Due to the differences between weather forecasting and history matching, the H is substituted by the sensitivity matrix G in reservoir history matching, which performs a complex non-linear transformation between model parameter field and the production data. Because neither Houtekamer nor the authors from our industry have mathematically validated the transformation in highly non-linear conditions, the localization transformation shown in Eq. 1, 2 and 3 has been applied in reservoir simulation history matching (Eq. 4) (it is the same equation as the Eq. 16 in Emerick (2011).

$$m_{i+1} = m_i + \rho_{MD} \circ C_M G^T (C_D + \rho_{DD} \circ G C_M G^T)^{-1} \times (d - g(m)) \quad (4)$$

In the updating equation, m is the parameter field that needs to be modified to reduce the difference between the simulation results and field production observation. In a typical problem, the parameter field can be porosity or permeability field. The m_i is the parameter field in the current iteration, while the m_{i+1} is the parameter field in the next iteration. The C_M is the variance matrix of the parameter field. Typically, the C_M is a diagonal matrix. The $g(m)$ is the simulation results with parameter field m. d is the observed production data, and C_d is the variance matrix of production data. A simple transform applied to Eq. 16 in Emerick (2011),$C_{MD} = C_M G^T C_{DD} = G C_M G^T$).

However, it may not be the best method for the transform from covariance localization to cross-covariance localization in reservoir history matching. Thus, the effectiveness of Houterkamer's method in reservoir history matching will be verified in this dissertation.

1.3.2 The problems in the history matching for the unconventional reservoirs

This dissertation believes that the use of ensemble methods to invert the position and shape of the fracture network is a promising direction. Since the ensemble methods are based on Bayesian theory, the highly non-linear problem makes the proper initial fields a critical factor for a successful history matching process. The fracture position and geometry history matching is a representative case of the non-linear problem. This is also the reason why reservoir engineers want to history matching the fracture's position and geometry. Features' existence will dramatically influence the well's production. However, its influence on a well's production is not a linear function of the fracture's angle or distance from the well. All the previous studies did not focus on the influence of prior information on this problem. This paper discusses the ensemble methods' matching quality with different types of initial fields, which combining different prior information, in the inversion problem of the fractures' geometry. Several examples with different matrix properties and different fractures network have been tested. The performance of the history matching program and the prior information in different kinds of reservoir models is compared and discussed by these numerical experiments.

Besides the prior information and in order to guide the efficient development of fractured oil and gas reservoirs, it is first necessary to select a proper simulator used in the history matching program, which can accurately describe the geometric characteristics and distribution of fracture networks in fractured oil and gas reservoirs. At present, dual-porosity, and dual-permeability models are the most commonly used fractured oil and gas reservoir modeling methods in the petroleum industry. Although the dual-continuous model is very effective, it is a very simple representation of a

complex naturally fractured reservoir. The traditional dual-porosity and dual-permeability models abstract fractures as fixed geometric structures that are not based on physical reality. This feature makes them insufficient to solve complex fluid flow problems in fractured reservoirs, which cannot be avoid in fracture position and geometry history matching. The dual continuum model is particularly suitable for reservoirs with a large number of highly connected small-scale fractures. The discrete fracture model (DFM) is a new type of model for simulating fractured oil and gas reservoirs and has received considerable attention in the past decade. As far as we know, although DFM can represent the flow in fractured reservoirs more accurately than traditional methods, there are still many limitations in its application in the industrial field. This is because when using DFM, a large number of small grid blocks are needed near the cracks, which leads to an increase in calculation time. In addition, most DFM methods need to generate unstructured grids to comply with the complexity of the fractures assigned to the domain of interest. Generating such grids for arbitrary fracture networks can be a huge challenge. The position and geometry of fractures are updated iteratively in the automatic history matching process with ensemble methods. A simulation method that can avoid re-discretizing or re-mesh calculation after every update is desired.

In this paper, Embedded Discrete Fractures Method (EDFM) was chosen as the simulation method because it has significant advantages (Yao & Chang) in the stated problem. During the history matching processes, a large calculation burden is unavoidable with other traditional simulation methods because the position and geometry of fractures can be non-orthogonal and different after every update. In order to use the advanced concepts in the dual continuum and discrete fracture model, Lee et al. (2000, 2001) and Li and Lee (2008) proposed a method for simulating fluid flow in a naturally fractured reservoir, called EDFM. This model draws on the concept of a dual continuum and clearly combines the effects of each fracture. EDFM uses a structured grid to represent the matrix and introduces additional fracture control volume by calculating the intersection of the fracture and the matrix grid. Therefore, the challenges

associated with unstructured grids are completely bypassed. In order to simplify the geometric design, Lee et al. (2000, 2001) and Li and Lee (2008) implemented the above methods only for vertical fractures. However, field characterization studies have shown that oblique fractures are very common in naturally fractured reservoirs (Walsh and Watterson, 1988; Angerer et al., 2002; Grechka and Tsuankin, 2004). Therefore, an extended EDFM method that considers realistic 3D discrete fracture media (including inclined fractures) is needed to model naturally fractured reservoirs in a robust and effective manner.

In EDFM, the changing of fracture position and geometry does not influence the discretization of the matrix because the discrete fractures are fully embedded in structured matrix grids. The fractures are discrete in unstructured grids, which means that each fracture grid connects to one single matrix grid. There are six different certain shapes when a plane (fracture) intersects into a cuboid (matrix grid). The transmissibility equations considering the shape effect were constructed by Shakiba (2014). In addition, the EDFM is easy to combine with a conventional reservoir simulator. The flow inside the matrix and fracture can be simulated separately, while the connection between fractures and matrix can be calculated with the non-neighboring connection (NNC). More details of the simulation methods and history matching methods applied in this paper will be introduced in Chapter III.

EDFM has the potential to significantly improve the simulation efficiency in the fractured reservoir history matching process. When integrating the EDFM and Ensemble methods into the fractures' position and geometry matching program. the problem needs to be transformed into a continuous, ideally gaussian distributed, field history matching problem through appropriate parameterization methods. Hough transform is introduced for this process. The details of this parameterization method will also be introduced in Chapter III.

In addition, the EDFM's performance with the coarser grids is tested and discussed in this dissertation, which is meant to further improve efficiency in the history matching process. Automatic history matching using ensemble methods is

computationally intensive. In the automatic history matching process, the numerical model may need to be run thousands of times, which proposes a higher efficiency requirement for the numerical simulator integrated into the automatic history matching program. Although the EDFM has obvious advantages to the dual-continuum model and DFM model, a model that contained numerous tiny fractures, such as the shale gas reservoir requires a high simulation accuracy to capture the sharp pressure change around the fracture which is caused by the enormous permeability contrast between the fracture and matrix. The use of dense grids to completely and clearly capture all the pressure drop around tiny fractures will still lead to a huge waste of computing resources. Thus, the trade-off between efficiency and accuracy will be discussed in this dissertation.

1.4 Research Objectives

In summary, three topics will be discussed in this dissertation: First, in the convention reservoirs, an Analysis of the performance of Ensemble Methods under a small ensemble size is conducted. A classic automatic history matching problem, the history matching of the permeability/porosity field is used as the example in this discussion. This is because the permeability or porosity field usually contains thousands of values. Meanwhile, the ensemble history matching method is updating dozens of simulation models at the same time. The statistical properties of these simulation models are used to estimate the value used to modify the permeability during the history matching process. The huge difference between the total number of permeability values and the total number of simulation models in the ensemble will cause the incorrect estimation of the modification value applied on the permeability field. A novel SVD supported localization method developed by the author will be introduced. Also, the effectiveness of Houterkamer's method in reservoir history matching is verified, which is called the generality from covariance localization to cross-covariance localization in reservoir history matching. The validation of generality will be discussed in two aspects. First, two appropriate roles of covariance localization will be introduced, then the generality can be validated by proving that the two roles of covariance localization can

be maintained in the transformation from Eq.1 to Eq. 2. In the discussion of covariance localization's two roles, the relation between the spurious correlation problem and the ill-posed problem is constructed. Then an SVD analytical solution is applied to the covariance localized EnKF updated equation to illustrate the two roles of covariance localization.

Second, the performance of Ensemble Methods with different prior information will be analyzed. The highly non-linear problem will make the proper initial fields a critical factor for a successful history matching process. The fracture position and geometry history matching is a representative case of the non-linear problem. Several numerical examples will be tested to demonstrate and discuss the ensemble method's different performance with different prior information. For the third topic, this dissertation will show the accuracy lost with coarser grid models when simulating with EDFM. then the reasons for the simulation error are analyzed and improved methods are proposed.

CHAPTER II

ANALYSIS OF PARAMETERIZATION AND LOCALIZATION WITH SINGULAR VALUE DECOMPOSITION (SVD) ANALYTICAL SOLUTION

2.1 The relationship between ill-posedness and spurious correlation

In this paper, history matching or parameter estimation in reservoir simulation is denoted as Eq. 5. The task is to find a parameter field, denoted generically by m, which, when used in the model will cause the resulting "output" g(m) of the model to match (approximately, at least) some observed data, denoted here by d.

$$g(\mathrm{m}) \cong d \tag{5}$$

Convex optimization is introduced to solve this problem by minimizing the least norm function $\mathrm{O}(\mathrm{m}) = \|d - g(m)\|$. In inverse problems, a regularization approach is used to deal with ill-posedness and over-fitting, which is based on ideas firstly advanced by Tikhonov & Arsenin and reviewed by Bell (1978). To deal with the ill-posedness, the objective functional is augmented with a regularizing functional $\|\cdot\|^2$ which can be based on a Sobolev seminorm. With a regularization functional $\|m\|$ that measures the semi-norm of model parameters, which can simply reduce the order of the problem and a weight α on the regularization functional, the objective function can be written as,

$$O(m) = \|d - g(m)\| + \alpha\|m\| \tag{6}$$

In this paper, this kind of regularized objective function is denoted as the first form regularized objective function.

A secondary form regularized functional $\|m - m_{pr}\|$ is also introduced in this paper. The term $\|m - m_{pr}\|$ incorporates additional statistical beliefs and describes the norm between updated the model parameter and prior information. The objective function with Bayesian theory can be written as (Oliver, Reynolds & Liu (2008)),

$$O(m) = -\frac{1}{2}\big(d - g(m)\big)^T (C_D)^{-1}\big(d - g(m)\big) - \frac{1}{2}\big(m - m_{pr}\big)^T (C_M)^{-1}\big(m - m_{pr}\big) \quad (7)$$

In this objective equation, m is the parameter field that needs to be modified to reduce the difference between the simulation results and field production observation. In a typical problem, the parameter field can be porosity or permeability field. The m_{pr} is the initial field, while the C_M is the variance matrix of the parameter field. Typically, the C_M is a diagonal matrix. The $g(m)$ is the simulation results with parameter field m. d is the observed production data, and C_d is the variance matrix of production data.

Given the definition of the norm in parameter space and observation space as the scalar product (Tarantola (2015)), the norm of a vector v can be calculated as $\|v\|^2 = (v, v) = v^t C^{-1} v$. For the Bayesian objective function,

$$O(m) = -\frac{1}{2}\big(d - g(m)\big)^T (C_D)^{-1}\big(d - g(m)\big) - \frac{1}{2}\big(m - m_{pr}\big)^T (C_M)^{-1}\big(m - m_{pr}\big)$$

$$= \|d - g(m)\| + \big\|m - m_{pr}\big\| \quad (8)$$

Thus, the Bayesian objective function has been described in the least norm theory with a secondary form regularized functional.

In ensemble maximum likelihood methods, spurious correlation mentioned in introduction section is a significant problem. When the ensemble size is small, the incorrect estimation of the covariance matrix is presented. The first order derivation of the original objective function,

$$\Delta \mathrm{O(m)} = \mathrm{G^T C_D^{-1}}(d - g(m)) \quad (9)$$

The second order derivation (Hessian matrix) of the original objective function,

$$\mathrm{H} = \mathrm{G^T} C_D^{-1} G \quad (10)$$

The quasi-Newton update equation for the least norm objective function without regularization,

$$m_{i+1} = m_i - \mathrm{H}^{-1}\Delta \mathrm{O}(\mathrm{m}) \tag{11}$$

$$m_{i+1} = m_i - (G^T C_D G)^{-1} G^T C_D^{-1}(g(m) - d) \tag{12}$$

The EnKF update equation can be written in the following form:

$$m_{i+1} = m_i + (\boldsymbol{C_m^{-1}} + G^T C_D G)^{-1} G^T C_D^{-1}\big(d - g(m)\big) \tag{13}$$

When undersampling causes underestimation of $\mathrm{C_m^{-1}}$ (Whitaker & Hamill, 2002), the update equation of the Kalman filter will degenerate to a Quasi-Newton update equation without regularization. In addition, its performance for ill-posed problems will be poor. Thus, in this section, the Bayesian objective function has been written in a least-norm form, and the spurious correlation problem is related to ill-posedness. An SVD analytical solution will be introduced to analyze the roles of localization methods in the next sub-section. The SVD analytical solution is originally used in parameterization to deal with ill-posedness.

2.2 The relationship between SVD parameterization and Localization

Recall the least norm objective function with the first-form regularization. The analytical solution of Eq. 6 with singular value decomposition (SVD) method can be written as,

$$m = -\sum_{i=1}^{n_{sv}} \frac{\sigma_i u_i^T d}{\sigma_i^2 + \alpha} v_i \tag{14}$$

In Eq. 14, linearize the simulator $g(m)$ to Gm, the SVD is applied to the G, then $G = \sum_{i=1}^{n} u_i \sigma_i v_i^T$. u_i is i^{th} left singular vector. v_i is i^{th}right singular vector. σ_i is i^{th} singular value. It is also easy to obtain the SVD solution for the original problem $\mathrm{O(m)} = \|d - g(m)\| = \big(d - g(m)\big)^T C_D^{-1}\big(d - g(m)\big)$ following the same procedures.

$$m = -\sum_{i=1}^{n_{sv}} \frac{\sigma_i u_i^T d}{\sigma_i^2} v_i \tag{15}$$

For a regularized objective function with a secondary-form regularization term $\|m - m_{pr}\|$ and a weight α on the regularization term, a transform can be applied to the equation, so that the SVD parameterization can be incorporated with such kind of equations. The details are shown in Appendix 2 and the SVD analytical solution can be written as,

$$\delta\widetilde{m} = -\sum_{i=1}^{n_{sv}} \frac{\sigma_i u_i^T r_0}{\sigma_i^2 + \alpha} v_i \tag{16}$$

In Eq, 16, the $O(m)$ is assumed to reach the local minimum at $m = m_{map}$. Map means maximum a posteriori. r_0 is the difference between the simulated well's production with the m_{map} and observed well's production. The SVD solution of Bayesian objective function can be written in a similar way,

$$\delta\widetilde{m} = -\sum_{i=1}^{n_{sv}} \frac{\sigma_i u_i^T r_0}{\sigma_i^2 + 1} v_i \tag{17}$$

However, instead of getting singular vector decomposition for $\mathrm{G} = \mathrm{U}\Sigma\mathrm{V}^{\mathrm{T}}$, an adjoint gradient matrix is decomposed by the SVD for Bayesian objective function. Considering the model parameters and observations of reservoir simulation history matching exist in different linear space, define the adjoint gradient matrix based on the scalar product, let G be a linear operator mapping M into D, the adjoint $\mathrm{G_D}$ of G is the linear operator mapping D into M. For any $\mathrm{d} \in \mathrm{D}, \mathrm{m} \in \mathrm{M}$

$$(G_D d, m)_M = (d, Gm)_D \tag{18a}$$

$$\mathrm{G_D} = C_D^{-\frac{1}{2}} G C_M^{\frac{1}{2}} = \mathrm{U}\Sigma\mathrm{V}^{\mathrm{T}} \tag{18b}$$

The same SVD analytical solution of the Bayesian objective function has also been derived with another method by Rodrigues (2006). However, there is no previous work that discussed the ensemble method and analyzed the roles of localization with this analytical solution.

In ensemble methods, such as EnKF, to eliminate the influence of covariance underestimation and keep the covariance matrix close to the desired "shape", the estimated covariance matrix is often modified with a localization matrix by Hadamard product (also named Schur product, it is an element-by-element product of matrix). The updated equation of covariance-localized Ensemble Kalman Filter is shown in Eq. 19, and search direction δm is shown in Eq. 20.

$$m_{i+1} = m_i + \mathrm{C_M G^T}(\mathrm{C_D^{-1}} + \mathrm{G}(\rho_\mathrm{M} \circ \mathrm{C_M})\mathrm{G^T})^{-1}(d - g(m_i)) \tag{19}$$

$$\delta m = \mathrm{G^T}(\mathrm{C_D^{-1}} + \mathrm{G}(\rho_\mathrm{M} \circ \mathrm{C_M})\mathrm{G^T})^{-1}(d - g(m)) \tag{20}$$

A typical covariance localization matrix is shown in Figure 1. If the color is bluer, the number represented by this small block is closer to 0. In the same way, if the color is yellower, the number represented by this small block is closer to 1. The area outside of the red square mainly consists of 0's or very small numbers, while the area in the red square is consist of larger numbers.

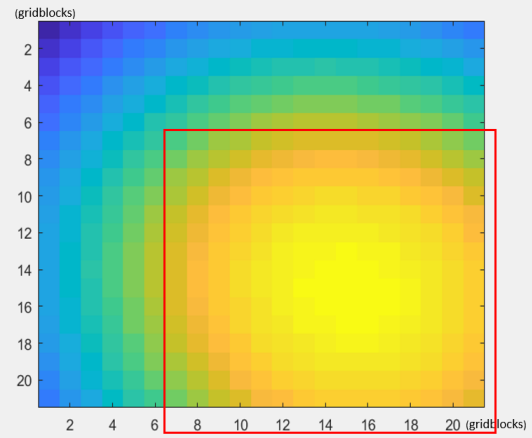

Figure 1. Localization Matrix

For the larger elements that are concentrated in a small area of the localization matrix (inside the red square in Figure 1, a Bayesian objective function with covariance localization can be denoted as,

$$\mathrm{O(m)} = \frac{1}{2}(G\delta m + r_0)^T C_D^{-1}(G\delta m + r_0) + \frac{\alpha}{2}(\sigma m)^T(\rho_M \circ \mathrm{C_M^{-1}})\sigma m \tag{21}$$

Recall the appendix 2, the SVD analytical solution can be derived and shown as,

$$\delta\widetilde{m} = -\sum_{i=1}^{n_{svd}} \frac{\sigma_i u_i^T r_0}{\sigma_i^2 + \widetilde{\rho_{M_i}}} v_i \tag{22}$$

$\widetilde{\rho_{M_i}}$ are covariance localization matrix elements in the parameterized space. $\widetilde{\rho_{M_i}}$ adjust the degree of regularization. If considering from probability theory perspective, $\widetilde{\rho_{M_i}}$ are the parameters measuring the confidence level of prior information.

Noticing the n_{svd} in the equation, the 0 elements area in localization matrix reduce the order of parameter space as truncation at n_{svd}. As the distributive law of matrix multiplication was used in the derivation of the update equation of Ensemble Kalman Filter, the dimension of all the δm in the objective function Eq. 21 should be the same and consistent with the dimension of $\rho_{M^n} \circ C_{M^n}^f$. Thus, the 0 elements and near 0 elements in the localization matrix ρ_i (outside of the red square in Figure 1) which makes the matrix sparse, actually reduce the order of $\mathrm{C_M}$ and parameter space.

Thus, in general, localization mainly plays two roles, first, non-zero elements in the localization matrix assign a weight on prior information (or be called "regularization term") to value the trust level of prior information (or to value the level of regularization), the localization matrix assigns a different weight to each element. In addition, the near zero elements in the localization matrix play a role to reduce the rank of parameter space, which is similar with the SVD truncate parameterization process.

Inversely, SVD truncate parameterization has a similar function with a localization matrix with only 0 and 1 as shown below (Eq. 23). All elements in the localization matrix which multiply truncated elements in the covariance matrix are 0, while the rest of the elements are 1. So, the method can reduce the order of parameter space and covariance matrix. It is obvious that assigning 1 to the regularization term will not fit for all possible scenarios.

$$\begin{bmatrix} 0 & 0 & \cdots & \cdots & 0 & 0 \\ 0 & 0 & \cdots & \cdots & 0 & 0 \\ 0 & 0 & 1 & \ldots & \ldots & 1 \\ 0 & 0 & 1 & \ldots & \ldots & 1 \\ 0 & 0 & 1 & \ldots & \ldots & 1 \\ 0 & 0 & 1 & \ldots & \ldots & 1 \end{bmatrix} \circ [C_M] \tag{23}$$

2.3 Generality from covariance localization to cross covariance localization and analysis of different correlation function

2.3.1 Generality in the first role

In this section, the generality from the covariance localization method to the cross-covariance localization method is studied. It is useful to analyze the construction of the cross-covariance localization matrix starting from the two roles of the covariance localization. In the following sections, the two roles of localization (parameterization and regularization) will be discussed separately. First, the parameterization function of the localization matrix will be analyzed. If Houterkamer's method is effective in reservoir history matching, the effectiveness of parameterization can be maintained in the transformation from Eq.1 to Eq. 2. In other words, the topic that needs to be proven in this section is that the same truncated distance can be used in both covariance and cross-covariance matrices.

Recall the analytical solution for δm in covariance localization, $\delta\widetilde{m} = -\sum_{i=1}^{n_{svd}} \frac{\sigma_i u_i^T r_0}{\sigma_i^2 + \widetilde{\rho_M}_i} v_i$ $\delta\widetilde{m}$ is of the same dimension as the truncated singular value matrix Σ of the adjoint gradient. If the cross-covariance matrices still have same same-size non-zero area as truncated Σ after the transformation from covariance localization to cross-covariance localization, the conclusion that can be proven is that cross-covariance localization matrix with a same truncated correlation length as the covariance matrix can have the same parameterization effect.

In the derivation process, a weaker assumption that C_D is diagonal is used to analyse the second localization matrix ρ_{DD}. This is reasonable to assume because the measurement errors in every observation point are independent. According to the

following theorem, suppose A, B is m × n matrices, and D and E are diagonal matrices of size m and n, respectively. Then,

$$\mathrm{D}(\mathrm{A} \circ \mathrm{B})\mathrm{E} = (\mathrm{DAE}) \circ \mathrm{B} = (\mathrm{DA}) \circ (\mathrm{BE}) = (\mathrm{AE}) \circ (\mathrm{DB}) = \mathrm{A} \circ (\mathrm{DBE}) \tag{24}$$

For the cross-covariance localized Kalman gain matrix,

$$K = \rho_{MD} \circ C_M G^T (C_D^{-1} + \rho_{DD} \circ G C_M G^T)^{-1}$$

$$= \rho_{MD} \circ C_M^{\frac{1}{2}} G_D^T \left(I + \rho_{DD} \circ C_D^{-\frac{1}{2}} G C_M^{\frac{1}{2}} C_M^{-\frac{T}{2}} G^T C_D^{\frac{T}{2}} \right)^{-1} C_D^{-\frac{1}{2}}$$

$$= \rho_{MD} \circ C_M^{\frac{1}{2}} G_D^T (I + \rho_{DD} \circ G_D G_D^T)^{-1} C_D^{-\frac{1}{2}} \tag{25a}$$

Recall the SVD of adjoint gradient $G_D = U \Sigma V^T$

$$\rho_{DD} \circ G_D G_D^T = \rho_{DD} \circ U \Sigma^2 U^T \tag{25b}$$

Thus, ρ_{DD} and ρ with the same same-size non-zero area as truncated Σ will have same parameterization effect. For ρ_{MD}, a stronger assumption is used in the discussion.

$$\sigma m = \rho_{MD} \circ C_M^{\frac{1}{2}} G_D^T (I + \rho_{DD} \circ G_D G_D^T)^{-1} C_D^{-\frac{1}{2}} \sigma d \tag{26a}$$

$$C_M^{-\frac{1}{2}} \sigma m = C_M^{-\frac{1}{2}} \left(\rho_{MD} \circ C_M^{\frac{1}{2}} G_D^T \right) (I + \rho_{DD} \circ G_D G_D^T)^{-1} C_D^{-\frac{1}{2}} \sigma d \tag{26b}$$

A stronger assumption is taken to analyze ρ_{MD}. Since only the size of the matrix is our current concern, an extreme scenario is considered where every element in the matrix ρ_{MD} is assumed to be the same and a new symbol ρ_{md} is used to represent this localization matrix with all the same elements. Notice that the dimension of ρ_{md} and ρ_{MD} remain the same, so it is reasonable to analyze the dimension of ρ_{md} instead of the dimension of ρ_{MD} to simplify the problem and without loss of generality. $C_M^{-\frac{1}{2}} \left(\rho_{\mathrm{md}} \circ C_M^{\frac{1}{2}} G_D^T \right) = C_M^{-\frac{1}{2}} \left(\rho C_M^{\frac{1}{2}} G_D^T \right)$, where ρ is a constant number. Since the matrix product is

linear, $C_M^{-\frac{1}{2}}\left(\rho C_M^{\frac{1}{2}} G_D^T\right) = \rho\left(C_M^{-\frac{1}{2}} C_M^{\frac{1}{2}} G_D^T\right) = \rho G_D^T = \rho' \circ G_D^T$ where ρ' is a matrix with constant number ρ and with the same dimension as G_D^T. Since $C_M^{\frac{1}{2}}$ is a square matrix, the dimension of ρ_{md}, ρ_{MD} are also the same as G_D^T. So, it is also reasonable to apply the transform, $\rho' \circ G_D^T = \rho_{md} \circ G_D^T$. Recall the SVD decomposition of G_D, $G_D^T = V\Sigma U^T$. $\rho_{md} \circ G_D^T = \rho_{md} \circ V\Sigma U^T$, Thus, ρ_{MD} and ρ with the same-size non-zero area as truncated Σ will have same parameterization effect.

2.3.2 Generality in the second role

The second role of localization, regularization, is discussed here. There are several types of correlation functions used to construct the covariance localization matrices: (1) Directly truncate the data beyond a given length (Arroyo & Datta-Gupta (2008)) (2) Gaspari and Cohn's correlation function (Eq. (4.10) in section 4.3 of Gaspari & Cohn (1999)) (3) Furrer and Bengtsson's method (Eq. 23 in Furrer & Bengtsson (2007)). Different correlation functions modify the covariance matrix in different shapes as shown in Figure 2.

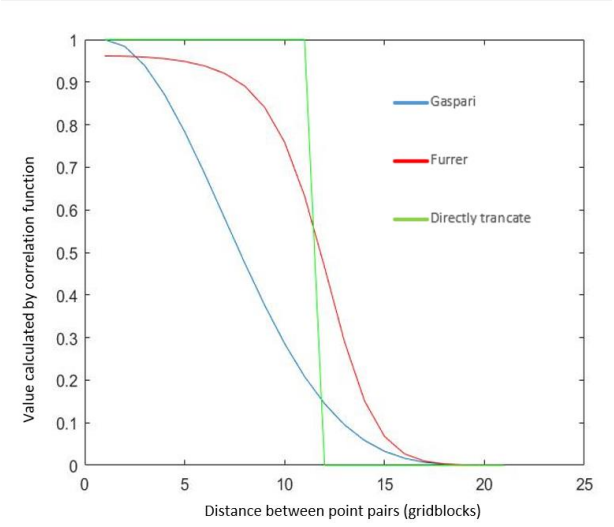

Figure 2. Comparison of different correlation functions

For covariance localization, analytically, the prior information at a local grid block should be trusted most. And the trust level should decrease as the prior

information's spatial distance increases away from a local grid block, which is measured by the covariance. For a L2 regularization term, $\frac{\alpha}{2}W^TW$, the function has a 0 mean and a $\frac{1}{\alpha}$ gaussian distribution prior information term. Thus, α should be the best reflection of the true covariance number in a L2 regularization term. In other words, for covariance localization, a covariance-shape liked matrix is preferred for the localization matrix. Because measurement error is always assumed to be white noise, both the observation field and the parameter field are assumed to be Gaussian distributions. Thus, the cross-covariance (the convolution of two Gaussian functions) is still in Gaussian distribution. Gaspari's function or a Furrer's function designed to Gaussian distribution sampling error are still preferred to evaluate the correlation between analysis points and observation points or between all pairs of observation points in cross-covariance localization. However, as Figure 2 showed, the discussion in this section is under the condition that both correlation functions and directly truncation have the same correlation length. Thus, the most important assumption for the above conclusions is the proper correlation length for correlation functions. In other words, a proper correlation length is a necessary precondition to ensure the correlation functions can perform better than direct truncation.

According to Gaspari and Cohn's work, the correlation function $\mathrm{C}_0(z,\frac{1}{2},c)$ (Eq. (4.10) in Gaspari & Cohn (1999)) for a Gaussian function $\mathrm{G}_0(z,L)=\exp\left(-\frac{z^2}{2L^2}\right)$ (Eq. (4.12) in Gaspari & Cohn (1999)) are similar when $\mathrm{L}=\mathrm{c}\sqrt{0.3}$ as the figure 6 (Figure 3) in their paper shows. Thus, when the parameter field is a random field with a Gaussian distribution, both the covariance function and the Gaspari's function are Gaussian, so the localization matrix formed with Gaspari's function is in the same shape as a covariance matrix, which is preferred.

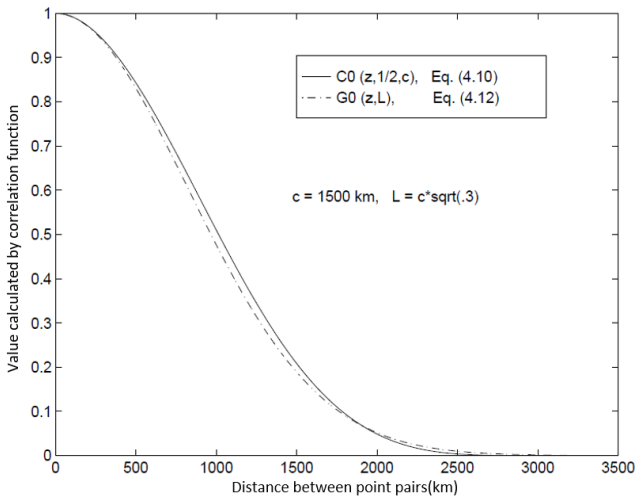

Figure 3. Comparison of Gaspari and Cohn correlation function and Gaussian function from Gaspari & Cohn (1999)

Furrer and Bengtson developed their work from a different start point, variability in the prior and posterior sample covariance matrices has been quantified by error measures. Their target was to minimize the error measures and they gave the expression a taper function with different covariance function and different ensemble size. Numerical experiments are used to test the performance of different correlation function and verify the analyses later.

2.4 SVD supported localization

An extremely challenging part of localization is the determination of the correlation length. A novel SVD support localization method developed by the author will be introduced here. The ensemble's mean model after each updating is simulated by the built-in simulator of the history matching program. Embedded in this simulator is a built-in adjoint method. The gradient matrix between the parameter and production data is obtained by solving $C_{MD}G = C_{DD}$ numerically. After applying SVD to $G_D = C_D^{-\frac{1}{2}} G C_M^{\frac{1}{2}}$, the right singular vector is mapped into a grid block map and set a proper truncate to the value of these singular vectors. This is used to obtain the area used to determine correlation length. This is labeled as the 'Flow Area'.

Instead of constructing one objective function which contains all predicted data, only the oil and water rates are set as predicted data in cost function. Then, this two-cost function is used to generate two areas from the SVD method. These two areas are combined to obtain the area which then is used to determine the correlation length. This is based on the observation that many items such as 'production rate' and 'production total' represent similar things. To eliminate the influence between the different related production terms, it is preferred to use only oil rate and water rate and construct two objective function.

Generally, the flow area should be an irregular shape, thus we are going to use an elliptical area to fit the flow area as Figure. 4 shows.

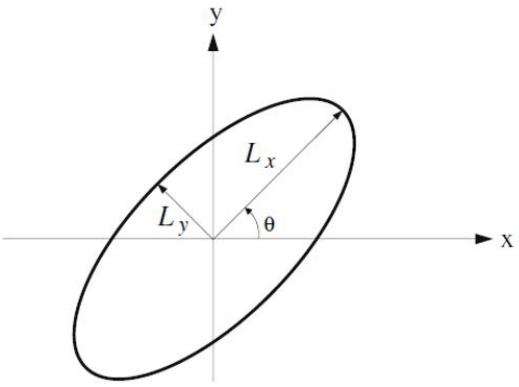

Figure 4. Elliptical area used to fit flow area

Only two parameters, L_x and L_y need to be adjusted. The Nelder-Mead method is used as the fitting algorithm. The least squares fitting equation is written as:

$$F(L_x, L_y) = \sum \left[s - e\left(\frac{\delta}{L}\right) \right]^2 \tag{27}$$

S is 1 in flow area, while it is 0 out of flow area. $\frac{\delta}{L}$ is the Euclidian distances between the target grid block and observed well, which is calculated with the following equation:

$$\frac{\delta}{L} = \sqrt{\left(\frac{\delta_{x'}}{L_x}\right)^2 + \left(\frac{\delta_{y'}}{L_y}\right)^2} \tag{28}$$

Euclidian distances are computed in the x and y directions and rotated to the main direction from prior geological information using

$$\begin{bmatrix}\delta_{x\prime}\\ \delta_{y\prime}\end{bmatrix} = \begin{bmatrix} cos\theta & sin\theta \\ -sin\theta & cos\theta\end{bmatrix}\begin{bmatrix}\delta_x\\ \delta_y\end{bmatrix} \tag{29}$$

After obtaining L_x and L_y, they are added to the correlation length from prior geological model. As explained by Emerick and Reynolds, assuming that the flow areas are somewhat related to the sensitivities, when we keep only the flow areas for localization, we are selecting a too small region, unless all model parameters are completely uncorrelated in the prior model.

Using the method of Emerick and Reynolds (2011), Equation. 27 indicates the localized updated equation of EnKF. The submatrices $\rho_{Y^nD^n}$, and $\rho_{D^nD^n}$ are computed. The following is the modified EnKF update equation:

$$y_j^{n,a} = y_j^{n,f} + \rho_{Y^nD^n} \circ C_{Y^nD^n}^f\left(C_{D_n} + \rho_{D^nD^n} \circ C_{D^nD^n}^f\right)^{-1} \times \left(d_{uc,j}^n - d_j^{n,f}\right) \tag{30}$$

As mentioned in the Appendix, the state vector of HIEnKF generally only includes uncertain model parameters

$$\mathrm{y} = [\mathrm{m^n}] \tag{31}$$

$$C_{Y^nD^n}^f = \left[C_{M^nD^n}^f\right] \tag{32}$$

$$\rho_{Y^nD^n} \circ C_{Y^nD^n}^f = \left[\rho_{M^nD^n} \circ C_{M^nD^n}^f\right] \tag{33}$$

The fifth-order compact correlation function defined by Gaspari and Cohn (1999) can be used to calculate the elements in correlation matrix $\rho_{M^nD^n}$, because every observation data value can be treated as a spatial data point located at the well position.

Chen and Oliver (2010) give the empirical equation to calculate $\rho_{D^nD^n}$ from $\rho_{M^nD^n}$, $\rho_{D^nD^n} = \rho_{M^nD^n}^{T}\rho_{M^nD^n}$

Equation 34, the correlation function presents a decline curve, which gives a ρ value of 0.21 at δ = L. We name L as correlation length and prefer to determine this length as the summation of correlated length from geological prior information and length get from SVD flow area. We apply the correlation function in one or two dimensions. In a two-dimension application, we use a elliptical area with two correlation length to represent the correlated area, In correlation equation, In Eq 34, $\frac{\delta}{L}$ gets the same definition as Eq 27.

$$\rho = -\frac{1}{4}\left(\frac{\delta}{L}\right)^5 + \frac{1}{2}\left(\frac{\delta}{L}\right)^4 + \frac{5}{8}\left(\frac{\delta}{L}\right)^3 - \frac{5}{3}\left(\frac{\delta}{L}\right)^2 + 1 \qquad 0 \le \delta \le 1 \ (34)$$

$$\rho = \frac{1}{12}\left(\frac{\delta}{L}\right)^5 - \frac{1}{2}\left(\frac{\delta}{L}\right)^4 + \frac{5}{8}\left(\frac{\delta}{L}\right)^3 + \frac{5}{3}\left(\frac{\delta}{L}\right)^2 - 5\left(\frac{\delta}{L}\right) + 4 - \frac{2}{3}\left(\frac{\delta}{L}\right)^{-1} \quad L \le \delta \le 2L \ (34)$$

$$\rho = 0 \qquad \delta > 2L \ (34)$$

2.5 Experiments and results

2.5.1 Experimental design

Based on the theoretical analysis, Houtermaker's transform from covariance localization to cross-covariance localization maintains the two roles of covariance localization, thus it is an effective and proper method for cross-covariance localization in reservoir history matching. The performances of localized EnKF methods with Houterkamer's transform and original EnKF method will be compared with two examples in this section. As discussed in the previous section, The Gaspari and Furrer's correlation function is preferred compared with direct truncation. In this section, Localized EnKF with different correlation functions will also be compared. For the method to obtain the correlation length for correlation function, two different methods will be introduced to make the experimental results more persuasive.

A popular method is to use streamlines to determine the correlation length for the correlation function for localization methods. This has been introduced by many authors with different correlation functions. Emerick and Reynolds (2011) introduced the streamline supported localization method with Gaspari's function. Arroyo, Devegowda, and Datta-Gupta (2008) introduced streamline assisted localization with direct truncation. The procedure of streamline supported localization is similar to the SVD supported localization. The correlation length of a specific producer is obtained from the area passed by streamlines linked between the producer and its neighbor injectors.

Localization plays two roles, including the parameterization to reduce the model's order. Thus, it is reasonable to use the SVD parameterization method to determine the correlation length. A new SVD supported localization method has been constructed by Jiang and Gorell (2018). In this localization method, a sensitivity map is generated by the SVD method, which is used to determine the correlation lengths for correlation functions. Both streamlines supported localization methods and SVD supported localization methods will be used in this section. In addition, if the SVD supported localization can have a similar or better performance than the streamline supported simulation, the result can also support the conclusions in this paper.

In this paper, we prefer to use a correlation length $L = \sqrt{.3}l$ in the correlation function or correlation function, in which l is the length obtained from SVD or streamline analysis via the ellipse matching method introduced in Jiang and Gorell (2018). This transform is implemented in all the localization methods with Gaspari and Cohn's function or Furrer and Bengtsson's function, which need a correlation length in the calculation. In this paper, both SVD and streamlines supported localizations are combined with different correlation functions is tested:

(1) SVD supported localization with Gaspari's function
(2) SVD supported localization with Furrer's function
(3) Streamline supported localization with Gaspari's function

(4) Streamline supported localization with Furrer's function

(5) Streamline supported localization with direct truncation

This section describes results of two different models. Before the history matching, models were created. These models are fictitious but are based on a reasonable set of parameters to mimic a single layer within a conventional reservoir. The models used specified prior information. The mean of permeability and porosity field in these models were set as uniform or with the permeability in the wells obtained from log and core. The permeability and porosity field were generated from geostatic methods, such as kriging and sequential Gaussian simulation (SGS). Further details about each model is given below in the example discussions. Matlab Reservoir Simulation Toolbox (MRST) is used as the basic simulator, and a self-made history matching module is applied to MRST.

2.5.2 The Criteria for Comparing Models

Measurement of the ill-posedness in an ensemble is a big challenge in experimental design. Based on the relationship between probability theory and statistics, the first measurement used in this paper is a misfit that measures the misfit between the mean of ensemble parameters and the real number. The following two steps are used to prove the appropriateness of this measurement:

- First, in Oliver & Reynolds (2008), it has been proved that the maximum likelihood answer in an ensemble method is equivalent to the local minimum that gradient method converges to. Ill-posedness makes the gradient method converge to a different answer compared with a real scenario. This can be described as the maximum likelihood answer deviated from real number.
- Second, when the ensemble size is sufficient, the likelihood distribution of the parameter can be reflected as the statical properties of a realizations' ensemble (Law of large numbers). The mean of the ensemble should be the maximum likelihood answer (highest probability point in a distribution). Thus, ill-posedness

will make the mean of ensemble parameters deviate from the real number. The same conclusion fits for ensemble forecasted production and conservation data.

However, if the assumption of sufficient ensemble size cannot be achieved then the mean of the ensemble does not reflect the maximum likelihood answer. We also consider the concept of Exchangeability, which is a weaker measurement to evaluate the quality of the ensemble. The concept of Exchangeability is designed to measure the compatibility of observation and ensemble forecasting based on the view from V. Fortin's paper (2014): when presented with a set of model forecasts and a set of verifying observations, an expert should not be able to distinguish the forecasts from the observations, given no other information. The real situation should be shown as a member in the history matching result ensemble, no matter it is "the most possible answer" (the mean of the ensemble) or an "extreme event" (at the tail of ensemble distribution). In this paper, the spread is also introduced to measure the variability of ensemble results. The ratio of misfit and spread is also calculated. It is a key point that this ratio is used to measure the Exchangeability and an ensemble smoother's reliability.

In summary, misfit, spread, and ratio are defined as follows. Assume $\mathrm{D} = \{\mathrm{d_t}, \mathrm{t} = 1, \dots, \mathrm{T}\}$ is a set of observation at different time t. an ensemble of forecasting from history matching program at time t is written as $\mathrm{G_t} = \{\mathrm{g(m)_{t,r}}, \mathrm{r} = 1, \dots, \mathrm{R}\}$,

$$\text{misfit} = \frac{1}{\mathrm{T}}\Sigma(\overline{G_t} - d_t)^2 \tag{35}$$

$$\mathrm{s} = \frac{1}{\mathrm{T}}\sum_{i=1}^{T}\frac{1}{R-1}\sum_{i=1}^{R}\left(\overline{G_t} - g(m)_{i,t}\right)^2 \tag{36}$$

$$\text{ratio} = \frac{\mathrm{s}}{\text{misfit}} \tag{37}$$

2.5.3 Example 1

A five-spot model (Figure. 5) with the relatively small ensemble is tested. The details of the example 2D reservoir model is described as follows. It is a 21 × 21 uniform size grid model with grid blocks' log-permeability as the history matching parameter.

The total length of the model is 1000m. And the rock saturation is set as uniform in the whole model, both initial water saturation and residual oil saturation are set at 0.2. Only two-phase flow is considered in the model. The viscosities of water and oil are set at 0.4 and 0.9, while the densities of water and oil are set at $1.014\mathrm{g/cm^3}$ and $0.859\mathrm{g/cm^3}$. All the fluids are set as incompressible. Relative permeability is calculated by an exponential function of saturation, $\mathrm{K_{or}} = S_0^4$, $\mathrm{K_{wr}} = S_w^4$. A random field was generated by a sequential Gaussian simulation with major a correlation length of the width of 28 grid blocks and minor correlation length of the width of 5 grid blocks oriented at 45°. The true permeability field (K) is generated by the random field R (Eq. 38). For the field R, the prior mean of all grid blocks and all realization is 1, and the prior variance is 1.0.

$$\mathrm{K} = 10 * \mathrm{e^R} \tag{38}$$

The permeability field shows a high heterogeneity as Figure. 5. The production will be very sensitive to the high permeable area. Thus, the spurious correlation will cause a severe problem if the high permeable area is updated incorrectly. Due to the high heterogeneity and the log-normal distribution, the log-permeability field is used to show the results. Porosities are simply calculated as a function of permeability (K), $\phi = 0.25 * \left(\frac{\mathrm{K}}{200}\right)^{0.1}$. In the simulation, the well's location follows the five-well pattern as shown in Figure. 5. all the producers are controlled by constant bottom hole pressure, 300 bars, while the injection well controls by injection rate of $150\ \mathrm{m^3}/d$. The observed data are oil and water production rates, water injection rates, water cut and bottom hole pressure. The simulation time step is 0.5 years, and the observation time interval is 2.5 years. The history matching time is 20 years with an updated interval at 5 years. After the history match, all models are simulated 10 more years and the results are plotted in the same plot with history matching results to indicate the predictability of the ensemble.

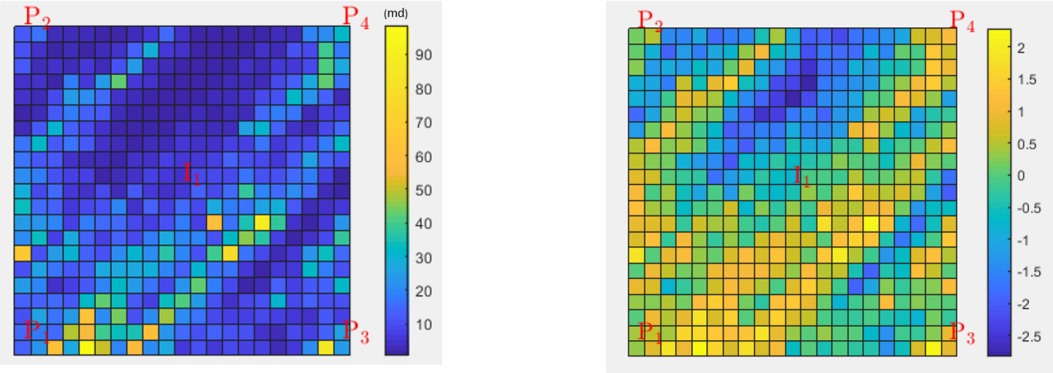

Figure 5. Example 1, Reference permeability (left) and log-permeability (right) field.

Using the original EnKF method, an ensemble of 10 models is not sufficient for this 441-parameter reservoir model. Figure. 6 and 7 show the history matching results from original EnKF. The red line shows the observation while the blue line represents the mean from the ensemble. Every grey line represents the result from one realization. The relatively small ensemble size causes underestimation of cross-covariance. Due to the conclusion in Section 2, it will reduce Bayesian term's ability to deal with ill-posedness.

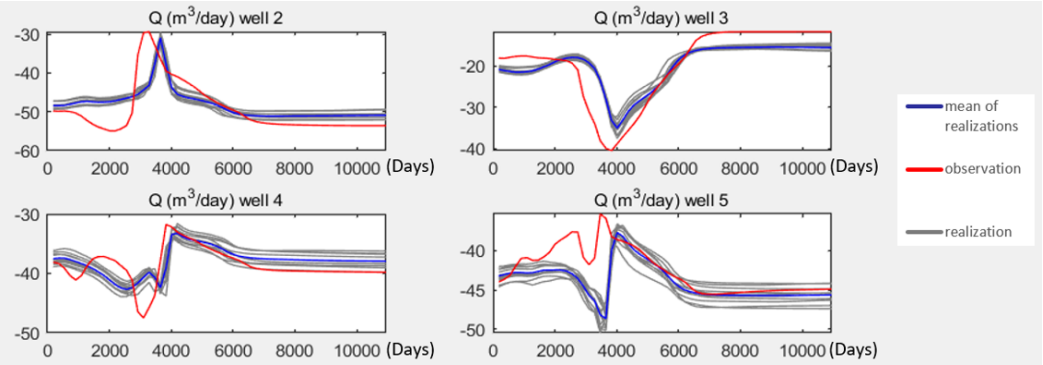

Figure 6. Example 1, Production rate history matching result from EnKF without localization

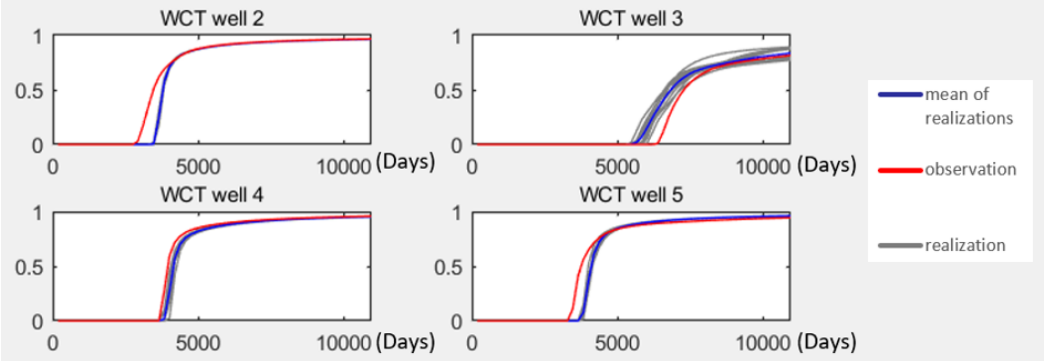

Figure 7. Example 1, water cut history matching result from EnKF without localization.

As shown in Fig 7, both the SVD method and streamline method are applied to obtain the correlation length. The flow areas used to determine the correlation length for producer 1 are shown in Figure 8. In the left plot of Figure. 8, yellow cells represent the cell's SVD value over the truncation. In the middle plot, the yellow area shows the area passed by the streamlines that connects the injector and producer 1. The streamlines map used to generate the middle plot is shown at the right plot. The same method as that introduced with the SVD supported localization is used to calculate the correlation length from the flow area, and the summary results are shown in Table 1. There is a difference between results from SVD and streamline.

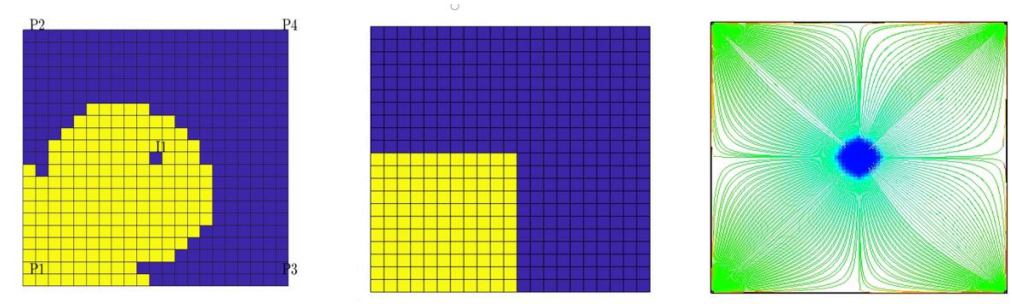

The flow area from SVD

The flow area from streamlines

The Streamlines map used to generate flow area

Figure 8. Example 1, the flow area maps for producer 1 and streamline map

Table 1. Example 1, Correlation length for each well

Well name	Correlation length from SVD	Correlation length from streamline
P1	18, 8	14, 9
P2	8, 18	9, 14
P3	8, 18	9, 14
P4	18, 8	14, 9

Figure . 9, 10, and 11 show the history matching results from different history matching methods. As Figure 9 shows, all methods did not show obvious differences in the log-permeability field matching results. However, the original EnKF method gets a poor match at production data (Figure 10 & 11). Because of the high heterogeneity, small differences in the log-permeability field can cause large differences in permeability field and even larger differences in production data. All localized methods give more reasonable results for the flow rate in producer 4 and water cut in producer 2. These producers were chosen to illustrate the effectiveness of the various methods because they had the poorest fit with the original EnKF method. Similar improvements have also been observed in other producers' production data matching results.

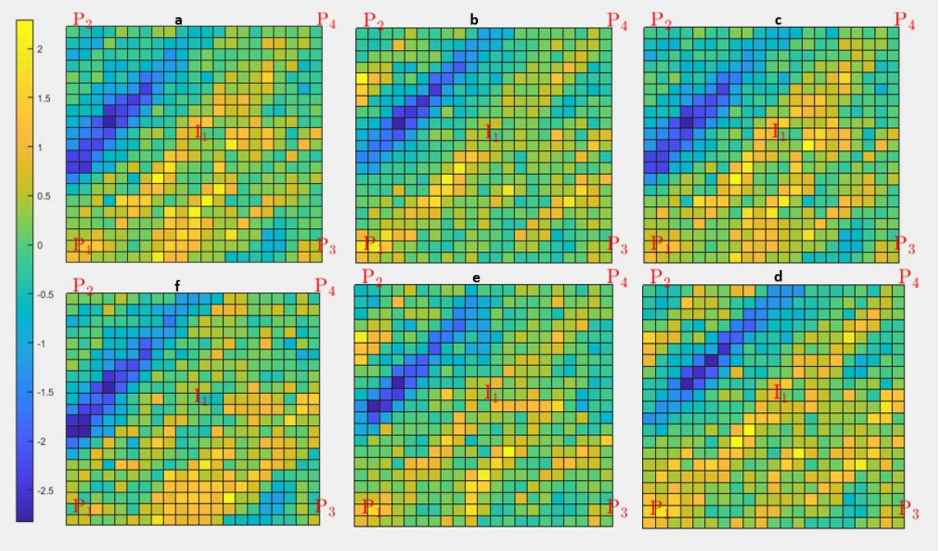

Figure 9. Example 1, Comparison of log-permeability field history matching results from different history matching methods.

First row: (a)Streamline supported localization with Gaspari's function; (b)Streamline supported localization with Furrer's function; (c)SVD supported localization with Gaspari's function.

Second row: (d)SVD supported localization with Furrer's function; (e)Streamline supported localization with direct truncation; (f)Original EnKF;

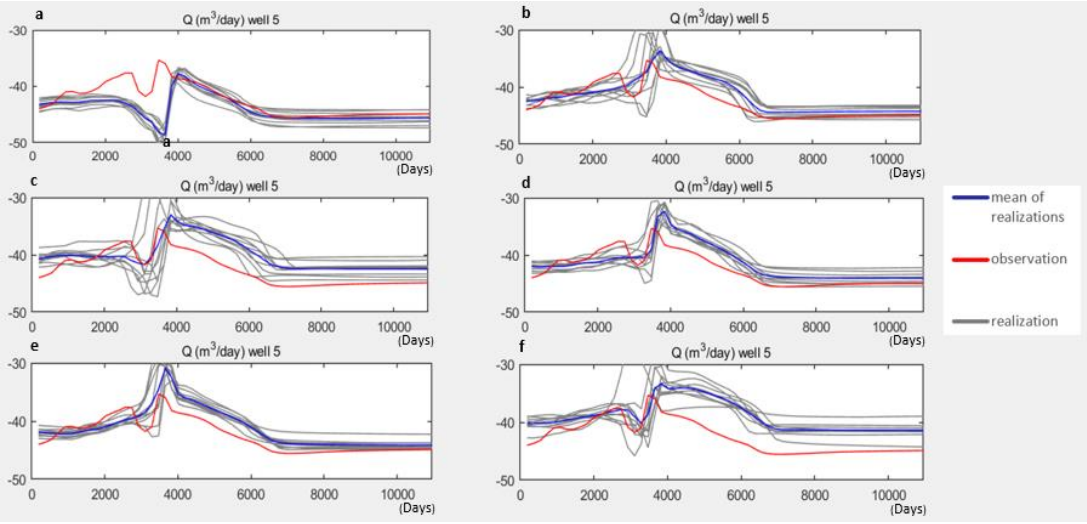

Figure 10. Example 1, Comparison of production rate history matching results from different history matching methods for Producer 4

First row: (a)Original EnKF; (b)Streamline supported localization with direct truncation.

Second row: (c)Streamline supported localization with Furrer's function; (d)Streamline supported localization with Gaspari's function.

Third row: (e)SVD supported localization with Gaspari's function; (f)SVD supported localization with Furrer's function.

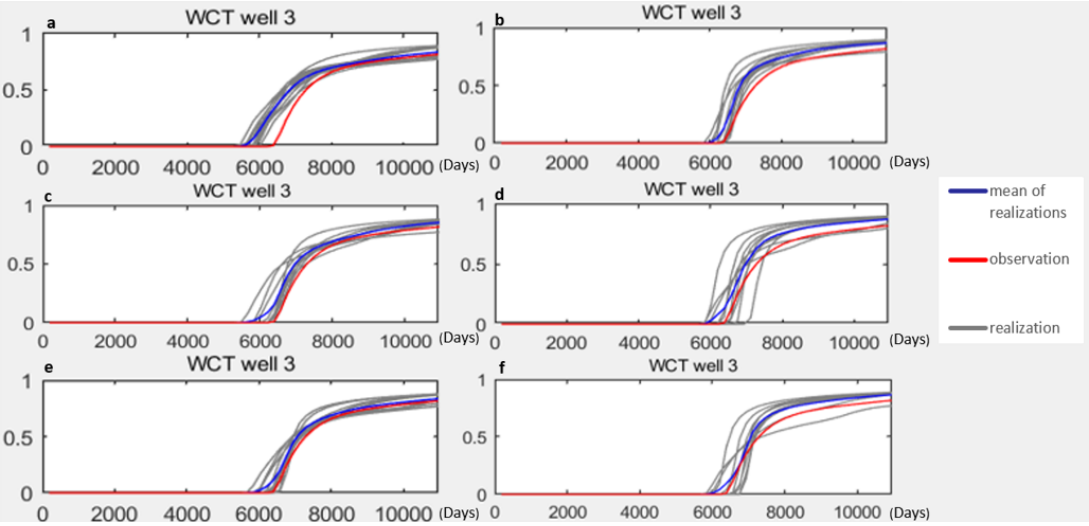

Figure 11. Example 1, Comparison of water cut history matching results from different history matching methods for Producer

Frst row: (a)Original EnKF; (b)Streamline supported localization with direct truncation.

Second row: (c)Streamline supported localization with Gaspari's function; (d)Streamline supported localization with Furrer's function.

Third row: (e)SVD supported localization with Gaspari's function; (f)SVD supported localization with Furrer's function.

Table 2 shows both data's misfit and spread. All the localized methods show significant improvement over the original EnKF, which supports our theoretical analysis conclusion. In this specific model, the streamline direct truncation shows better performance than streamline supported Gaspari's function in results misfit, which is not

expected in theoretical analysis. For the reason of these unexpected results, it can be attributed to correlation. It can be noticed that SVD supported Gaspari's function performs better than directly truncation in misfit, which means the streamline determined correlation length may not be the most suitable correlation length for Gaspari's function. More numerical experiments need to be conducted to research this problem in the future. The streamline directly truncation loses in comparison with Furrer's correlation function as the conclusion in the theoretical section. No matter the correlation lengths are determined by streamline or SVD, Furrer's function performs better than Gaspari's function in this example. Furthermore, SVD supported localization performs better than streamline-supported localization in misfit, which also supports the conclusion in previous sections. For the computational cost, the program was run on a computer with Intel Xeon E3-1285 CPU and 32G memory. The original EnKF cost 32.8s in these cases, while the SVD supported localized EnKF takes around 28s, and streamline supported localized EnKF takes around 26s. different correlation functions do not make big differences in computational cost.

Table 2. Example 1, misfit and spread of different history matching methods

	misfiit	spread	ratio
Original	0.0317	0.0023	0.0726
SVD with Gaspari & Cohn	0.0146	0.0033	0.2260
SVD with Furrer	0.0111	0.0097	0.8739
Streamline with Gaspari & Cohn	0.0193	0.0039	0.2021
Streamline with Furrer	0.0139	0.0134	0.9640
Streamline with directly truncation	0.0172	0.0076	0.4419

2.5.4 Example 2

Although, a five-spot model is reasonable to test the performance of different correlation functions. It is not sufficient to make definitive conclusions on the

comparison of these correlation functions. Therefore, a more complex model (Figure 12) with 10 realizations was tested. The details of this model are as follows. It is a 41 × 41 uniform size grid models with gridlock log-permeability as the history matching parameter, whose total length is still 1000m. The rock saturation, fluid properties are the same as Example 1. The true permeability field was still generated by a sequential Gaussian simulated random field with a major correlation length of the width of 56 grid blocks and minor correlation length of the width of 10 grid blocks oriented at 45°. The function from random field R to permeability field (K) is Eq. 39. The prior mean of R of all realization is 1, and the prior variance of R is 1.0

$$\mathrm{K} = 0.1 * \left(1 + \frac{\mathrm{R} - \mathrm{R}_{\min}}{\mathrm{R}_{\max} - \mathrm{R}_{min}} * 1000\right) \tag{39}$$

Porosity (ϕ) is still set as a function of permeability, $\phi = 0.25 * \left(\frac{\mathrm{K}}{200}\right)^{0.1}$. Compared with the exponential function, which was used in Example 1, the permeability field is more homogeneous with this function (Figure 12). However, there is a significant highly permeable channel in the reference permeability field. It is easier for us to value the different methods' performance on the permeability field with this high permeable channel. There are 6 producers and 1 injector, all the wells open at the beginning of the simulation. The well positions are also shown in Figure 12. In the simulation, all the producers are controlled by constant bottom hole pressure, 300 barsa, while the injection well controls by injection rate at $150\ \mathrm{m}^3/d$. The observed data are oil and water production rates, water injection rates, water cut and bottom hole pressure. The simulation time step is 0.25 years, and the observation time interval is 0.5 years. The history matching time is 4 years with an updated interval at 0.5 years. After the history match, all models are simulated 1 more year.

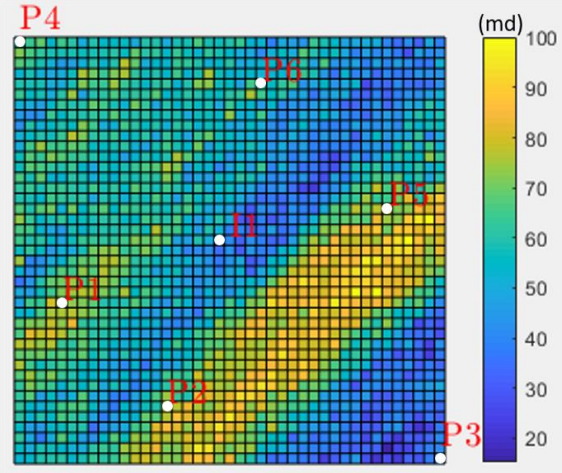

Figure 12. Example 2, Reference permeability field

The same problem of cross-covariance poor estimation is caused by the relatively small ensemble as the example 1. Both the SVD method and streamline method are applied to obtain the correlation length. The correlation length of each producer is shown in Table 4. There is still a difference that can be observed between results from SVD and streamline. The resulting history matching permeability fields are shown in Figure 13. The localized EnKF methods give a better match of the highly permeable channel than original EnKF, which support the theoretical analysis. Both Gaspari's and Furrer's function shows more obvious channel than directly truncation. SVD methods show a more obvious high permeable channel than streamline methods. These observations also support the theoretical sections.

Table 3. Example 2, Correlation length for each well

Well name	Correlation length from SVD	Correlation length from streamline
P1	21, 9	14, 8
P2	21, 9	14, 8
P3	25, 14	9, 22
P4	13, 33	9, 22
P5	17, 8	13, 9
P6	17, 8	13, 9

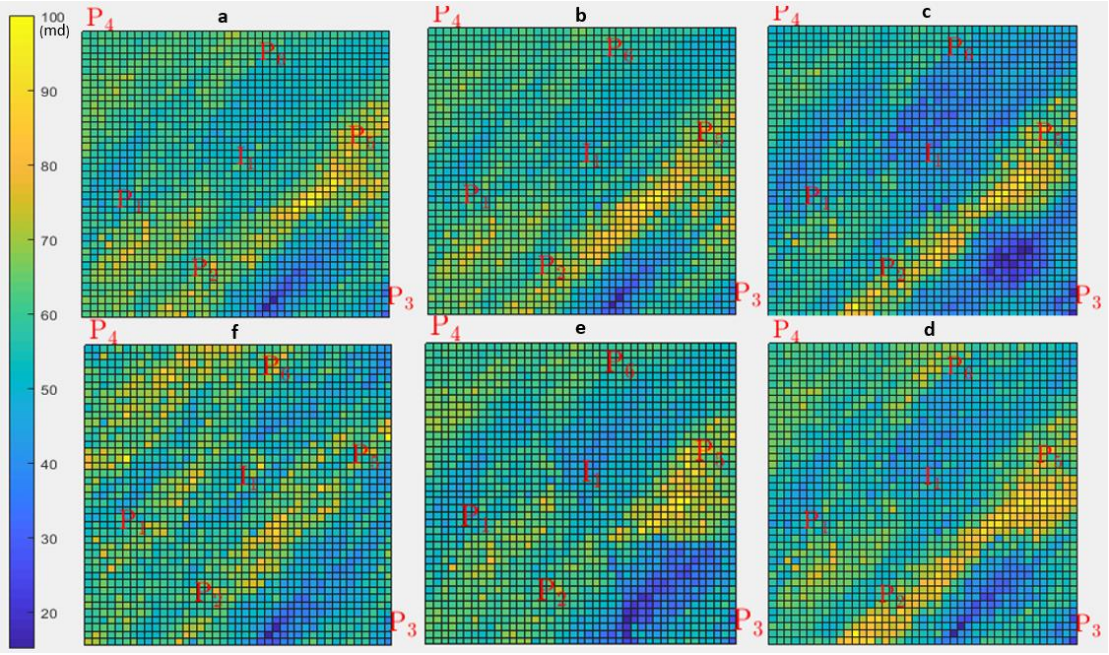

Figure 13. Example 2, Comparison of log-permeability field history matching results from different history matching methods.

First row: (a)Streamline supported localization with Gaspari's function;(b) Streamline supported localization with Furrer's function; (c)SVD supported localization with Gaspari's function.

Second row (from left to right): (d)SVD supported localization with Furrer's function; (e)Streamline supported localization with direct truncation; (f)Original EnKF.

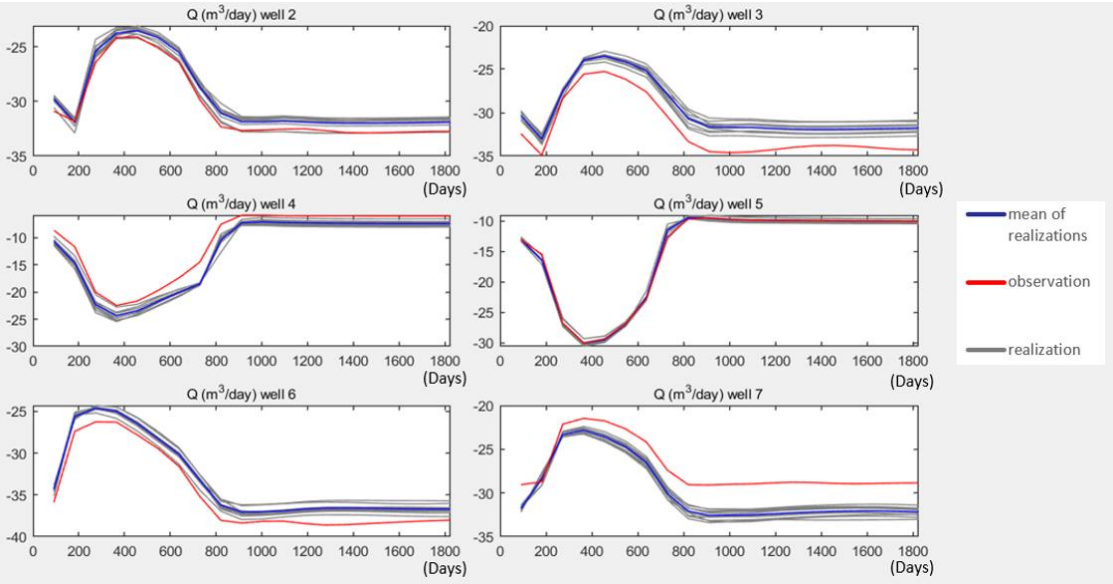

Figure 14. Example 2, Production rate history matching result from EnKF without localization

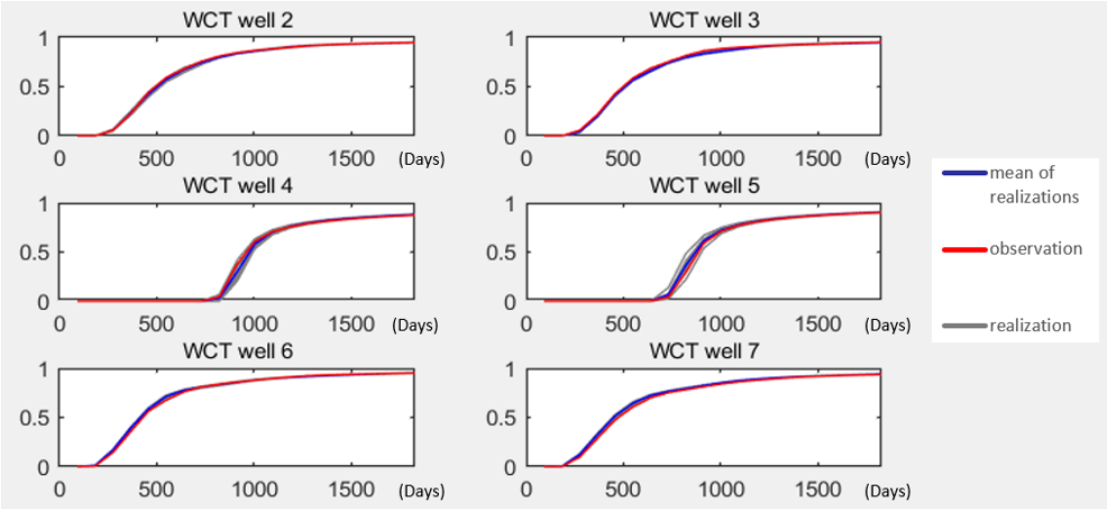

Figure 15. Example 2, water cut history matching result from EnKF without localization

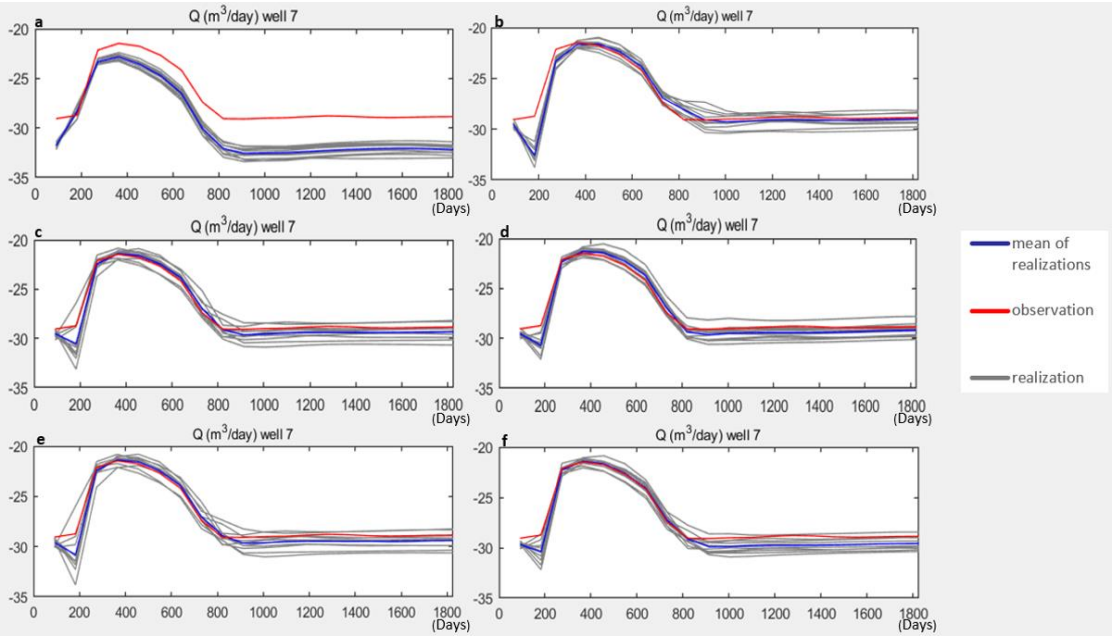

Figure 16. Example 2, Comparison of prduction rate history matching results from different history matching methods for Producer 6

First row: (a)Original EnKF; (b)Streamline supported localization with direct truncation.

Second row: (c)Streamline supported localization with Gaspari's function; (d)Streamline supported localization with Furrer's function.

Third row: (e)SVD supported localization with Gaspari's function; (f)SVD supported localization with Furrer's function.

Figures 14 & 15 show the production history matching result from different history matching methods compared with the original EnKF. In example 2's more homogeneous model, original EnKF's production data match is better than that in example 1. Only producer 6's the total production matching result from different methods are picked to show the match quality (Figure 16), because the water cut matching quality from original EnKF is acceptable. All localized methods give more reasonable results for the flow rate in producer 6 to support this paper's conclusion. The same improvements have also been observed in the other producers' total production rate history matching results.

Because the ensemble size is the same as Example 1, the ideal misfit and spread ratio of this example should be 0.91 as the same. From Table 5, for both data misfit and results reliability, all the localized methods show improvement over the original EnKF in this example. Both Gaspari's and Furrer's function perform better in misfit than directly truncation. The Furrer's function perform similar with directly truncation in results' reliability while the Gaspari's function perform better. All these results verify the conclusion in previous analysis. It should be noticed that Gaspari's function does not only perform better than the directly truncation but also perform better than the Furrer's function, which is different from the last example. Thus, the performances of different correlation methods are highly depended on specific models. Localization with SVD still performs better than localization with streamline with respect to the misfit and reliability. The results again support the theoretical analysis.

Table 4. Example 2, misfit and spread of different history matching methods

	misfit	spread	ratio
Original	0.0025	0.0009	0.36
SVD with Gaspari & Cohn	0.0012	0.0017	0.706
SVD with Furrer	0.0013	0.0030	0.433
Streamline with Gaspari & Cohn	0.0018	0.0029	0.62
Streamline with Furrer	0.0018	0.0045	0.4
Streamline with directly truncation	0.0031	0.0097	0.42

2.6 Conclusion

Based on the theoretical analysis, the spurious correlation problem in EnKF is related to ill-posedness. The two roles of localization have been clearly identified. The covariance and cross-covariance localization play roles of both parameterization and regularization. Houtermaker's method used to construct the cross-covariance localization matrix is an effective and proper improvement method for the spurious correlation problem in reservoir history matching. The covariance localization matrix and cross-covariance matrix can offer similar effects with the same correlation length.

Based on the numerical experiment results, localized EnKF with Houterkamer's method performs better than the original EnKF in two examples. The theoretical analysis has been verified. Also, both Gaspari and Cohn's function and Furrer and Bengtsson's function are preferred in cross-covariance localization. They perform better than direct truncation in most comparisons. However, direct truncation can still perform better or similar with the other two correlation functions sometimes. it is still difficult to determine whether one of these correlation functions is consistently better. More numerical experiments need to be conducted for the comparison of the different correlation functions in future research.

In addition, the author proposed SVD supported localization method demonstrates its effectiveness in the experimental examples and supported the conclusion in this paper.

CHAPTER III

THE IMPORTANCE OF PRIOR INFORMATION ON THE FRACTURE GEOMETRY INVERSION WITH ENSEMBLE METHODS

3.1 Methods

In this paper, self-developed EDFM module was coded and applied into the MATLAB Reservoir Simulation Toolbox (MRST), which was used as the reservoir simulator. The EDFM uses structured grids to represent the matrix and explicitly incorporates the fracture with unstructured elements in the matrix. Comparing to the traditional simulator, EDFM builds three additional flow connection between the fractures and matrix with non-neighboring connections. In our model, the transmissibility of these three NNC are calculated with the equation proposed by Shakiba (2014) to measure the mass transportation in the computational domain:

1. Flow between a fracture segment and a grid block
2. Flow between Two fracture planes in One grid block
3. Flow between Two fracture segments in two grid blocks

In our research, a self-coded EnKF module is developed upon the EDFM simulator. The ensemble method has been researched and applied to tweaking the continuous fields for a long time. Permeability and porosity field history matching is a representative ensemble method's application in reservoir engineering. The objective function used in the ensemble method is shown below. This function is based on the Bayesian theory:

$$O(m) = \frac{1}{2}\left(m - m_{pr}\right)^T C_M^{-1}\left(m - m_{pr}\right) + \frac{1}{2}(g(m) - d)^T C_D^{-1}(g(m) - d) \quad (40)$$

In the objective equation, m is the parameter field that needs to be modified to reduce the difference between the simulation results and field production observation. In a typical problem, the parameter field can be porosity or permeability field. The m_{pr} is the initial field, while the C_M is the variance matrix of the parameter field. Typically,

the C_M is a diagonal matrix. The $g(m)$ is the simulation results with parameter field m. d is the observed production data, and C_d is the variance matrix of production data.

The ensemble methods reduce the objective function iteratively by modifying the parameter filed m with the incremental which defined as below:

$$\delta m = m_{l+1} - m_l \tag{41}$$

The incremental can be calculated with an equation involving the gradient G between the simulation results $g(m)$ and parameter field m, and also involving the differences between the observed production data d and the simulation result $g(m)$. Calculating the gradient directly will be extremely expensive due to the parameter field's scale (permeability etc.). In the ensemble methods, an ensemble of the geological models that follows the same geostatistical properties is updated at the same time. In EnKF, the gradient calculation is avoided, and the gradient term is combined into two covariance terms C_{MD} and C_{DD}. The C_{MD} and C_{DD} can be obtained based on the statistic properties of the ensemble after every update. The incremental calculation equation of EnKF is shown below:

$$\delta m = C_{MD}(\mathrm{C_D^{-1}} + \mathrm{C_{DD}})^{-1}(d - g(m_l)) \tag{41}$$

So, if the fractures' position and geometry problem can be transferred into a continuous-field history matching problem similar to the permeability history matching, it means the ensemble methods can be applied to the fracture geometry and position problems. Following Lu & Zhang's work (2015), Hough transformation is introduced as a parameterization method to achieve this target. A 2D example is used to illustrate the Hough transformation applied in our research.

Hough transformation can map the existence possibility of any line in a Cartesian coordinate field into an angular coordinate field. In Figure 17, the green line can be located by two parameters, angle (θ), and distance (ρ) from the line to the coordinate origin. In Figure 18, the X-axis is the angle, and the y-axis is the distance, Thus, each cell in this plot represents a line in the upper plot. The color in each cell

represents the probability of the line's existence, Blue is 0, which means this line does not exist in Figure 17. Yellow is 1, which means this line exists in the upper plot, such as the green line corresponds to a yellow point which is shown as the cell in the red square in Figure 18.

However, if the Hough field only contains 0 and 1, it is still not a desired "continuous field" in the ensemble history matching program. In practice, a smooth transition needs to be added between the yellow and blue as shown in Figure 18. The yellow cell in the red square is also not exactly 1, it is a local maximum in the entire field. This transition is actually more reasonable in physics. It reflects the uncertainty in the history matching process. It means The line most likely exists at the cell in the red square, but also possible to exist at the cells around the red squared cell. These cells represent lines that have very close orientation and position as the line represented by the red square cell. The probability number is named “Hough Value”. When coming with L(Length) and D(displacement), this method can measure the existence of line segments, as the red one. With the Hough transformation, the parameter field m in the Eq. 40 is:

$$m = \begin{bmatrix} H \\ D \\ L \end{bmatrix} \tag{42}$$

The results for 2D fracture representation can be easily extended to 3D by using two-line segments and resulting in a parallelogram. The detailed introduction of Hough-transform can be found in Hough (1962) and Duda and Hart (1971).

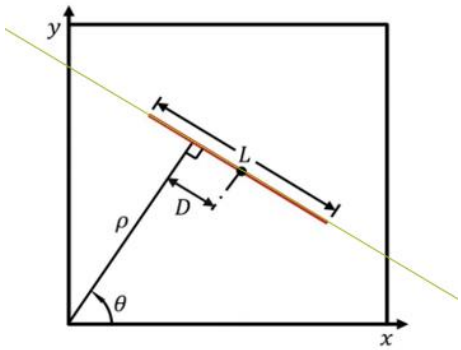

Figure 17. Fracture in Cartesian coordinates

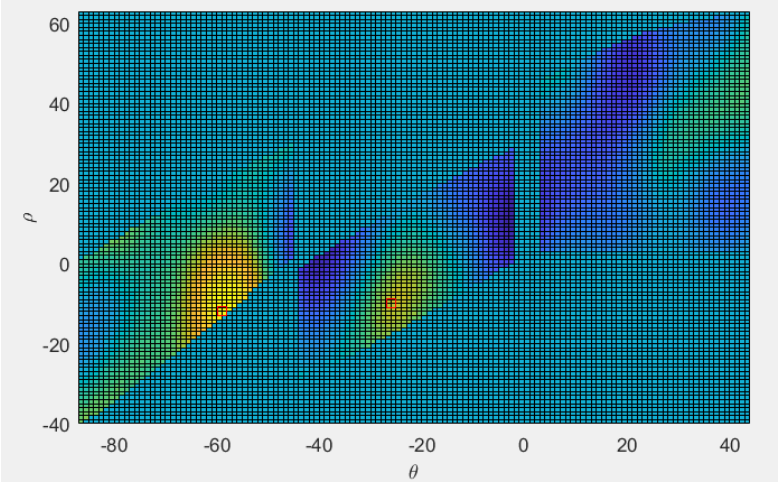

Figure 18. Hough field with local maximums

After every history matching iteration, when a Hough value local maximum is also over the truncation, in the history matching process, a fracture's Cartesian coordinate position can be calculated by that point's angle coordinates ρ and θ, the correlated fracture length L and displacement D value of that point. The fracture's Cartesian coordinates are used to build the reservoir simulation model. The Sequential-Gaussian simulation can easily control the number of local maximums into a proper number in the initial fields. And when checking the history matching results, truncated local maximums in the Hough fields' mean map are treated as the fractures in the final history matched model.

In the ensemble methods, the prior information is included in the initial fields. Which is the parameter fields before the first updating. In each individual example, the prior information combined into the initial field is different. Thus, the methods to generate the initial fields will be introduced separately with each example in the next section.

3.2 Numerical Experiments

Three representative simulation models were tested in this dissertation. In each model, three different types of initial fields are applied. Since the generation method of the initial fields is slightly different due to the specific fractures' geometry various in every single case. The details of the initial-field generation methods will be introduced

in every case's sub-section. The history matching results with different initial fields are compared and discussed in this section.

An automatic history matching program with the algorithm introduced in the second section is used to obtain the geometry information of fractures, such as the number, position, and length of fractures. In all the example models, the fracture permeability is set as 1000D, Fracture aperture is set to 0.04 meters, and the fracture porosity is set as 0.8. Thus, the fractures are almost infinite conductive. The matrix rock properties and fluid properties in the model are also set to known and homogenous. Reference models are used to generate the "production data" used in automatically history matching process. So, the history matching results can be verified by comparing them to the reference model.

3.2.1 Example 1

The first case is a high permeability case, in which, the matrix permeability is 100md. And the matrix porosity is set as 0.26. The model scale is 450m×450m. The entire model is discretized into 45×45 grid-blocks. This case contains both injectors and producers. This is because we want to design the first case as the simplest one. When we use the production data to obtain the fracture geometry inversely, the injection well can provide extra data as the water rate. For the same reason, the factures' geometry is very simple in this case. There are two crossed fractures crossed at the center of the model. The fracture distribution and well positions are shown in Figure 19 which is a saturation map after 4 years simulation. Well 1 is an injector, while Well 2,3, and 4 are producers. The producers are produced at a constant bottom hole pressure (30 bar), The injector is set at a constant rate (150m^3/day). Assume there is only a two-phase flow (Oil and Water) in the model. The simulation time is 4 years. The updating interval of the history matching program is one year. Total production rate, water cut, and injection bottom hole pressure were used as the observed data in the history matching process.

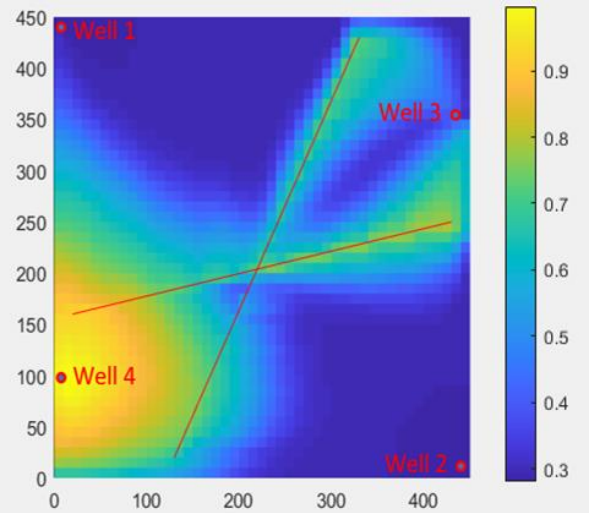

Figure 19. Saturation map of Example 1 reference model after 4 years simulation

In this example, to show the performance improvement of the history matching with prior information, the Type 1 initial fields are without prior information, while the Type 2 and 3 initial fields are with different types of prior information. The EnKF history matching program ran with all three types of initial fields, in order to compare the quality of history matching results. the details of generating all three types of initial fields will be introduced in the following.

Type 1:

The ensemble methods need ensembles of the initial Hough value fields, initial length fields, and initial displacement fields. Every single realization needs its own initial Hough value field, own length field, and displacement field. So, for the cases without prior information, the initial Length (L) fields ensemble and Displacement (D) fields ensemble is constructed by totally random numbers. Initial Hough value fields ensemble is generated by a Sequential-Gaussian simulation process with Mean 1 and Variance 1. The mean of the initial Hough value fields ensemble is shown in Figure 20. The cells with high probability in the Hough map indicate the existence of a corresponded lines. And there are no significant high probability spots in the mean map, which means the existence probability of every cell's corresponded line is almost equal.

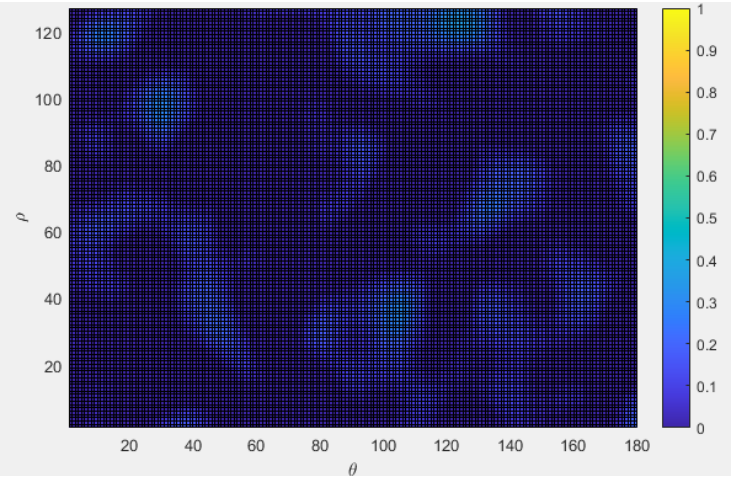

Figure 20. Mean map of initial Hough value fields in Type 1 initial fields.

Type 2:

A particularly important feature in the reference model is that the two fractures intersect at the center of the map. Therefore, in Type 2 initial fields, this information is selected as the prior information and is assigned in the initial Hough fields. The type 2 initial fields still need to be the ensembles, the Hough value fields ensemble is generated by the following steps: (1) an ensemble of fracture maps is generated (Figure 21). All these maps contain two fractures crossed at the center of the model; however, the fractures' length and orientation are random in these maps. (2) the fracture maps are converted to Hough map, length map, and displacement map. (3) The Gaussian filter is applied on the Hough field ensemble. Following these steps, the following prior information is added to the history matching process: (1) there are two fractures in the model. (2) the two fractures must pass the center of the model. The Figure. 22 is a Hough value plot converted from one of the fracture maps in the Figure. 21. The Figure 23 is the mean map of all the Hough value plots converted form the fracture maps in the ensemble.

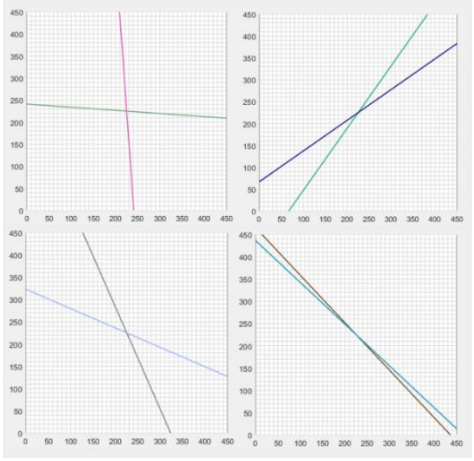

Figure 21. Fracture map used to generate initial Hough fields in Type 2 initial field.

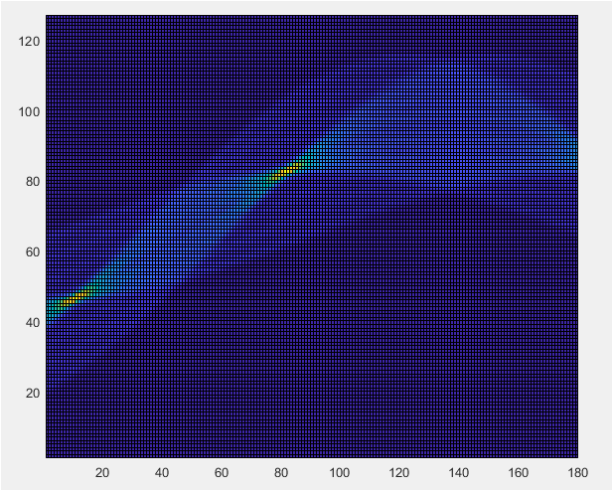

Figure 22. Mean map of initial Hough value fields in Type 1 initial fields.

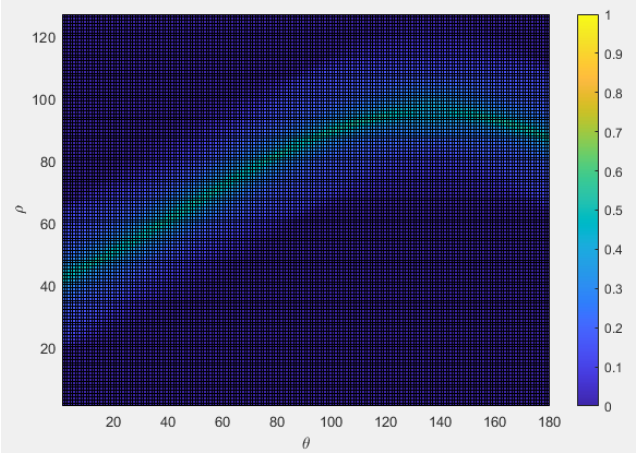

Figure 23. Mean map of initial Hough value fields after Gaussian filter in Type 1 initial fields.

Type 3:

The type 3 initial fields with prior information are more complex. Since a line consists of many points in geometry, we call these points on a fracture line, the fracture points. When two fractures are crossed at the center of the model, no matter the fractures' orientation and length, the possibility of the points on the fracture' existence at the center of the model is 1. The possibility decreases from the center to the edge. For example, at the right upper corner of the model, only the fracture in 45-degree orientation and long enough, a fracture point will be existed at here.

This message needs to be transformed into a mathematical language and tell the program. So, a set of point plots is generated to be used as prior information in the program (Figure 24 is an example). The yellow dots in Figure 24 represent the fracture points, and they follow a normal distribution from the model center to the edge, whose possibility is 1 at the center and decrease from the center to the edge.

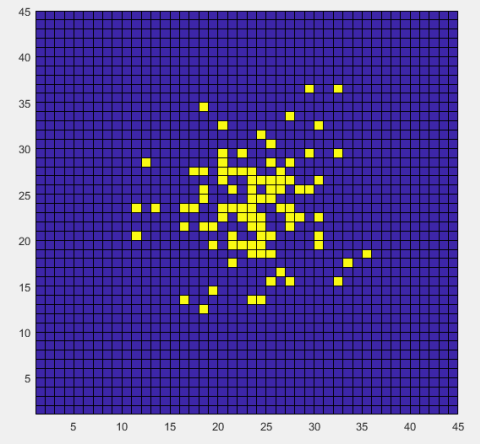

Figure 24. Cartesian map with random points.

A forward Hough transform is applied to the point map (Figure 25, left), and then the Gaussian filter is applied to blur the Hough value field into a continuous field (Figure 25, right). Figure 26 shows the average of these initial Hough value fields. The second type of prior information shows our thoughts on how to get the prior information, this point map is remarkably similar to the micro-seismic events map, so maybe we can obtain the prior information from the sources such as the micro-seismic records.

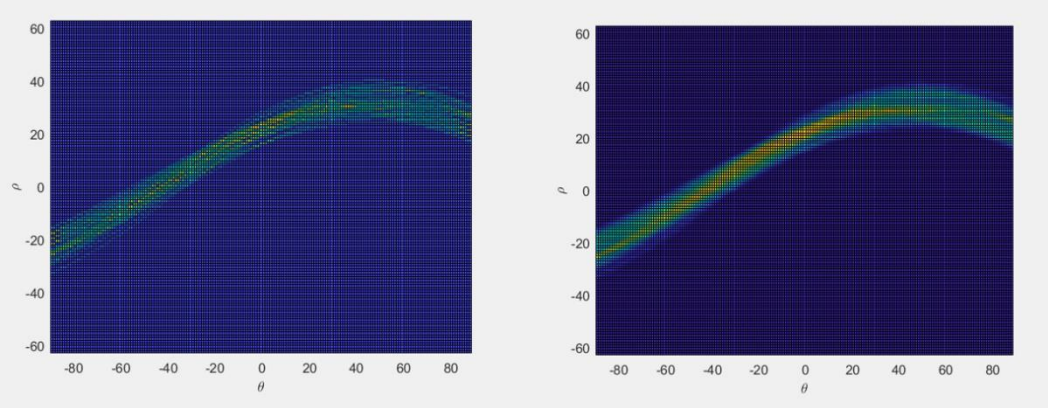

Figure 25. a representative of the Original Hough value fields and Hough value fields after Gaussian filter in Type 3 initial fields.

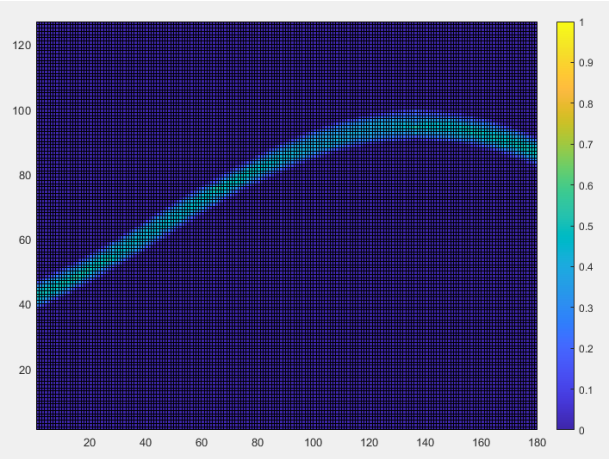

Figure 26. Mean map of initial Hough value fields after Gaussian filter in Type 3 initial fields.

From the history matching program with Type 1, 2, and 3 initial fields, the mean maps of the updated Hough fields are shown in Figure 27. Figure 27 are still Hough Value maps in the angular coordinate. The corresponded fracture maps are shown in Figure 28. The red squares in Figure 27 show local maximums, while Figure 28 shows the fractures represented by these local maximums in Figure 27. From the fracture geometry history matching results, it can be easily observed that the history matching program with Type 1 initial fields failed to obtain one of the fractures. The history matching program with both Type 2 and 3 initial fields are obtained fracture maps with correct crossed fracture geometry, while the fracture's orientation is slightly different

from the reference model. The history matching programs with Type 2 and 3 initial fields lead to a better performance in the fractures' geometry history matching.

In addition, the history matching program with Type 1 initial fields generated the fracture connecting wells No. 1 and No. 4 in a position close to the correct position. However, the fracture far away from any production wells is not inversed correctly. So, besides the previous conclusion, the history matching results with Type 1 initial fields also indicate that the performance of the history matching method is highly related to the fracture's sensitivity to the well production when there is no prior information.

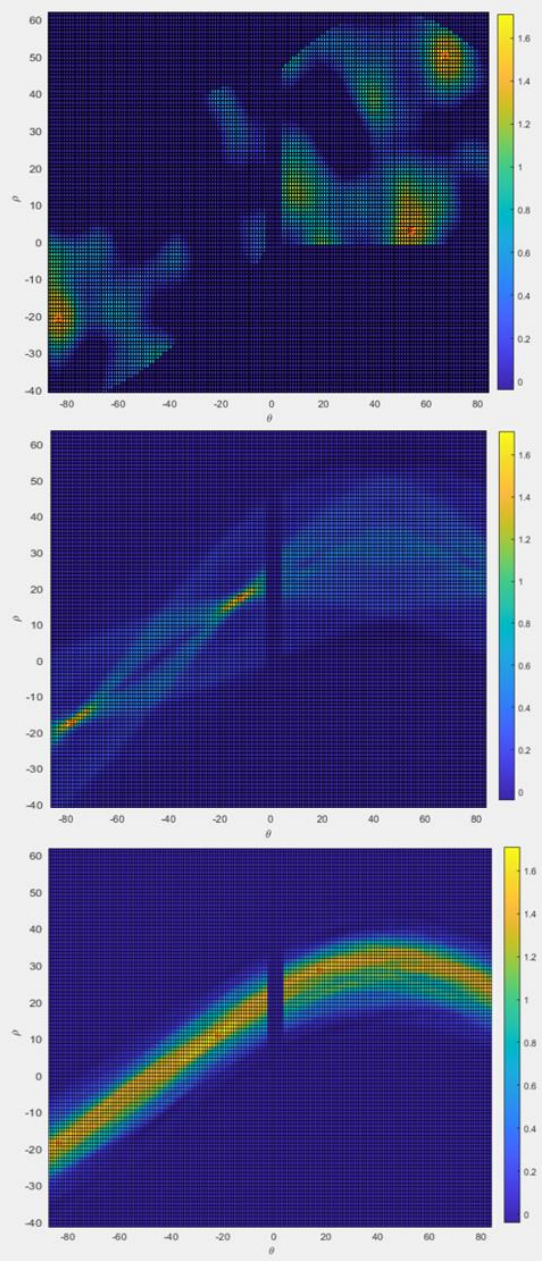

Figure 27. Mean of Hough value fields history matching results. (From the top to the bottom: Type 1, Type 2, Type 3)

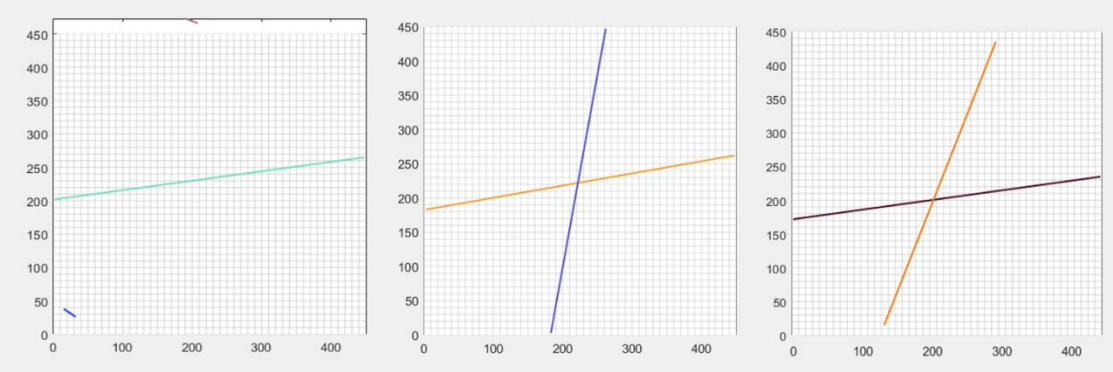

Figure 28. fracture geometry history matching results. (From the left to the right: Type 1, Type 2, Type 3)

The production data matching results are shown in Figure. 29. In this figure, the red lines indicate the observation. Each gray line is an implementation simulation result in the ensemble, while the blue lines represent the average of all implemented simulation results. Table. 1 is the mean-square error (MSE) measured between the observed production data and model simulation results after the history matching. In this chapter, a different parameter (MSE) is used to replace three parameters in the last chapter, which is more efficient to evaluate the performance of the history matching program. The equation used to measure the MSE is shown below:

$$MSE = \frac{1}{n_e}\sum\frac{\left(d - g(m)\right)^2}{C_D} \tag{43}$$

From the production data history matching plots and MSE table, it can be concluded that the history matching program with Type 2 initial fields leads to the best match. Compared to the history matching program with no prior information (Type 1 initial fields), the history matching program with Type 3 initial fields shows a slight improvement on the production data history matching.

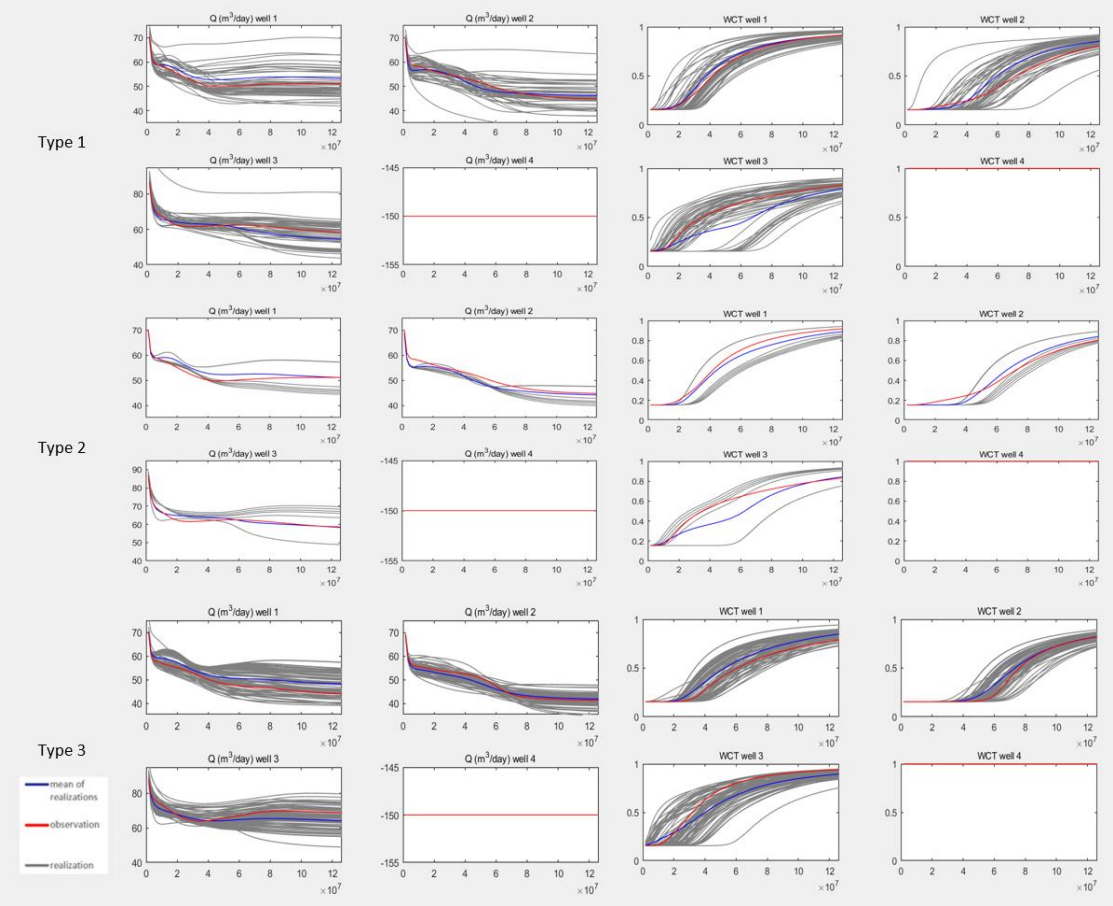

Figure 29. The production history matching results

Table 5. MSE of Example 1

Initial fields	**Type 1**	**Type 2**	**Type 3**
MSE	37.6007	19.1745	36.4869

3.2.2 Example 2

In this example, the prior information generated by the same method as in Example 1, Since the reference model still contains two fractures crossed at the center of the model, which is very similar to Example 1. A similar fracture geometry can help us to conduct analysis and get conclusions by the control variates method when comparing Example 1 and 2. The changes in the Example 2 reference model are the well pattern and matrix permeability.

The history matching program's performance is tested in a model without the injection well in this Example. All five wells in this model are production wells with a constant bottom hole pressure of 131 bar. Only the pressure data from these producers is used as observation data in history matching, because of the missing injector. The model assumes that there is only oil flow in the model and the fluid properties are the same as the last example. The simulation time is still 4 years. For the history matching programs, updates are made at the end of each year and the model is restarted after the update.

The missing injector is a situation commonly in unconventional reservoirs. To make our numerical tests more meaningful for the unconventional reservoir, the matrix permeability in this example is set as 1 mD. Several factors are considered when determining the matrix permeability. Only the main fractures are shown, and there is no dual-porosity matrix. Thus, the permeability is much higher than the nano-darcy level which is commonly seen in shale reservoirs. However, 1 mD can still provide high contrast with Example 1. Figure 30 shows the pressure map of the reference model after 4 years simulation.

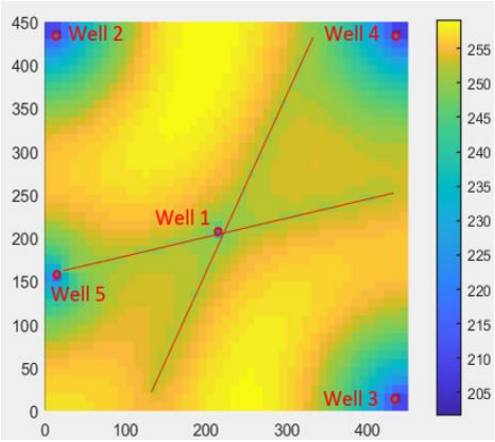

Figure 30. Pressure map of Example 3 reference model

The mean of the history matching program updated Hough fields are shown in Figure 31. The axis title and each cell's parameter type are the same as in Figure 27. The fracture geometry maps after history matching are shown in Figure 32. the generation process of Figure 32 is the same as Figure 28. In this example, only the history matching

program with Type 2 initial fields can obtain a history matched model with the correct fracture amount. The fractures' geometry in this model is also very similar to the reference model. From Figure 31, it can be observed that only the history matching program with Type 2 initial fields delivers two clear maximums. The other two history matching programs lead to more than 2 local maximum spots, which indicates a worse convergence of the history matching programs with Type 1 and 3 fields.

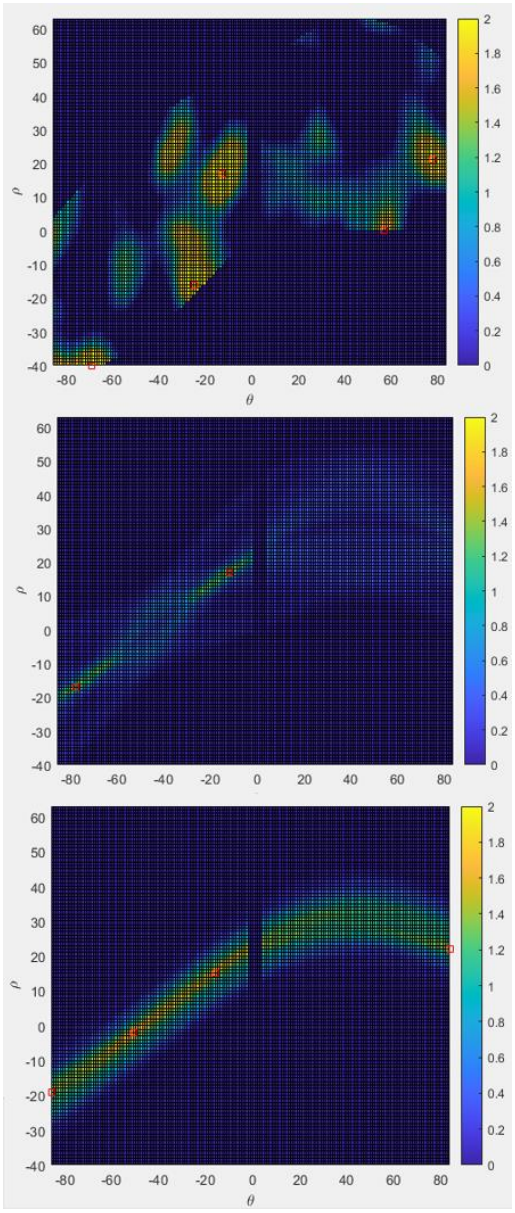

Figure 31. Mean of Hough value fields history matching results. (From the top to the bottom: Type 1, Type 2, Type 3)

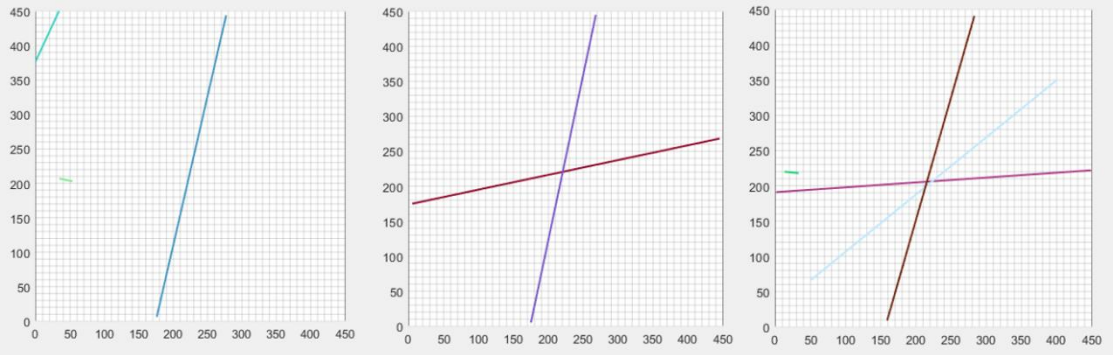

Figure 32. fracture geometry history matching results. (From the left to the right: Type 1, Type 2, Type 3)

The history matching of production data is shown in Figure 33 and the MSE is shown in Table 2. Figure 33's legend and axis title are the same as Figure 29 in Example 1. The history matching programs with both Type 2 and 3 initial fields gain performance improvements. Although the history matching results with Type 3 initial fields still get a relatively wide distributed gray-line ensemble. The grey-line ensemble from the history matching program with Type 3 initial fields is closer to the observed data than the ensemble from the history matching program with the Type 1 initial fields. Comparing with the results with Type 1 fields, the blue line and red line are closer in results with Type 3 fields, especially in Well 1. The Type 2 initial fields lead to a lower MSE than the Type 3 initial fields, which is the same as Example 1.

Well 2, 3, and 4 show a relatively good match in the results with all three types of initial fields. It should be mentioned here, wells 2, 3, and 4 ‘s "better" matching may not be good evidence of the history matching programs' actual performance. Since these wells are not very sensitive to unconnected fractures in these relatively low permeability reservoirs. This scenario also reveals the main challenge faced in a low-perm reservoir. The production data used for history matching is much less due to the low permeability and no water injection. For example, in this case, there is no water cut data that can be used in the history matching process. The pressure data in Well 2, 3, and 4 are also useless in the history matching because of the extremely low sensitivity between the fractures’ geometry and Well 2, 3, and 4’s pressure data. This shortage of observation data will challenge the convergence of the algorithm. The prior information will be more

important in low-perm cases, which can greatly narrow the scope of the problem. With fewer production data, the prior information should be more specific to provide more data in the history matching process. For example, the history matching program with Type 3 initial fields obtained a very similar fracture geometry with the reference model in Example 1. However, the performance of the program with Type 3 fields is weaker in this example as the mean Hough field contains more local maximums than the fractures' amount in the reference model.

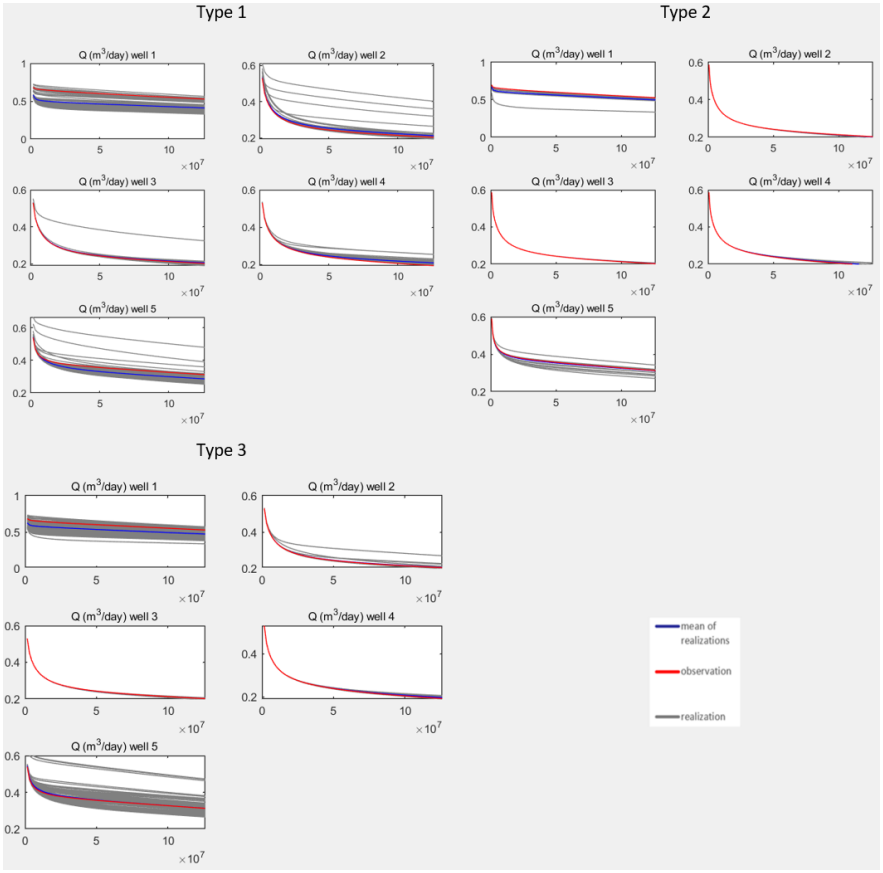

Figure 33. The production history matching results

Table 6. MSE of Example 2

Initial fields	**Type 1**	**Type 2**	**Type 3**
MSE	52.0954	26.5724	32.9123

3.2.3 Example 3

In this example, a fracture system with one main fracture and several secondary fractures is tested with ensemble methods in this example. Because the fracture system in this example is more complex, the history matching of this case is conducted with water injection in a high-perm reservoir to provide more data in the history matching process. The reservoir properties in this example are the same as Example 1, which allows us to conduct analysis and get conclusions by comparing the program performance with Example 1.

The model scale is 450m×450m. The entire model is discretized into 90×90 grid-blocks. The well plot and fracture geometry of the reference is shown in Figure 34, which is a saturation map of the reference model after 4 years simulation. Well 1 is an injector, while Well 2, 3, 4, and 5 are producers. The producers are produced at a constant bottom hole pressure (162 bar), while the injector is injecting at a constant rate (150m^3/day). Two-phase flow (Oil and Water) is simulated in the model. The simulation time is 4 years. Because the fracture system is more complex, in order to keep the simulation accuracy, this model contains 4-times grid blocks than other examples. The updating interval is one year. Total production rate, water cut, and injection bottom hole pressure are used in history matching.

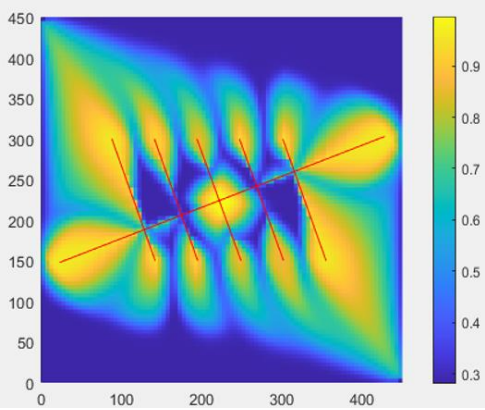

Figure 34. Saturation map of Example 4 reference model after 4 years simulation.

Because the fracture geometry in the reference model has dramatic changes when comparing to Examples 1 and 2. The initial fields generation methods have also been applied corresponded modification:

Type 1:

The generation method of the Type 1 initial field keeps the same as the Example 1 and 2. The initial Length (L) fields ensemble and Displacement (D) fields ensemble is constructed by totally random numbers. Initial Hough value fields ensemble is generated by a Sequential-Gaussian simulation process with Mean 1 and Variance.

Type 2:

For the Type 2 initial fields, the Hough value fields ensemble is generated by the following steps: (1) an ensemble of fracture maps is generated (Figure 35). All these maps contain six fractures, which is the same as the reference model. Five of the fractures are parallel and have the same interval as the reference model. The one fracture left is perpendicular to the rest four fractures. The orientation of the entire fracture network and the length of each fracture is random. (2) the fracture maps are converted to Hough maps, length maps, and displacement maps. (3) The Gaussian filter is applied to blur the Hough fields. Figure 36 shows the mean map of the transformed Hough fields ensemble. The figure's axis title and each cell's parameter type are the same as Figure 4. Since the model's cell number is 4 times as it in Examples 1 and 2. And the Hough field keeps the same resolution as that in Example 1 and 2 (In angle axis, each cell length represents 1 degree. In distance axis, each cell length represents 1 simulation model's cell length). The total cell amount in the Hough field is increased. Figure 20 displays all the grids to show the resolution of the Hough field. However, it makes the color in each cell hard to read. Thus, the later shown Hough field maps in this example will remove the grid.

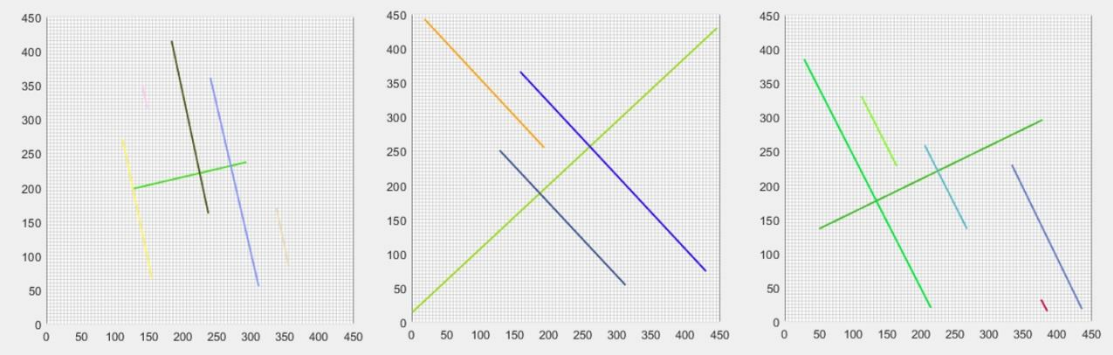

Figure 35. Fracture map used to generate initial Hough fields in Type 2 initial field.

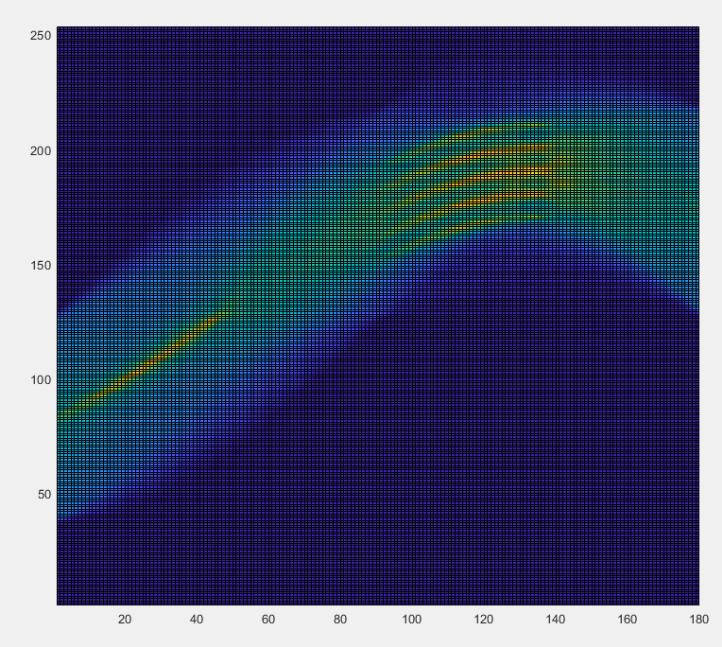

Figure 36. Mean map of initial Hough value fields after Gaussian filter in Type 2 initial fields.

Type 3:

The type 3 initial fields with prior information still include an ensemble of Hough fields which are generated from the point maps. There are five fractures' crossed points in the reference model, which is selected as the prior information. The initial Hough fields are generated by the following steps: (1) an ensemble of point maps is generated. The points in the map are followed normal distributions which use the fracture cross points as the centers (the probability of point existence is 1 at this point) of these distributions. A representative of the point maps is shown in Figure 21. (2) the

ensemble of point maps is transformed into Hough fields, Figure 22 is the mean map of the Hough fields ensemble, the figure's axis title and each cell's parameter type are the same as Figure 20. At meanwhile, the initial Length (L) fields ensemble and Displacement (D) fields ensemble is generated by totally random numbers.

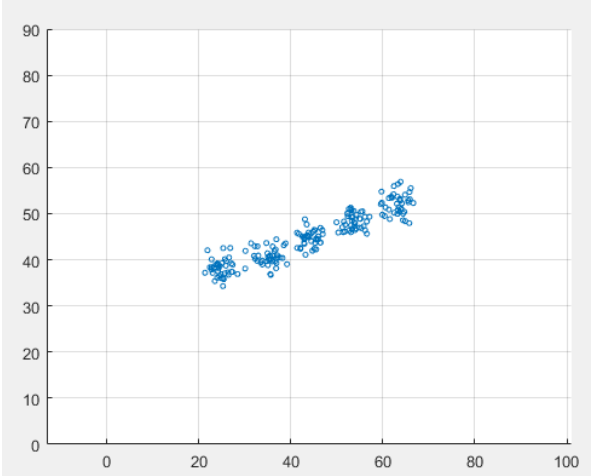

Figure 37. A representative of the point maps.

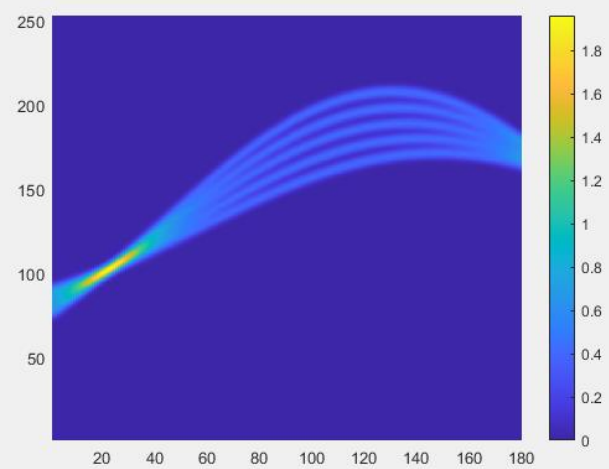

Figure 38. Mean map of initial Hough value fields after Gaussian filter in Type 3 initial fields.

When there is no prior information provided, the ENKF history matching program shows very weak abilities on this problem. The program failed to obtain the correct fractures' geometry (Figure 40). With Type 2 fields, the history matching program can provide a very similar position and geometry of fractures as the reference model (Figure 39 & 40). It seems like that the history matching program with Type 3

initial fields leads to even worse matching results than the program with Type 1 initial fields. The results with Type 3 fields do not reflect the “fishbone” fracture geometry at all.

The enlightenment reflected from the experimental results with Type 3 fields is that, when the points map containing five dependent normal distributed points sets in a straight line, the points map may not tell the history matching program the prior information we expect to tell. It is reasonable to suspect that the initial fields actually tell the program that there is a high probability of the fracture points' existence on the straight line through which all the fractures' crossed points go. This can partly explain the reason why the history matching results show two fractures whose orientation and length very close to the fracture containing all five cross points in the reference model.

The production data is shown in Figure 41 and the misfit of the production data is measured by MSE in Table 3. The Type 2 initial fields show a dramatic improvement in this example when comparing to the history matching results with Type 1 initial fields, while the results with Type 3 fields are worse than the results with Type 1 fields. This matches what can be observed in the fracture geometry matching results.

From this example, it can be concluded that a more complex fracture system also leads to more challenges in the history matching program. The method generating the initial field should ensure the desired prior information is delivered to the history matching program when the fracture system is complex. Complex fracture geometry always leads to complex prior information, which requires a more wisely initial field generation method design. Combining the information from different sources and different detection methods into the initial fields also gives more problems in the generation method design.

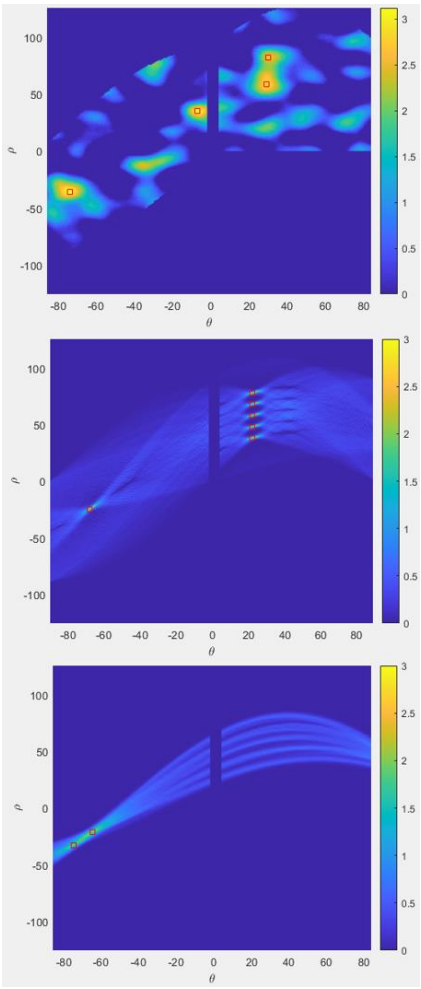

Figure 39. Mean of Hough value fields history matching results. (From the top to the bottom: Type 1, Type 2, Type 3)

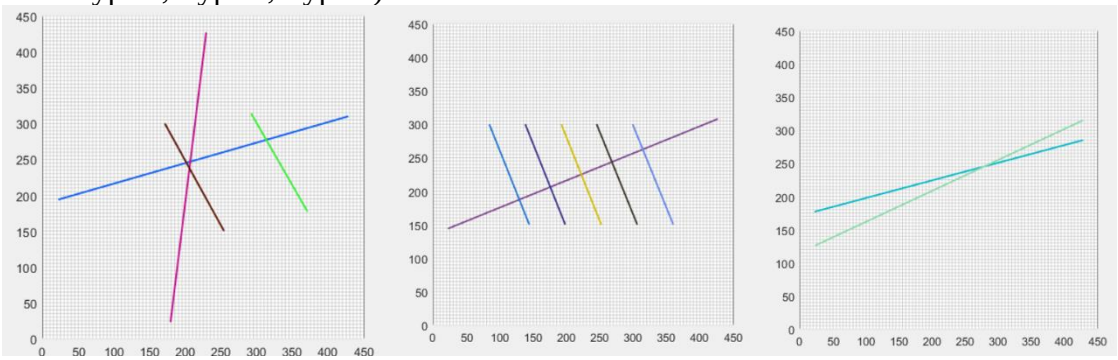

Figure 40. Fracture geometry history matching results. (From the left to the right: Type 1, Type 2, Type 3)

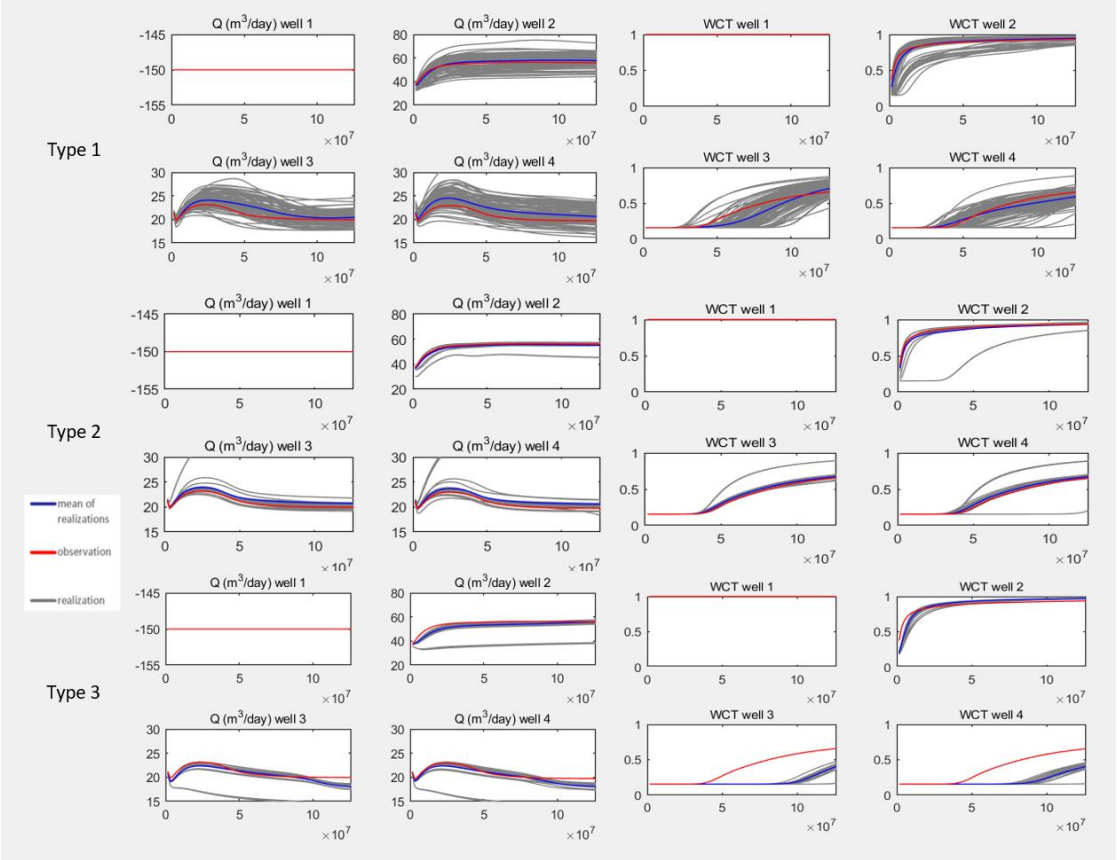

Figure 41. The production history matching results.

Table 7. MSE of Example 3

Initial fields	**Type 1**	**Type 2**	**Type 3**
MSE	39.6536	23.1706	49.5445

Conclusion

In this paper, ensemble history matching programs' performance with different prior information is tested in three examples representing reservoirs with various matrix properties and fractures networks. From all the three examples, it can be concluded that comparing the cases without prior information, specific and proper prior information can give a dramatic performance improvement in fractures' geometry history matching process. It still needs to be noticed that, from Example 3, initial fields that do not deliver the desired prior information may lead to even worse performance.

When comparing Example 1 with Example 2 and 3, it can be concluded that both the low permeability (Low permeability reservoirs always lead to the missing injectors) and

the complex hydraulic fracture system provide more challenges to the history matching program. Thus, the prior information is more critical in the unconventional reservoirs which always contain these two features. When the reservoir has a low permeability, the prior information is a powerful tool to deal with the shortage of observation data in the history matching. the prior information in the initial fields should be more specific. When the fractures have more complex geometry, to make sure the initial fields delivered expected prior information is a challenge to the design of initial field generation algorithms.

CHAPTER IV

THE PERFORMANCE ANALYSIS OF EDFM WITH DIFFERENT TOTAL GRID NUMBER

4.1 The Verification of the Simulator

Many fractured reservoirs, such as shale gas reservoirs, have fractures in various scales. The width of natural fractures ranges from micrometers to millimeters and the lengths of natural cracks range from centimeters to meters. The width of hydraulic fractures is from millimeters to centimeters, and the length is in meters. In fractured reservoirs such as shale gas reservoirs, the permeability between the matrix and the fractures varies greatly, and the pressure changes around the fractures are huge and rapid. Even when the EDFM method is applied, it is critical to select an appropriate grid size. The size of the grid should ensure that the main pressure changes can be captured, and the calculation cost can be minimized. In this chapter, the performance of EDFM under different grid densities is tested, the main causes of numerical simulation errors are analyzed, and the performance of different improvement methods is discussed. In this chapter, we mainly want to research the EDFM's performance in the shale gas reservoir. So, we selected an open-source shale gas module (Open Shale) based on the MRST, which has been verified with CMG. The Figure. 42 is the comparison between the Open Shale and CMG (Bin Wang, 2020). The EDFM model shows a 3.04% error in the 30 years cumulative production, which is acceptable for the practical use. For the gas transport mechanisms, only the Langmuir adsorption is considered in the following simulations.

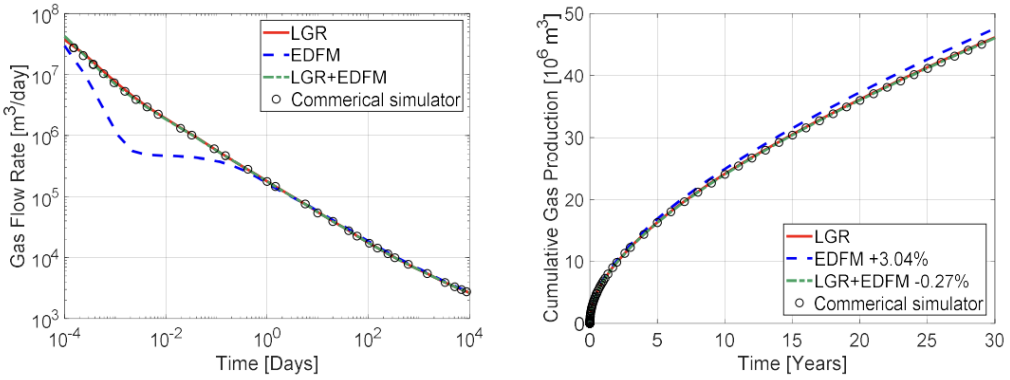

(a) log-log gas flow rate (b) cumulative production

Figure 42. Comparison of gas flow rate (a) and cumulative production (b), (Bin Wang, 2020)

The "+3.04%" and "-0.27%" in the Figure 42(b) indicates the simulation errors of different simulation methods.

4.2 EDFM models with complex fracture geometry

In the first case, the EDFM models commonly used in a field case are tested under the different total grid numbers (Figure 43). The blue lines in this model represent the hydraulic fractures, while grey lines in this model show the random distribution of the natural fractures. In this model, horizontal wells are represented by rows of straight wells, as shown by black dots. Three different meshed models are tested in this example. The total grid numbers in these three models are 31 X 7/ 121 X 15/ 241 X 31 respectively. The reservoir properties used in the simulation are shown in Table. 8. The pressure maps after 30 years of simulation are shown in Figure. 44. From the production plots (Figure. 45), the coarsest model shows an obvious difference in the cumulative production when comparing with the other two model's production. And from the production rate plot, a significant difference starts from around 1 day to 100 days. In the rest of this chapter, the reason for this difference is attempted to be located and the methods to improve this problem are discussed.

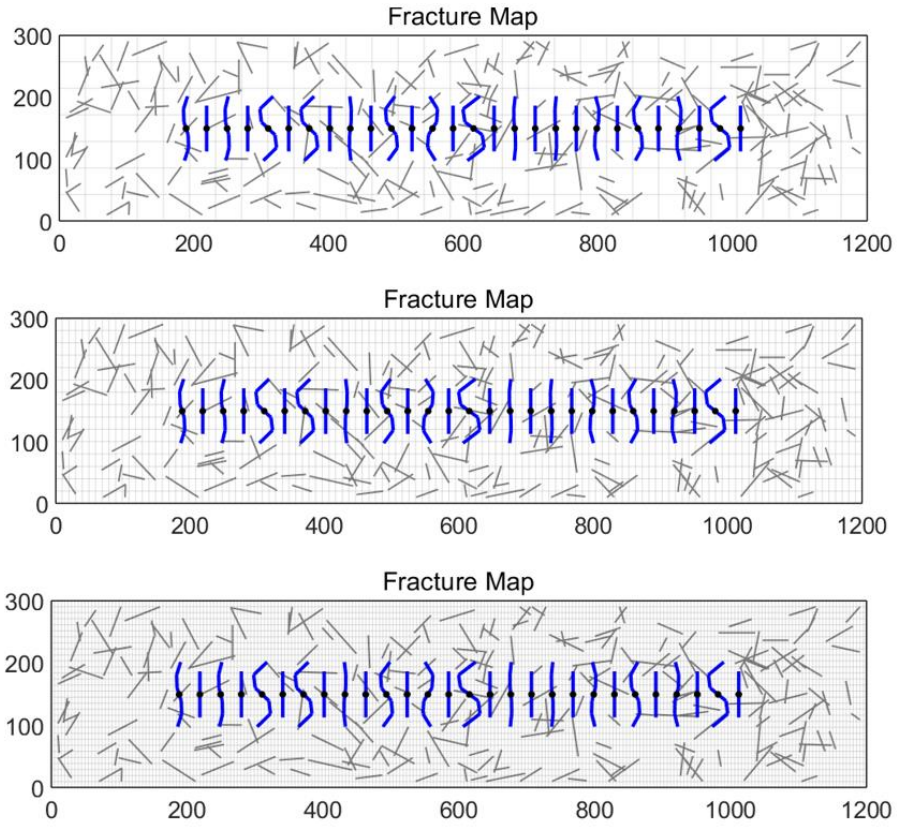

Figure 43. The grid mesh of the simulation models

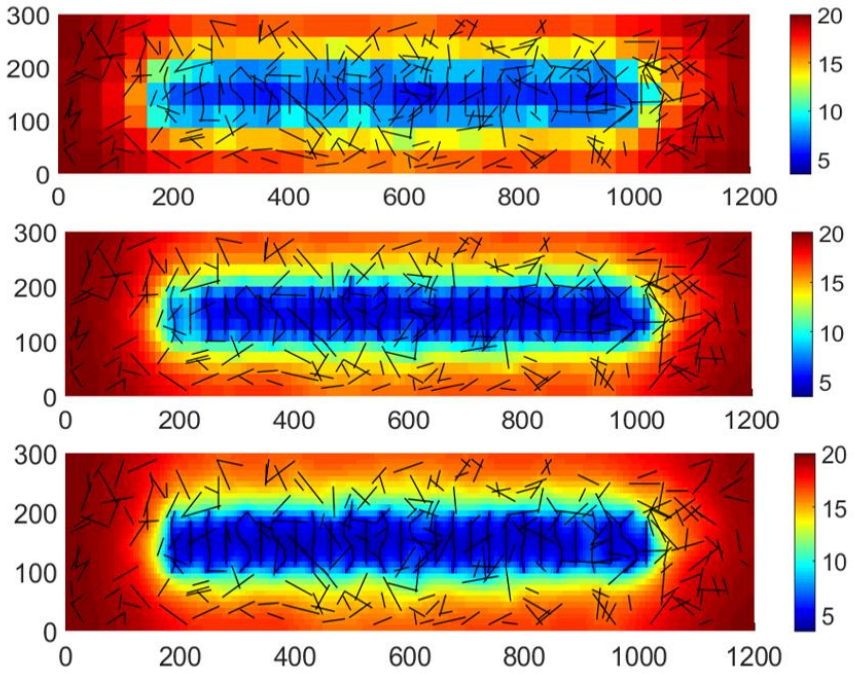

Figure 44. The pressure maps after 30 years simulation

Table 8. Reservoir properties

Properties	Unit	Value
Domain dimensions (x,y)	m	1200;300
Depth	m	5463
Formation thickness,	m	90
Initial reservoir pressure	MPa	20.34
Temperature	K	352
Rock density	kg/m3	2500
Langmuir pressure	MPa	4.47
Langmuir volume	m3/kg	0.00272
Matrix porosity		0.03
Matrix compressibility	1/Pa	1.50E-10
Fracture compressibility	1/Pa	1.00E-08
Matrix permeability	nD	100
Hydralic Fracture permeability	mD	100
Fracture width	m	0.003
Fracture spacing	m	30.5
Fracture half-length	m	47.2
Fracture conductivity	md-ft	1
Nature Fracture permeability	mD	10
Well BHP	MPa	3.69
Correction skin factor	-	19
Production time	days	1600

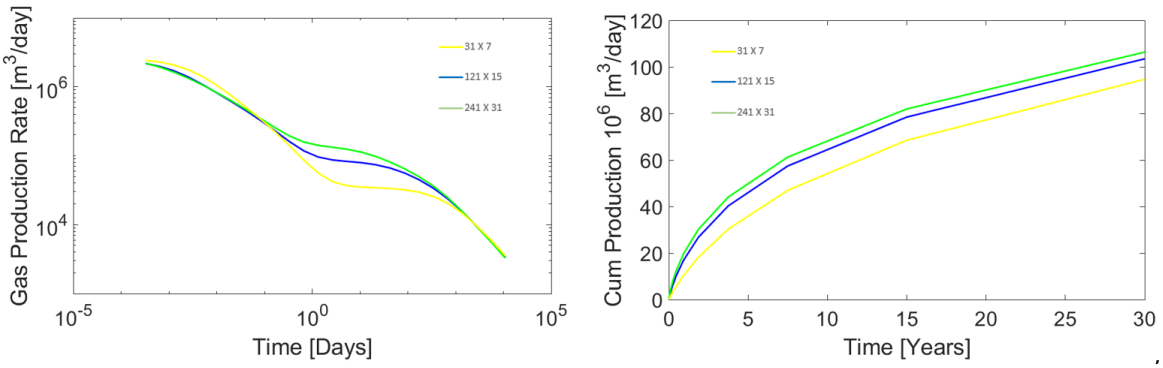

Figure 45. The production rate plot and cumulative production plot

4.3 EDFM models with single fracture

In order to locate the reason for the cumulative production difference, the second model tested in this chapter is a single fracture model, the fracture is parallel to the model's edge. The production data from four different meshes are compared (Figure. 46). In the Figure 46, from the left to the right, the first model is a traditional log LGR model with 253X65 cells. The log LGR explicit fracture model is used as the reference. Three EDFM models with different total grid numbers are simulated. The corresponding pressure maps after 30 years of simulation are shown in Figure. 47, while the good production is shown in Figure. 48. The scenario is similar to the last case. There is a huge cumulative production difference between the 19 X 15 model and the rest three models. The production rate shows a difference lasting around 100 days, which may be the reason for the gap in the cumulative production. The properties of the model are shown in Table. 9. The grid number of the fracture is related to the matrix mesh in the EDFM (every matrix cell only contains 1 fracture cell). According to the control variates method, extremely high conductivity is assigned to the fracture in this case and the next three cases, in case the different inside-fracture pressure drop caused by the different fracture grid influence the cumulative production. The fracture-matrix mass transportation can be analyzed first. The finite conductivity case will be tested later in this chapter.

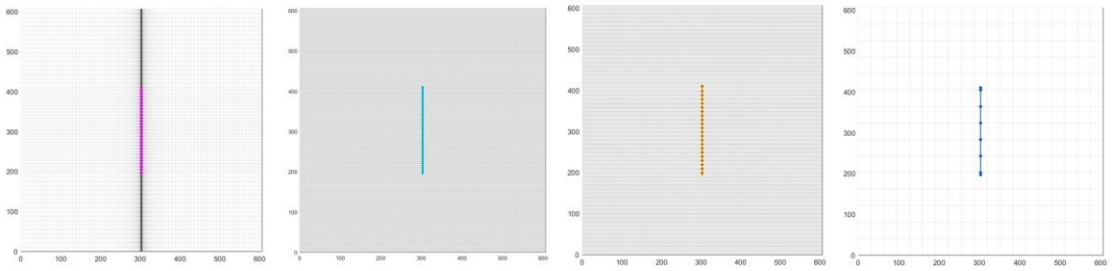

Figure 46. The grid mesh of the simulation models

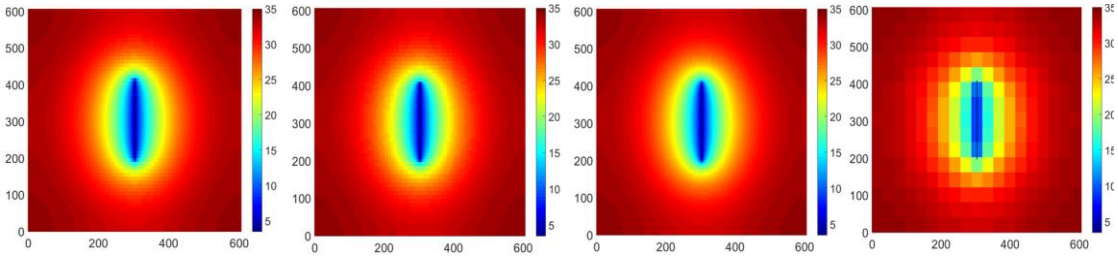

Figure 47. The pressure maps after 30 years simulation

Table 9. Reservoir properties

Properties	Unit	Value
Domain dimensions (x,y)	ft	1900;1900
Formation thickness,	ft	150
Initial reservoir pressure	MPa	34.47
Temperature	K	327.6
Langmuir pressure	MPa	8.96
Langmuir volume	m3/kg	0.0041
Matrix porosity		0.07
Matrix compressibility	1/Pa	1.45E-10
Matrix permeability	nD	500
Hydralic Fracture permeability	D	1000
Fracture width	ft	0.01
Fracture half-length	ft	350
Well BHP	MPa	3.45
Production time	years	30

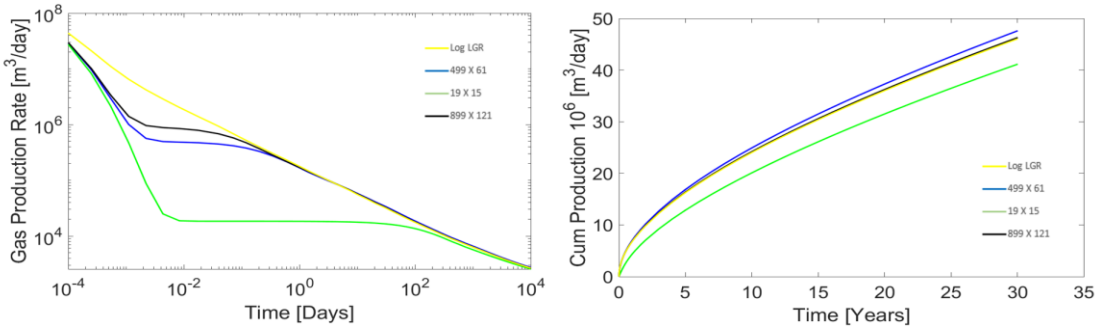

Figure 48. The production rate plot and cumulative production plot

There are three possible reasons which may cause the error in the well's production. Firstly, the assumption of linear flow between the fracture and matrix in EDFM cannot accurately capture the sharp unsteady state pressure drop. Secondly, when the fracture segment in a matrix cell is much smaller than the grid size, the tip effect of the fracture will appear, and the pressure drop area of the fracture will appear elliptical. It is obviously inappropriate to consider only the linear pressure drop on both sides of the fracture. Thirdly, If the fracture direction is not parallel to the edges of the matrix grid, the resulting grid diagonal effect (numerical viscosity) may affect the accuracy of the simulation. In the following three cases, three methods to improve these three problems respectively will be applied to the model with one infinite-conductivity fracture. The main reason for the cumulative production error can be identified if the error is obviously eliminated with any of these three improvement methods.

4.4 Improve the simulation accuracy of pressure drop around fracture

To improve the simulation accuracy of the sharp unsteady-state pressure drop, the LGR method is applied to the EDFM model. Two models are tested in the following case. The total grid number in both models is 19 X 15, which is as same as the coarsest model in the last case. The difference between the two models is that: one model (Model 1)'s cells are uniform y-direction thickness, so there is a grid partially penetrated by the fracture tip. The other model (Model 2)'s cells are modified to make the fracture fully penetrated all the connected cells (Figure. 49). The cells connected to the fracture are divided into 37 cells. The pressure maps after 30 years of simulation are presented in

Figure. 50. These two models' production data show as the red lines in Figure. 51 & 52. The red lines are the EDFM models with the LGR, while the other lines are the same line in the last case's production plot (Figure 48) with the same legend. The early production rate is significantly improved. However, the cumulative productions from the two models with different fracture tip treatments are different. This is because the tip effect shows up, which can be observed from the pressure map (Figure. 50). In the two models, the fracture lengths are the same, however, the low-pressure areas (blue area) are not the same length.

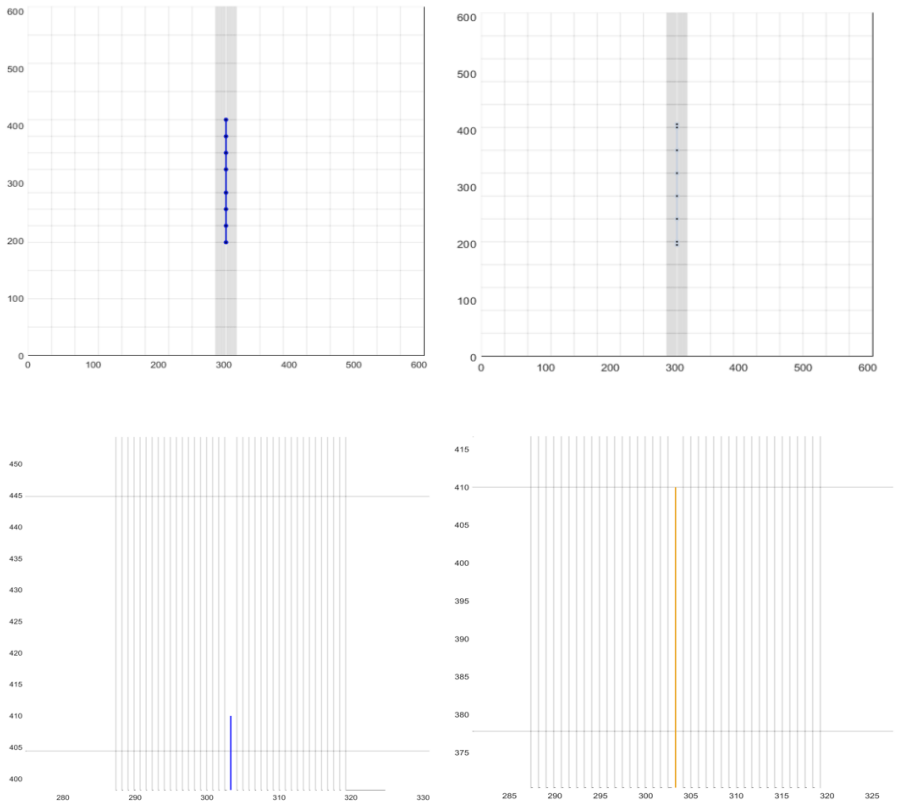

Figure 49. The grid mesh of the LGR models and Zoom-in plots for the matrix cell containing the fracture tip

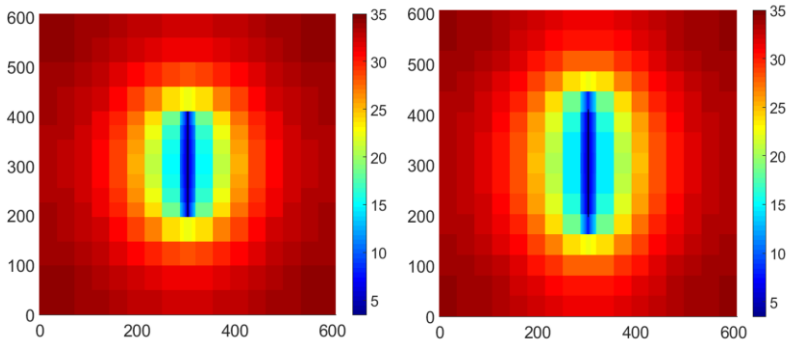

Figure 50. The pressure maps after 30 years simulation

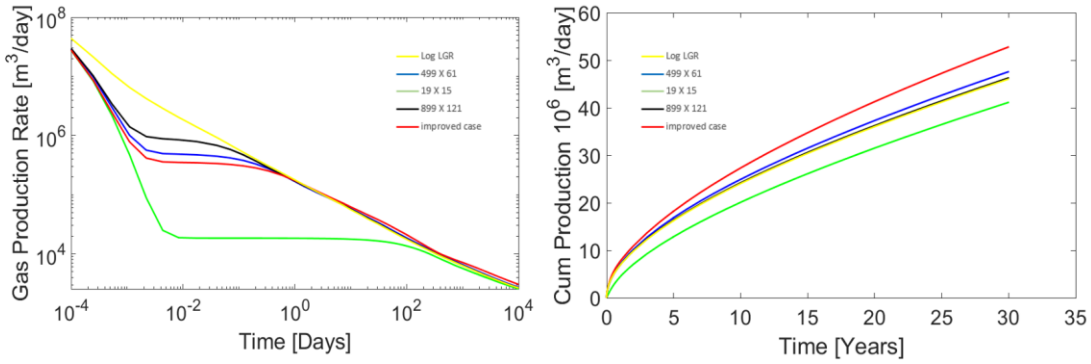

Figure 51, The production rate plot and cumulative production plot of the Model 1

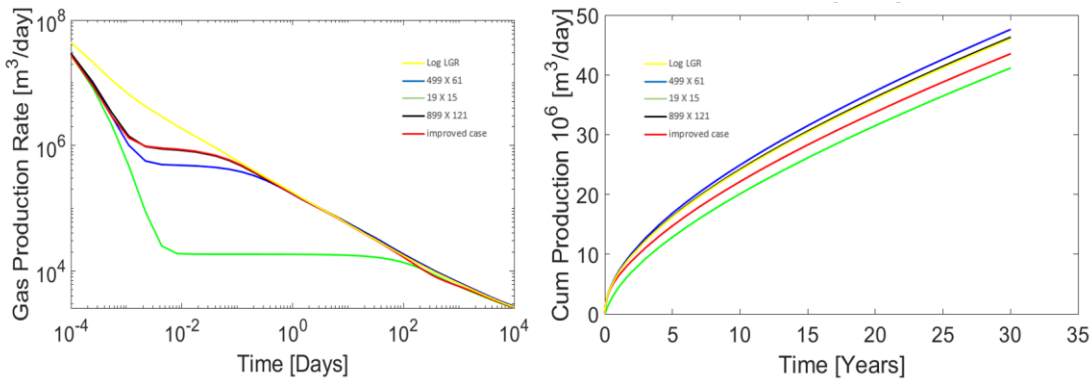

Figure 52. The production rate plot and cumulative production plot of the Model 2

4.5 Improve the simulation quality with the tip effect

To improve the simulation quality with the tip effect, the fourth case in this chapter applies a new semi-analytical fracture-matrix transmissibility developed by Shao (2020). In this method, the fracture is treated as an ensemble of point sinks (Figure. 53). In other words, the fractures in a matrix cell are treated as a bunch of wells.

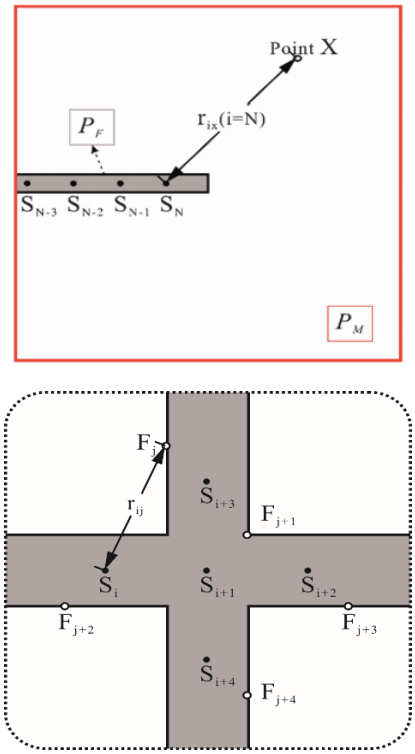

Figure 53. The illustration of the semi-analytical transmissibility (Shao, 2020)

The well model which is the analytical solution of the steady-state radial flow combined with the superposition principle of potential is used to calculate the pressure drop caused by the fractures. Assume the fracture segment in a matrix cell is consisted by N point sinks $s_i(i = 1{\sim}N)$, the pressure at any location x inside the matrix cell can be written as.

$$\Phi_x = \sum_{i=1}^{N} \frac{q_{s_i}}{2\pi h} \ln(r_{ix}) + C \tag{44}$$

To solve the q and C, Build the same equation from the Fracture center to the edge:

$$\Phi_F = \sum_{i=1}^{N} \frac{qs_i}{2\pi} lnr_{ij} + C \ (j = 1 \ to \ N) \tag{45}$$

The unknown q and C are combined into a new parameter ξ_i:

$$\xi_i = \frac{qs_i}{\phi_F - C} \tag{46}$$

Thus, the parameter ξ_i can be solve by a linear equation set:

$$\sum_{i=1}^{N} \frac{\ln(r_{ij})}{2\pi} \xi_i = 1 \tag{47}$$

The pressure of a matrix can be solved with double integral:

$$P_X = \left(\frac{\sum_{i=1}^{N} \xi_i \ln(r_{ix})}{2\pi h} - 1 \right) \left(\frac{P_M - P_F}{\epsilon - 1} \right) + P_F \tag{48}$$

Combine with the define of the transmissibility,

$$T = \frac{K_M \sum_{s_i \subset M} \xi_i}{\epsilon - 1} \tag{49}$$

The first model in the fourth case is the 19 X 15 LGR-EDFM model with the new semi-analytical fracture-matrix transmissibility. The mesh of the model and the corresponded pressure map after 30 years of simulation is shown in Figure. 54. In the well's production plot (Figure. 55), the red line is the model with new transmissibility, while the rest lines are the same line as the line with the same color in the case 3' s production plot. From the pressure map, the new transmissibility successfully eliminates the tip effect, and an obvious improvement can be seen in the cumulative production plot.

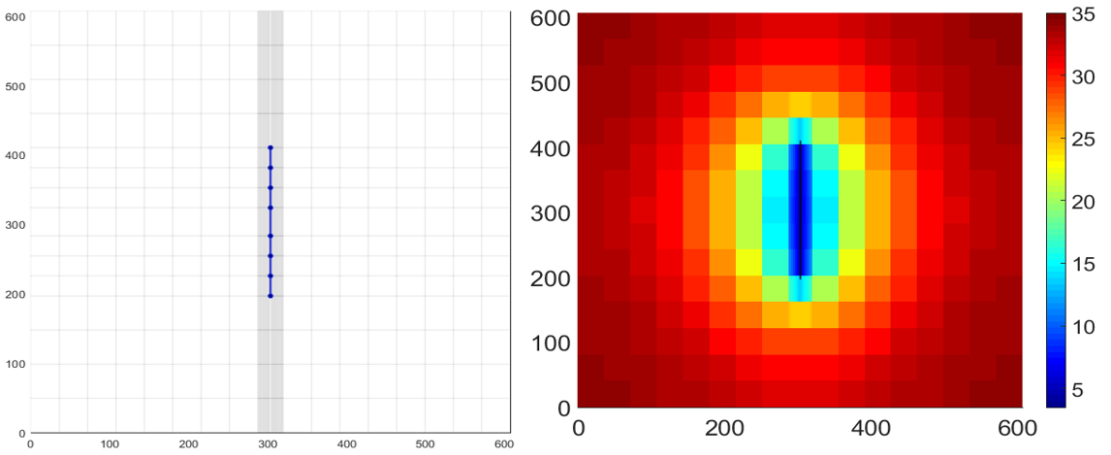

Figure 54. The grid mesh of the simulation models and the pressure map at the end of the simulation of the model with LGR

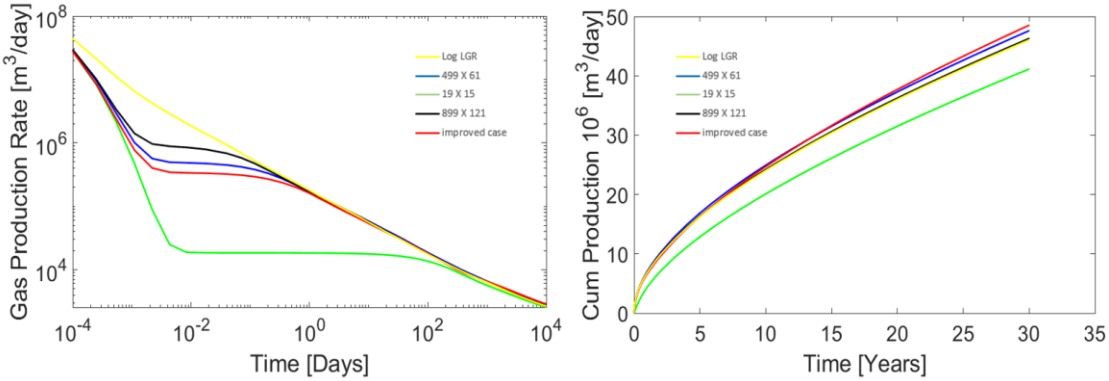

Figure 55. The production rate plot and cumulative production plot of the model with LGR

However, another model does not show the same improvement as the last model. When the new transmissibility is directly applied into the 19 X 15 EDFM model without LGR (Figure. 56), there is no improvement on the constant rate period in the production rate plot, which leads to an even worse match on the cumulative production rate (Figure. 57).

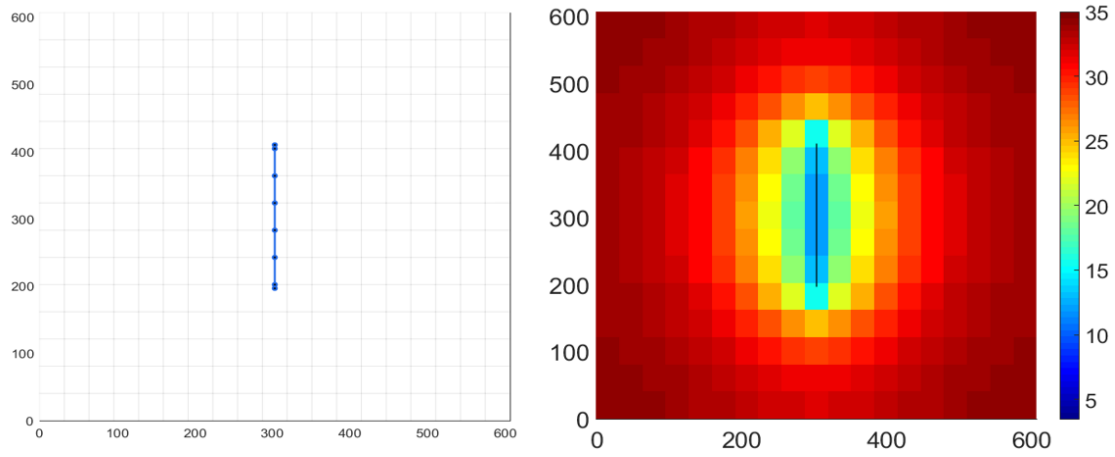

Figure 56. The grid mesh of the simulation models and the pressure map at the end of the simulation of the model without LGR

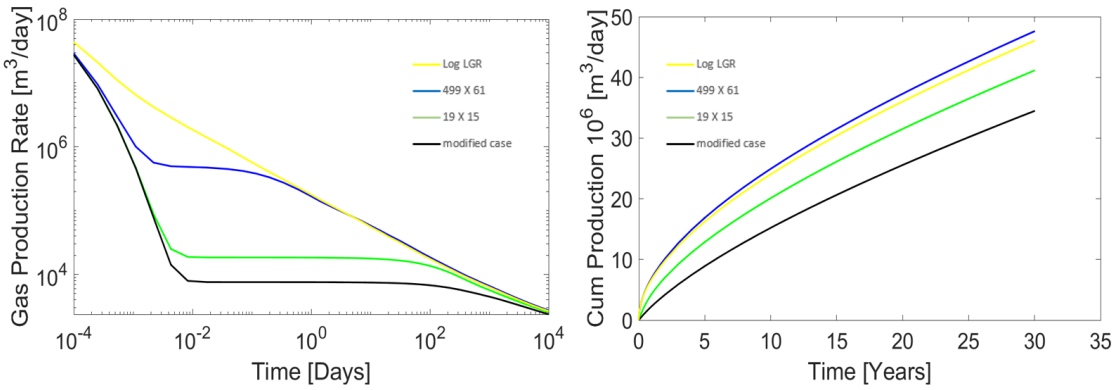

Figure 57. The production rate plot and cumulative production plot of the model without LGR

When analyzing the gas production rate plot from case 2 (Figure. 58), the period shows an obvious error can be divided into two sub-period, which are called “period 1” and “period 2”. In period 1, the production rate shows a decrease with a constant rate in the log-log plot, which indicates a transient flow period. Then, the production rates reach different constant rates with the model’s different total grid numbers. For the 19 X 15 EDFM model, Figure. 59 is a section view of the pressure drop in the cells which is connected and neighbored by the fracture at the beginning and the end of period 2. The cell connected to the fracture is located at the 0 in the X-axis, other cells have been assigned from “Grid block 1” to “Grid block 4” follow from far to near as shown in Figure. 60. there is almost no pressure drop in Grid block 2. The sharp pressure drop

caused by the low permeability takes a long time to make the grid block 2' pressure drop significantly. The boundary between Grids blocks 1 and 2 is acting as an open boundary. Thus, the transient flow in period 1 is when the pressure wave moves in Grid 1, the steady-state flow in period 2 is when the pressure wave hits the boundary between Grids block 1 and 2 (Figure. 60).

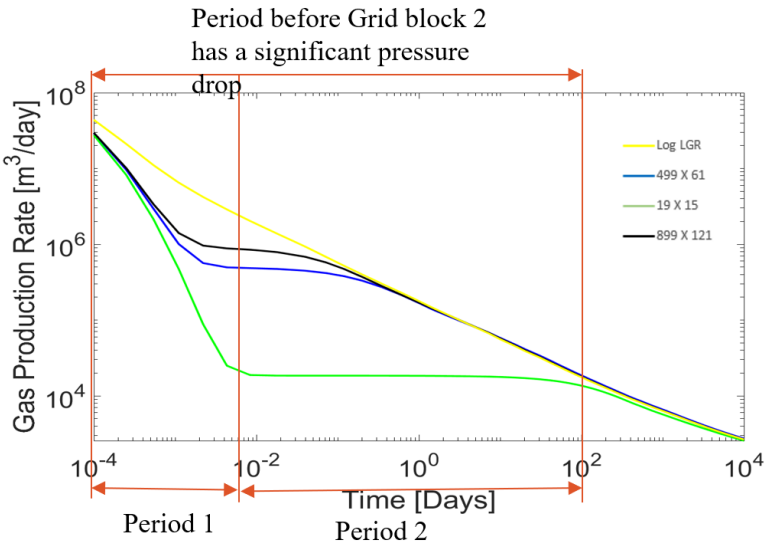

Figure 58. Production rate plot analysis

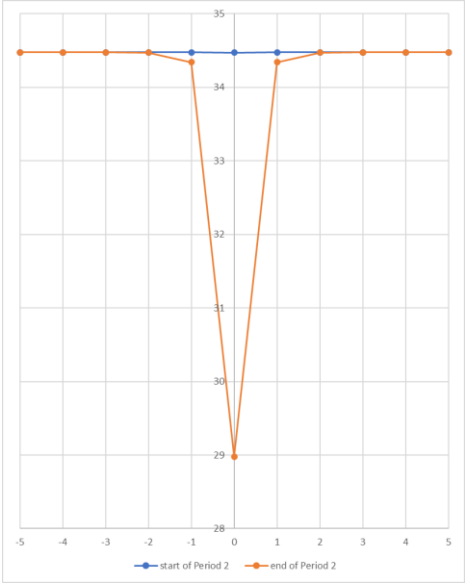

Figure 59. The pressure-drop around the facture

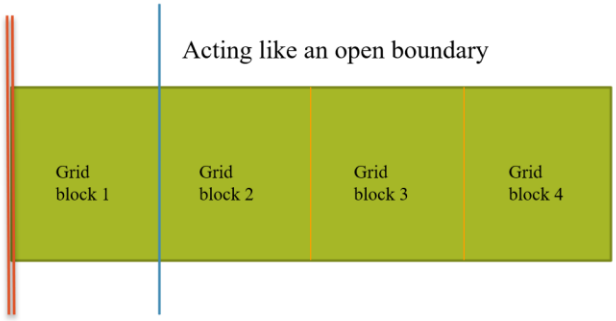

Figure 60. The illustration of the fracture and its neighboring cells

In conclusion, the sharp pressure drops around the fracture cannot be captured by the linear flow equation with coarse grids, which causes an incorrect "steady-state flow period". This is the main reason for the simulation error in the cumulative production. the LGR is effective and necessary to capture the sharp pressure drop around the fracture while a coarse grid is used in EDFM. However, when the LGR is applying, refinement cannot be in only one direction, otherwise, the tip effect should be taken care of by other methods, such as the semi-analytical transmissibility introduced here. This new transmissibility considers the ellipse pressure drop around the tip.

4.6 Improve the grid diagonal effect

To test the grid diagonal effect's influence on the well's production, a fracture that is not paralleled to the model's edge is assigned to a model with the same matrix properties as Case 1. The fracture's half-length in the model is 676ft, while the fracture conductivity is 10 D·ft. the fracture can seem like infinite conductivity. Three EDFM models with 240X60 grids/61X15 grids/19X5 grids have been simulated for 30 years. From the pressure map (Figure. 61), it can be observed that points in the white cell have a higher pressure than the points with the same distance from the fracture in the blue circle, which is called the grid diagonal effect. When the grid is coarse enough, the pressure drop area lost the elliptical shape. From the production plot, the simulation error in Case 5 is similar to the previous 4 cases. The incorrect steady-state flow period also shows up in this case. To improve the grid diagonal effect, extra connections have been built between the fracture and not directly connected cells in the diagonal direction as the blue lines shown in the last plot of Figure. 62. The modified case's production

data is plotted as the red line in Figure. 62. There is no obvious improvement to the steady-state period in the production rate plot, and the long-time production rate is over the reference model which makes the cumulative production increase too fast in the long production time. Thus, the grid diagonal effect is not the main reason that caused the simulation error in the EDFM model with the coarse grid.

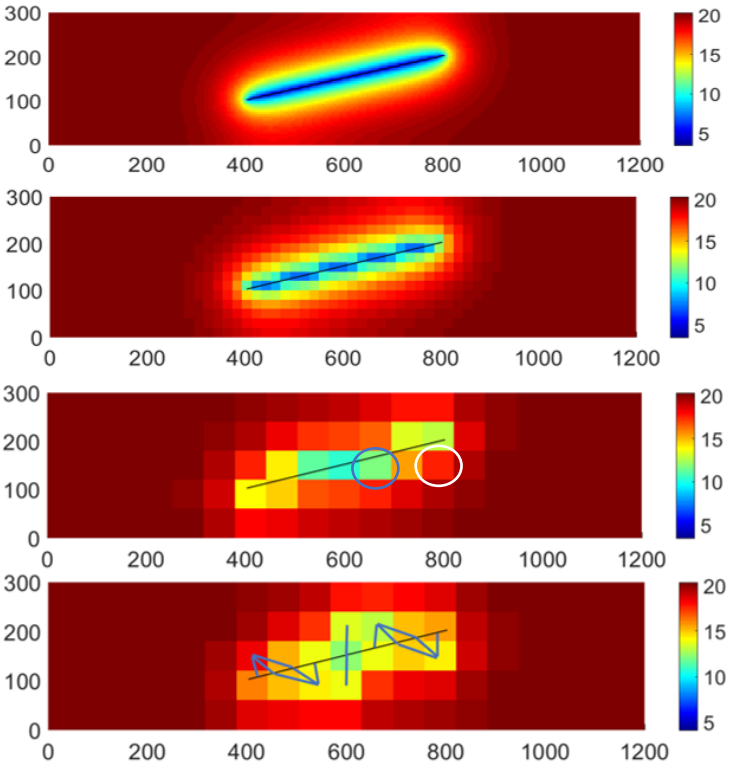

Figure 61. The pressure maps after 30 years simulation

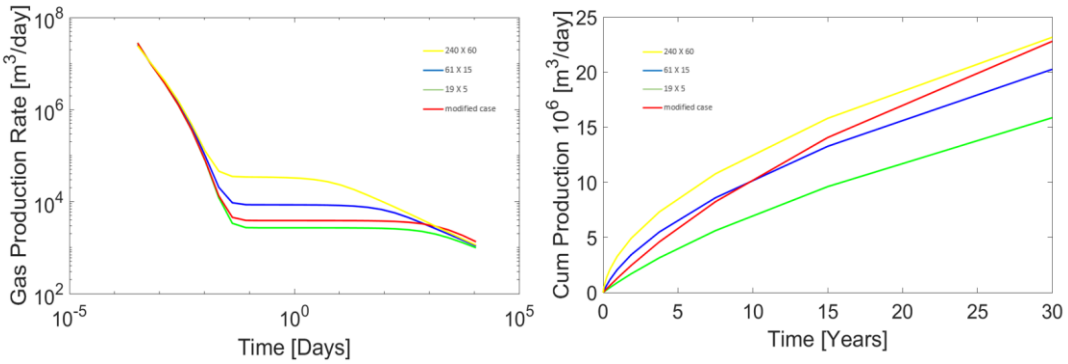

Figure 62. The production rate plot and cumulative production plot

4.7 Single fracture model with low fracture permeability

The last case study in this chapter simulates four models with the same properties and mesh as the models in Case 2. The fracture in this model also has the same location and properties as Case 2 except the fracture permeability is only 100md in this case. From the pressure map (Figure. 63), the pressure drop inside the fracture can be observed. From the production plot (Figure. 64), the coarser the grid is, the later the steady-state flow shows up. In addition, there is a transitional period between the transient and steady-state flow. When the same LGR and semi-analytical transmissibility applied into this finite conductivity case (red lines in Figure. 65), the error in early-time production rate and the cumulative production has been eliminated effectively. Although the coarser matrix gird leads to a coarser fracture gird mesh, this is not the main reason to cause the simulation error in the well's production.

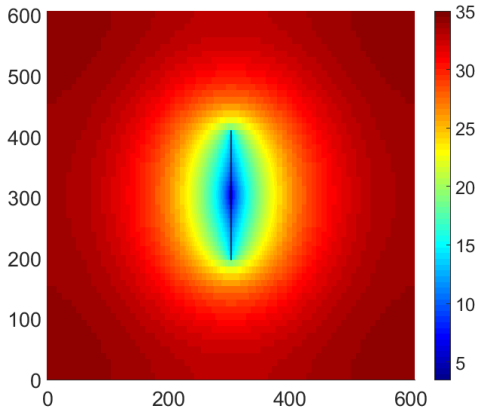

Figure 63. The pressure map after 30 years simulation

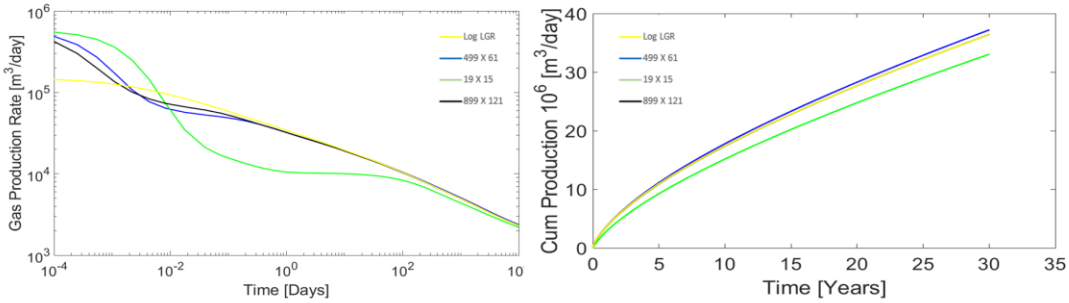

Figure 64. The production rate plot and cumulative production plot of the model without improvement methods

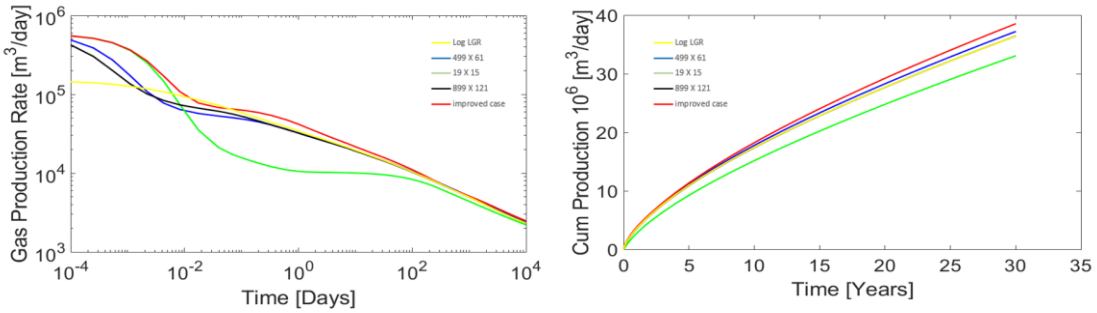

Figure 65. The production rate plot and cumulative production plot of the model with improvement methods

Apply the LGR in several directions in the EDFM model with complex fracture geometry, such as the models in Case 1, is not practical. Thus, Combining the MINC (Multiple Interacting Continua) model with the EDFM is a more realistic choice. The method is an extension of the dual-porosity (DP) concept. The dual porosity concept is often expressed by postulating a "sugar-cube" model for a fractured-porous reservoir, in which discontinuous matrix blocks are separate from each other by thoroughgoing fracture. The crucial point in which the MINC and the conventional dual-porosity methods differ is in the nature of the matrix-fracture flow. The double-porosity method assumes that matrix-fracture flow is "quasi-steady" or "transient". The flow rate between the matrix and fracture is calculated by the "quasi-steady" or "transient" analytical solution. while in the MINC model, matrix-fracture flow is done by computing a numerical linear approximation to the gradients (of pressure, temperature, etc.) which drive flow at the matrix-fracture contact. Thus, the MINC model divided each "sugar-cube" into several "sub-cube" which is encapsulated one by one.

Farah & Wu (2019) introduced a DFM-MINC model, which can directly be applied to the EDFM-MINC model. The distance between the factures' continuums and matrix continuums is calculated. The critical step in the EDFM-MINC method is to calculate the volume of each MINC sub-grid, which can be calculated by the following steps: a bunch of random points is generated inside each matrix cell. The distance of each point to the nearest fracture is calculated. account the percentage of the points with similar distance in the total points and calculate the MINC sub-grids volume with these

percentages. However, there is still a dilemma to apply the MINC-EDFM model into an ensemble history matching program. The EDFM is applied in the iterated fractured reservoir history matching because it is unacceptable to mesh the matrix once the fracture's geometry is changing. But MINC-EDFM model needs to mesh again when the fracture's geometry is changing. Besides using more grids (MINC model, LGR), analytical solution (DP model) is another option to capture the sharp, non-steady-state pressure drop between the fracture and matrix. However, the matrix-fracture flow equation in the DP model is not fit for the EDFM model. The pseudo-steady and transient flow equation used in the DP assumes a closed boundary, which needs a matrix block to be fully surrounded by the fractures. This is not true in the EDFM model. The analytical solution of transient radio flow for an infinite reservoir can be written as:

$$P(r,t) = P_0 - \frac{q\mu}{4\pi kh}\left[-Ei\left(-\frac{r^2}{4\left(\frac{k}{\mu C}\right)t}\right)\right] \tag{50}$$

Without closed boundaries, the time term t cannot be eliminated from the analytical solution. In conclusion, if the computation resources are very limited, there is no need to present all the randomly small fractures which only penetrate less than three matrix cells explicitly. Only use the EDFM to present main fractures and use a dual-porosity model for all the small fractures may be a wiser way to simulate in the history matching program.

CHAPTER V

CONCLUSIONS

From the research of the three topics listed at the beginning of this dissertation, the following conclusions can be summarized: When the ensemble size is much smaller than the amount of the parameters that need to be matched, the Ensemble Methods do not perform well. Houtermaker's method used to construct the cross-covariance localization matrix is an effective and proper method to eliminate this problem in reservoir simulation history matching. For the specific permeability/porosity history matching in the conventional reservoir, both SVD supported localization performances and streamline-supported localization can improve this problem. both Gaspari and Cohn's function and Furrer and Bengtsson's functions are preferred in cross-covariance localization. They perform better than direct truncation in most comparisons. However, direct truncation can still perform better or similar to the other two correlation functions sometimes. it is still difficult to determine whether one of these correlation functions is consistently better. In the highly non-linear problem, the performance of the Ensemble Methods is very different with different prior information. For the specific problem of fracture position and geometry history matching, the more complex the fractures' geometry, the more specific the prior information in the initial fields should be. Combining the desired prior information into the initial fields also proposes challenges to the design of initial field generation algorithms. When combing with the ensemble fracture geometry history matching program, The EDFM shows advantages over other traditional simulation methods. However, the EDFM still faces problems capturing teh sharp pressure drop around the fracture in the shale gas reservoirs, which leads to obvious simulation error in the final cumulative production. Combining the MINC or analytical matrix-fracture flow equation into the EDFM still faces limitations in the fracture geometry history matching process. If the computation resources are very limited, only using the EDFM to present main fractures and using the dual-porosity model for all the small fractures is a wiser way to simulate in the history matching program.

BIBLIOGRAPHY

Aanonsen, S. I., Nævdal, G., Oliver, D. S., Reynolds, A. C., & Vallès, B. (2009). The ensemble Kalman filter in reservoir engineering--a review. Spe Journal, 14(03), 393-412.

Agarwal R, Li Y K, Nghiem L. A regression technique with dynamic parameter selection or phase behavior matching[C]//SPE California Regional Meeting. Ventura, California: Society of Petroleum Engineers, 1987: 207-214

Angerer, E., Horns, S.A., Gaiser, J.E., Walters,R., Bagala, S., and Vetri, L., 2002, Characterization of dipping fractures using PS mode-converted data, SEG Annual International Meeting, Salt Lake City, UT, October 6-12.

Arroyo, E., Devegowda, D., Datta-Gupta, A., & Choe, J. (2008). Streamline-assisted ensemble Kalman filter for rapid and continuous reservoir model updating. SPE Reservoir Evaluation & Engineering, 11(06), 1-046.

Bandis, S.C., Lumsden, A.C., and Barton, N.R., 1983, Fundamentals of rock joint deformation, International Journal of Rock Mechanics and Mining Sciences and Geomechanics, Abstract. 20 (6), 249-268.

Barton, N.R., Bandis, S.C., and Bakhtar, K., 1985, Strength, deformation and conductivity coupling of rock joints, International Journal of Rock Mechanics and Mining Sciences and Geomechanics, Abstract. 22 (3), 121-140.

Bell, J. (1978). Mathematics of Computation, 32(144), 1320-1322. doi:10.2307/2006360

Bissell, R. (1994). Calculating optimal parameters for history matching. In ECMOR IV-4th European Conference on the Mathematics of Oil Recovery.

Bryant, E. C., Hwang, J., & Sharma, M. M. (2015, February). Arbitrary fracture propagation in heterogeneous poroelastic formations using a finite volume-based cohesive zone model. In SPE Hydraulic Fracturing Technology Conference. Society of Petroleum Engineers.

Chai, Z., Yan, B., Killough, J. E., & Wang, Y. (2018). An efficient method for fractured shale reservoir history matching: The embedded discrete fracture multi-continuum approach. Journal of Petroleum Science and Engineering, 160, 170-181.

Chang, H., & Zhang, D. (2018). History matching of stimulated reservoir volume of shale-gas reservoirs using an iterative ensemble smoother. Spe Journal, 23(02), 346-366.

Chavent G, Dupuy M, Lemmonier P. History matching by use of optimal theory[J]. Society of Petroleum Engineers Journal, 1975, 15(1): 74- 86.

Chen W H, Gavalas G R, Seinfeld J H, et al. A new algorithm for automatic history matching[J]. Society of Petroleum Engineers Journal, 1974, 14(6): 593-608.

Chen, Y., & Oliver, D. S. (2010). Cross-covariances and localization for EnKF in multiphase flow data assimilation. Computational Geosciences, 14(4), 579-601.

Chen, Y., & Oliver, D. S. (2012). Ensemble randomized maximum likelihood method as an iterative ensemble smoother. Mathematical Geosciences, 44(1), 1-26.

Chen, Y., & Oliver, D. S. (2017). Localization and regularization for iterative ensemble smoothers. Computational Geosciences, 21(1), 13-30.

Chen, Z., Liao, X., Yu, W., Sepehrnoori, K., Zhao, X., Li, X., & Sun, H. (2017, September). A Diagnostic Approach to Identify Complex Fracture Geometries in Unconventional Reservoirs Using a Semi-Analytical Model. In Unconventional Resources Technology Conference, Austin, Texas, 24-26 July 2017 (pp. 2145-2171). Society of Exploration Geophysicists, American Association of Petroleum Geologists, Society of Petroleum Engineers.

Chen, Z., Liao, X., Zhao, X., Dou, X., Zhu, L., & Sanbo, L. (2017). A finite-conductivity horizontal-well model for pressure-transient analysis in multiple-fractured horizontal wells. SPE Journal, 22(04), 1-112.

Chen, Z., Liao, X., Zhao, X., Lv, S., & Zhu, L. (2016, April 1). A Semianalytical Approach for Obtaining Type Curves of Multiple-Fractured Horizontal Wells with Secondary-Fracture Networks. Society of Petroleum Engineers. doi:10.2118/178913-PA

Coats K H, Dempsey J R, Henderson J H. A new technique for deter**-**mining reservoir description from field performance data[J]. Society of Petroleum Engineers Journal, 1970, 10(1): 66-74.

Costa L A N, Maschio C, José Schiozer D. Application of artificial neural networks in a history matching process[J]. Journal of Petroleum Science and Engineering, 2014, 123: 30-45.

Cullick A S, Johnson W D, Shi G. Improved and more rapid history matching with a nonlinear proxy and global optimization[C]//SPE Annual Technical Conference and Exhibition. San Antonio, Texas: Society of Petroleum Engineers, 2006: 1-13

Devegowda, D., Arroyo, E., Datta-Gupta, A., & Douma, S. G. (2007, January). Efficient and robust reservoir model updating using ensemble Kalman filter with sensitivity-based covariance localization. In SPE Reservoir Simulation Symposium. Society of Petroleum Engineers.

Dougherty E L. Application of optimization methods to oilfield problems: Proved, probable, possible[C]//Fall Meeting of the Society of Petroleum Engineers of AIME. San Antonio, Texus: Society of Petroleum Engineers, 1972: 1-20.

Duda, R. O., & Hart, P. E. (1971). Use of the Hough transformation to detect lines and curves in pictures (No. SRI-TN-36). SRI INTERNATIONAL MENLO PARK CA ARTIFICIAL INTELLIGENCE CENTER.

Emerick, A. A. (2017). Investigation on principal component analysis parameterizations for history matching channelized facies models with ensemble-based data assimilation. Mathematical Geosciences, 49(1), 85-120.

Emerick, A., & Reynolds, A. (2011). Combining sensitivities and prior information for covariance localization in the ensemble Kalman filter for petroleum reservoir applications. Computational Geosciences, 15(2), 251-269.

Fortin, V., Abaza, M., Anctil, F., & Turcotte, R. (2014). Why should ensemble spread match the RMSE of the ensemble mean? Journal of Hydrometeorology, 15(4), 1708-1713.

Furrer, R., & Bengtsson, T. (2007). Estimation of high-dimensional prior and posterior covariance matrices in Kalman filter variants. Journal of Multivariate Analysis, 98(2), 227-255.

Gao G, Li G, Reynolds A C. A stochastic optimization algorithm for automatic history matching[C]//SPE Annual Technical Conference and Exhibition. Houston, Texas: Society of Petroleum Engineers, 2004: 1- 23.

Gao Huimin. Inversion solution of formation parameters by using automatic history matching technology[J]. Well Testing, 1994, 3(4): 18-24.

Gaspari, G., & Cohn, S. E. (1999). Construction of correlation functions in two and three dimensions. Quarterly Journal of the Royal Meteorological Society, 125(554), 723-757.

Gavalas G R, Shah P C, Seinfeld J H. Reservoir history matching by Bayesian estimation[J]. Old SPE Journal, 1976, 16(6): 337-350.

Gomez S, Gosselin O, Barker J W. Gradient-based history-matching with a global optimization method[C]//SPE Annual Technical Conference and Exhibition. Houston, Texas: Society of Petroleum Engineers, 1999: 1-13.

Grechka, V. and Tsuankin, I., 2004, Characterization of dipping fractures in transversely isotropic background, Geophysical Prospecting, Vol. 68, 1399-1407.

Hajizadeh Y. Ants can do history matching[C]//SPE Annual Technical Conference and Exhibition. Florence, Italy: Society of Petroleum Engineers, 2010: 1-15.

Haugen V E J, Natvik L J, Evensen G, et al. History matching using the ensemble Kalman filter on a North Sea field case[C]//SPE Annual Technical Conference and Exhibition. San Antonio, Texas: Society of Petroleum Engineers, 2006: 1-9.

Hough, P. V. (1962). U.S. Patent No. 3,069,654. Washington, DC: U.S. Patent and Trademark Office.

Houtekamer, P. L., & Mitchell, H. L. (1998). Data assimilation using an ensemble Kalman filter technique. Monthly Weather Review, 126(3), 796-811.

Houtekamer, P. L., & Mitchell, H. L. (2001). A sequential ensemble Kalman filter for atmospheric data assimilation. Monthly Weather Review, 129(1), 123-137.

Houtekamer, P. L., Mitchell, H. L., Pellerin, G., Buehner, M., Charron, M., Spacek, L., & Hansen, B. (2005). Atmospheric data assimilation with an ensemble Kalman filter: Results with real observations. Monthly weather review, 133(3), 604-620.

Jacquard P, Jain C. Permeability distribution from field pressure data [J]. Society of Petroleum Engineers Journal, 1965, 5(4): 281-294

Jahns H O. A rapid method for obtaining a two- dimensional reservoir description from well pressure response data[J]. Society of Petroleum Engineers Journal, 1966, 6(4): 315-327.

Jiang, J., & Gorell, S. (2018). Principle Component Analysis Methods for Covariance Localization in the Ensemble Kalman Filter History Matching. Society of Petroleum Engineers. doi:10.2118/190015-MS

Jiang, J., & Gorell, S. B. (2019). Analysis of localization methods in ensemble Kalman filter with SVD analytical solution. Journal of Petroleum Science and Engineering, 175, 919-931.

Jiang, J., Sheng, J., & Gorell, S. (2019, October). Inversion of Production Data Using an Ensemble Smoother to Determine the Geometry of Hydraulic Fractures. In SPE Liquids-Rich Basins Conference-North America. OnePetro.

Kaydani H, Mohebbi A, Eftekhari M. Permeability estimation in heterogeneous oil reservoirs by multi-gene genetic programming algorithm [J]. Journal of Petroleum Science and Engineering, 2014, 123: 201- 206.

Kazemi A, Stephen K D. Optimal parameter updating in assisted history matching of the Nelson field using streamlines as a guide[C]//SPE EUROPEC/EAGE Annual Conference and Exhibition. Barcelona, Spain: Society of Petroleum Engineers, 2010: 1-15.

Kern, M. (2016). Numerical Methods for Inverse Problems. John Wiley & Sons.

Lee, S.H., Jensen, C.L., and Lough, M.F., 2000, Efficient finite-difference model for flow in a reservoir with multiple length-scale fractures, SPE Journal, Vol. 5, 268-275.

Lee, S.H., Lough, M.F., and Jensen, C.L., 2001, Hierarchical modeling of flow in naturally fractured formations with multiple length scales, Water Resources Research, Vol. 37, 443-455.

Li, L. and Lee, S.H., 2008, Efficient field-scale simulation of black oil in a naturally fractured reservoir through discrete fracture networks and homogenized media, SPE Reservoir Evaluation and Engineering, Vol. 11, 750-758.

Li, R., Reynolds, A. C., & Oliver, D. S. (2001, January). History matching of three-phase flow production data. In SPE reservoir simulation symposium. Society of Petroleum Engineers.

Liu N, Oliver D S. Critical evaluation of the ensemble Kalman filter on history matching of geologic facies[C]//SPE reservoir simulation symposium. Houston, Texas: Society of Petroleum Engineers, 2005: 1- 12.

Liu N, Oliver D S. Ensemble Kalman filter for automatic history matching of geologic facies[J]. Journal of Petroleum Science and Engineering, 2005, 47(3): 147-161.

Lorenz, J.C., 1999, Stress sensitive reservoirs, Journal of Petroleum Technology, Vol.51, 61-63.

Lu, L., & Zhang, D. (2015). Assisted history matching for fractured reservoirs by use of hough-transform-based parameterization. SPE Journal, 20(05), 942-961.

MacMillan D J. Automatic history matching of laboratory core floods to obtain relative- permeability curves[J]. SPE Reservoir Engineering, 1987, 2(1): 85-91.

Mattax C C, Dalton R L. Reservoir simulation[J]. Journal of Petroleum Technology, 1990, 42(6): 692-695.

Naevdal G, Mannseth T, Vefring E H. Near-well reservoir monitoring through ensemble Kalman filter[C]//SPE/DOE Improved Oil Recovery Symposium. Tulsa, Oklahoma: Society of Petroleum Engineers, 2002: 1-9

Nasralla R A, Daoud A M, Fattah K A, et al. Fast and efficient sensitivity calculation using adjoint method for three-phase field-scale history matching[J]. Journal of Petroleum Science and Engineering, 2011, 77(3): 338-350

Oliver D S, Chen Y. Recent progress on reservoir history matching: A review[J]. Computational Geosciences, 2011, 15(1): 185-221.

Oliver, D. S., & Chen, Y. (2011). Recent progress on reservoir history matching: a review. Computational Geosciences, 15(1), 185-221.

Oliver, D. S., Reynolds, A. C., & Liu, N. (2008). Inverse theory for petroleum reservoir characterization and history matching. Cambridge University Press.

Oliver, D. S., Reynolds, A. C., & Liu, N. (2008). Inverse theory for petroleum reservoir characterization and history matching. Cambridge University Press.

Ouenes A, Brefort B, Meunier G, et al. A new algorithm for automatic history matching: application of simulated annealing method (SAM) to reservoir inverse modeling[J]. SPE 26297, 1993: 1-31.

Ping, J., & Zhang, D. (2013). History matching of fracture distributions by ensemble Kalman filter combined with vector-based level set parameterization. Journal of Petroleum Science and Engineering, 108, 288-303.

Quenes A, Saad N. A new fast parallel simulated annealing algorithm for reservoir characterization [C]//SPE Annual Technical Conference and Exhibition. Houston, Texas: Society of Petroleum Engineers, 1993: 19-29.

Rodrigues, J. R. P. (2006). Calculating derivatives for automatic history matching. Computational Geosciences, 10(1), 119-136.

Rodrigues, J. R. P. (2006). Calculating derivatives for automatic history matching. Computational Geosciences, 10(1), 119-136.

Sahni I, Horne R N. Generating multiple history- matched reservoir model realizations using wavelets[C]//SPE Annual Technical Conference and Exhibition. Houston, Texas: Society of Petroleum Engineers, 2004: 1-11.

Saleri N G, Toronyi R M. Engineering control in reservoir simulation: part I[C]// SPE Annual Technical Conference and Exhibition. Houston, TX: Society of Petroleum Engineers, 1988: 1-42.

Schiozer D J, Leitão H C. A new automated history matching algorithm improved by parallel computing[C]//Latin American and Caribbean Petroleum Engineering Conference. Caracas, Venezuela: Society of Petroleum Engineers, 1999: 1-11.

Schulze-Riegert R W, Axmann J K, Haase O, et al. Evolutionary algorithms applied to history matching of complex reservoirs[J]. SPE Reservoir Evaluation & Engineering, 2002, 5(2): 163-173.

Sen M K, Datta-Gupta A, Stoffa P L, et al. Stochastic reservoir modeling using simulated annealing and genetic algorithm[J]. SPE Formation Evaluation, 1995, 10(1): 49-56.

Shakiba, M. (2014). Modeling and simulation of fluid flow in naturally and hydraulically fractured reservoirs using embedded discrete fracture model (EDFM) (Doctoral dissertation).

Slater G E, Durrer E J. Adjustment of reservoir simulation models to match field performance[J]. Society of Petroleum Engineers Journal, 1971, 11(3): 295-305.

Tan T B, Kalogerakis N. A fully implicit, three- dimensional, three phase simulators with automatic history- matching capability[C]//SPE Symposium on Reservoir Simulation. Anaheim, California: Society of Petroleum Engineers, 1991: 35-46

Tan T B, Kalogerakis N. A three-dimensional three-phase automatic history matching model: Reliability of parameter estimates[J]. Journal of Canadian Petroleum Technology, 1992, 31(3): 34-41.

Tarantola, A. (2005). Inverse problem theory and methods for model parameter estimation (Vol. 89). siam.

Thomas L K, Hellums L J, Reheis G M. A nonlinear automatic history matching technique for reservoir simulation models[J]. Society of Petroleum Engineers Journal, 1972, 12(6): 508-514.

van den Bosch B, Seinfeld J H. History matching in two-phase petroleum reservoirs: Incompressible flow[J]. Society of Petroleum Engineers Journal, 1977, 17(6): 398-406.

van der Wilk, M., Rasmussen, C. E., & Hensman, J. (2017). Convolutional Gaussian Processes. In Advances in Neural Information Processing Systems (pp. 2845-2854).

Veatch Jr R W, Thomas G W. A direct approach for history matching [C]//Fall Meeting of the Society of Petroleum Engineers of AIME. New Orleans, Louisiana: Society of Petroleum Engineers, 1971: 1-12.

Walsh, J.J. and Watterson, J., 1988, Dips of normal faults in British coal measures and other sedimentary sequences, Journal of Geologic Society, Vol. 145, 859-873.

Wang Shuguang, Guo Dezhi. Popularization of NelderMead simplex algorithm and its application in automatic history matching[J]. Petroleum Geology & Oilfield Development in Daqing, 1998, 17(4): 25-27

Wasserman M L, Emanuel A S, Seinfeld J H. Practical applications of optimal-control theory to history-matching multiphase simulator models[J]. Society of Petroleum Engineers Journal, 1975, 15(4): 347-355.

Wathelet, M. (2008). An improved neighborhood algorithm: parameter conditions and dynamic scaling. Geophysical Research Letters, 35(9).

Watson A T, Seinfeld J H, Gavalas G R, et al. History matching in two- phase petroleum reservoirs[J]. Society of Petroleum Engineers Journal, 1980, 20(6): 521-532.

Whitaker, J. S., & Hamill, T. M. (2002). Ensemble data assimilation without perturbed observations. Monthly Weather Review, 130(7), 1913-1924.

Xavier C R, Santos E P D, Vieira V D F, et al. Genetic algorithm for the history matching problem[J]. Procedia Computer Science, 2013, 18: 946-955

Yan Xia, Li Yang, Yao Jun, et al. Automatic history matching of reservoirs using the streamline based EnKF method[J]. Acta Petrolei Sinica, 2011, 32(3): 495-499

Yang P H, Watson A T. Automatic history matching with variable-metric methods[J]. SPE Reservoir Engineering, 1988, 3(3): 995-1001.

Yao, M., Chang, H., Li, X., & Zhang, D. (2018). Tuning fractures with dynamic data. Water Resources Research, 54(2), 680-707.

Yin J, Park H Y, Datta-Gupta A, et al. A hierarchical streamline-assisted history matching approach with global and local parameter updates[J]. Journal of Petroleum Science and Engineering, 2011, 80(1): 116-130.

Zafari M, Reynolds A C. Assessing the uncertainty in reservoir de- scription and performance predictions with the ensemble Kalman filter [C]//SPE Annual Technical Conference and Exhibition. Dallas, Texas: Society of Petroleum Engineers, 2005: 1-18.

Zafari, M., & Reynolds, A. C. (2005, January). Assessing the uncertainty in reservoir description and performance predictions with the ensemble Kalman filter. In SPE Annual Technical Conference and Exhibition. Society of Petroleum Engineers.

Zeng L, Chang H, Zhang D. A probabilistic collocation based Kalman filter for history matching[J]. SPE Journal, 2011, 16(2): 294-306.

Zhang F, Skjervheim J A, Reynolds A C, et al. Automatic history matching in a Bayesian framework, example applications[C]//SPE Annual Technical Conference and Exhibition. Denver, Colorado: Society of Petroleum Engineers, 2003: 1-14

Zhang X, Hou J, Wang D, et al. An automatic history matching method of reservoir numerical simulation based on improved genetic algorithm[J]. Procedia Engineering, 2012, 29: 3924-3928.

Zhang, F., Reynolds, A. C., & Oliver, D. S. (2002). Evaluation of the reduction in uncertainty obtained by conditioning a 3D stochastic channel to multiwell pressure data. Mathematical geology, 34(6), 715-742.

Zhang, Y., & Oliver, D. S. (2011). History matching using the ensemble Kalman filter with multiscale parameterization: A field case study. SPE Journal, 16(02), 307-317.